공학박사학위논문

in-situ Transmittance Evaluation of Solutions for Cu Electroless Deposition and Its Applications

구리 무전해 도금 용액의 실시간 투과율 평가 및 그 응용

2013년 8월

서울대학교 대학원

화학생물공학부

박 경 주

in-situ Transmittance Evaluation of Solutions for Cu Electroless Deposition and Its Applications

구리 무전해 도금 용액의 실시간 투과율 평가 및 그 응용

지도교수 김 재 정

이 논문을 공학박사 학위논문으로 제출함
2013 년 4 월

서울대학교 대학원
화학생물공학부
박 경 주

박경주의 공학박사 학위논문을 인준함
2013 년 6 월

위 원 장 _____

부위원장 _____

위 원 _____

위 원 _____

위 원 _____

Abstract

Cu electroless deposition (ELD) has extensive applications with representative practical use in ultra large scale integration (USLI) interconnection. It is important to figure out the characteristic of solutions related to the reliability. Thus, many analytical methods of solution estimation have been reported in *ex-situ* and *in-situ*.

In this study, *in-situ* transmittance measurement to verify the solution performances of the stability and the reactivity on SnPd colloidal surface was proposed as an alternative tool for chemical-sensitive electrochemical analysis, and its feasibility was contemplated. Its advantages lie in both the simplicity of the analysis and the *in-situ* allowance in time-dependent characterization. Applicatively, the relation of material properties with Cu particles and Cu film was demonstrated and qualified solution was applied to form Cu seed layer in through silicon via (TSV).

To understand the basic behaviors of Cu ELD solution, the change of transmittance with the size of Cu particles by the injection of SnPd colloids were observed. Based on the relationship between the transmittance and the Cu particle growth, *in-situ* monitoring was applied to determine the effect of complexing agents, reducing agents, and the organic additives, which are the important elements in determination of solution performance, on stability and reactivity.

In application of *in-situ* measurements to performance test with various complexing agents, it was confirmed that the stability and reactivity of each solution were well described by *in-situ* transmittance measurement. The merits of methods which reflect the real environmental impact by supporting SnPd catalyst helped to exhibit the characteristics of solutions. The validity of the *in-situ* transmittance monitoring was supported by comparison with the consequence from the actual film deposition on Ta substrate.

In the same way, reducing agents were evaluated. Aldehyde based reducing agents showed the similar trends in transmittance and Cu powder so that the reactivity could also be predicted. In contrast, other reducing agents exhibited different trends and some limitations. It is expected that those problems would be solved with suggested modification of equipment. These results implied the validity of widening in application to various kinds of solutions.

Measurement with organic additives, usually used for bottom-up filling was also implied for reactivity test. The change of reaction time from transmittance curve represented the acceleration and suppression effect, and the concentration range affected was same as that in Cu film deposition. Cu powder also allowed us to forecast the reactivity of solution and surface roughness of Cu film. Additionally, material properties of Cu powder with organic additives were measured to find out whether it can indicate those of Cu film. As a result, though precise prediction was difficult, they have considerable relationship in the aspect of the grain size and the surface roughness.

For another application, one of the optimal compositions in the aspect of the stability and the reactivity, EDTA-HCHO based-solution, was selected by *in-situ* transmittance measurement. With this solution, the formation of Cu seed layer in high aspect ratio of via was performed. The additional improvement of the stability with RE-610® and 2,2'-dipyridyl facilitated the achievement of adhesive Cu film. To overcome the structural drawbacks of non-Bosch TSV, more optimization and the modification of process were required. In a bid for it, pretreatment conditions were optimized and convection system was adopted. Optimal time was achieved by populating the Cu nuclei at the bottom of the vias, and the continuity and conformality of the seed layer were enhanced by finding the optimal rotating speed. Finally, conformal Cu seed layer was obtained, on which Cu was successfully filled by electrodeposition (ED) without voids.

In conclusion, proposed *in-situ* transmittance measurement was proved to be applicable for not only the evaluation of performances with various kinds of solutions but also the prediction of material characters. It was confirmed that this monitoring method has potentials to be applied in various field including Cu interconnection.

Keywords: electroless deposition, Cu, stability, reactivity, *in-situ* analysis, complexing agent, reducing agent, organic additive, film property, seed layer

Student number: 2008-21073

Contents

List of Tables

List of Figures

CHAPTER I

Introduction

1-1. Electroless deposition (ELD)

Electroless deposition (ELD) is one of the wet processes to make various metal deposits. Although the composition and the reactions of ELD solution are complicated, ELD is widely applicable to interconnection technique of semiconductor fields, printed circuit board, or the synthesis of catalyst.[1-5] The structure of deposited metal can be controlled by process parameters in ELD. Form of deposit may be film or particles, which depends on the requirements of application. ELD does not need any external electron supplement because necessary electron can be afforded by self-reduction. Besides, with catalyzing process before deposition, metals can be easily deposited on various substrates regardless of their conductivity.

The process of ELD is classified with 3 steps; (i) surface treatment, (ii) catalyzation, and (iii) metal deposition. The methods of surface treatment are diverse according to the types of substrate. For example, in the case of polymer substrate, the pretreatment to eliminate organic contaminants should be applied prior to ELD.[6-7] When metals are used as a substrate, native oxides have to be removed.[8-9] Catalyzation means the formation of novel metal catalyst particles

on substrate to initiate the ELD. Once the reaction starts on catalyst, as-deposited metal acts as new catalyst so that metal can be continuously deposited. Therefore, ELD is announced as autocatalytic reaction. Fig. 1.1 shows the metal candidates that can be used in ELD that has required properties such as self-catalytic characteristic or co-deposition.

Generally, ELD solution is composed of 4 components; (i) metal source, (ii) complexing agent, (iii) reducing agent, and (iv) pH adjustor. Metal source is a supplier of metal ions to be deposited, and the complexing agent makes the solution stable by chelating with free-metal ions. Chelating ability depends on the formation constant (pK_f), also referred to as stability constant, and the adsorption affinity of complexing agents.[10-12] Control of complexing agent is vital because strong chelating ability impinges the slow deposition rate and weak complexing ability mediates the decomposition of solution. Therefore, the selection of complexing agent and the control of its concentration are required for reactivity control. Reducing agent provides the electrons needed to reduction of metal by oxidation itself. Commonly used reducing agents are listed in Table.1.1.[13-14] It usually oxidizes by releasing hydrogen atom so that the evolution of hydrogen bubble accompanies. However, the reducing agent should be selected by making allowance for different thermodynamic favor of metals on its oxidation reaction. As Fig. 1.2 shows, Pd has a great catalytic activity over various types of reducing agents.[13] In addition, appropriate pH of solution by pH adjustor is also important to obtain the desirable deposits or kinetics.

Metal deposits are generated by simultaneous two reactions as shown Fig. 1.3. and Eq. 1-A to 1-C. That is, the reduction reaction that metal (Me) ions with complexing agent (L) is reduced and the oxidation reaction that reducing agent (Re) oxides with serving electrons.

Oxidation reaction: $Re \rightarrow Re^{n+} + ne^-$ (Eq. 1-A)

Reduction reaction: $MeL^{a-} + ne^- \rightarrow Me^0 + L^{(a+n)-}$ (Eq. 1-B)

Overall reaction: $Re + MeL^{a-} \rightarrow Me^0 + L^{(a+n)-} + Re^{n+}$ (Eq. 1-C)

Such reactions of ELD are theoretically explained by the mixed potential theory as depicted in Fig. 1.4. Each cathodic and anodic reaction gives the current-potential curve. When the anodic current (i_{anodic}) and cathodic current ($i_{cathodic}$) are the same, net current became zero. The potential at this point is defined as mixed potential ($E_{mixed\ potential}$) and absolute current is to be mixed current, i_m, which represents the deposition rate. However, there is a limitation that the mixed potential theory is based on the half-cell reactions so that it cannot reflect precisely the full reactions that is more complicated.

Table. 1.1 Oxidation Reactions of Various Kinds of Reducing Agents[13-14]

Name	Molecular formula	Reaction
Formaldehyde	HCHO	$HCHO + 3OH^- \rightarrow HCOO^- + 2H_2O + 2e^-$
Glyoxylic acid	CHOCOOH	$CHOCOOH + 3OH^- \rightarrow HC_2O_4^- + 2H_2O + 2e^-$
Hydrazine	N_2H_4	$N_2H_4 + 4OH^- \rightarrow N_2 + 4H_2O + 4e^-$
Dimethylamineborane (DMAB)	$(CH_3)_2NHBH_3$	$(CH_3)_2NHBH_3 + 3H_2O + OH^- \rightarrow (CH_3)_2NH_2^+ + B(OH)_4^- + 5H^+ + 6e^-$
Sodium borohydride	$NaBH_4$	$BH_3OH^- + 6OH^- \rightarrow B(OH)_4^- + 3H_2O + 6e^-$
Cobalt ion	Co^{2+}	$Co^{2+} \rightarrow Co^{3+} + e^-$
Sodium hypophosphite	NaH_2PO_2	$H_2PO_2^- + 3OH^- \rightarrow HPO_3^{2-} + 2H_2O + 2e^-$

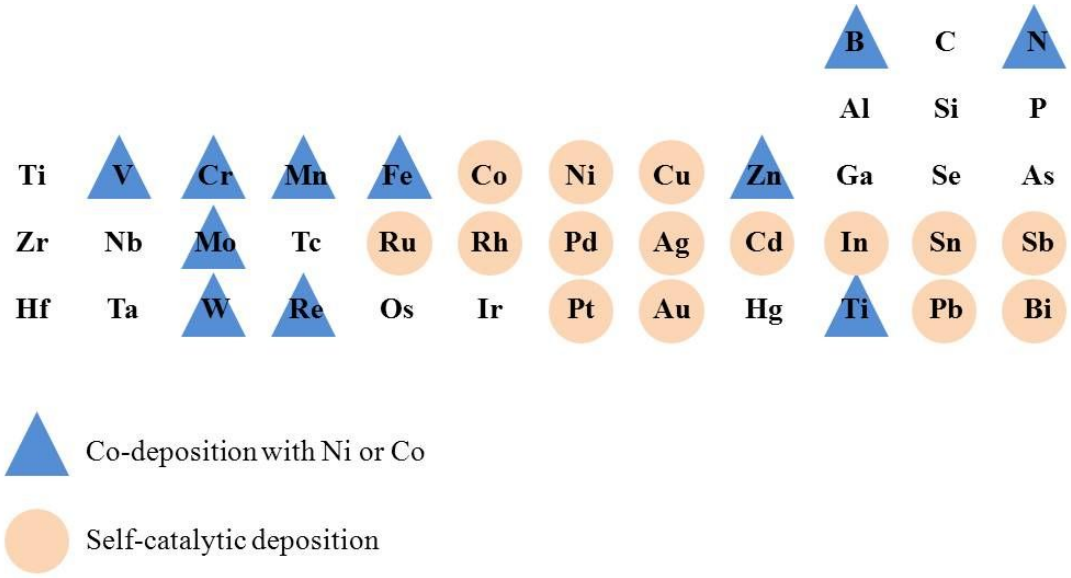

Fig. 1.1. Possible elements for the application on the electroless deposition.[13]

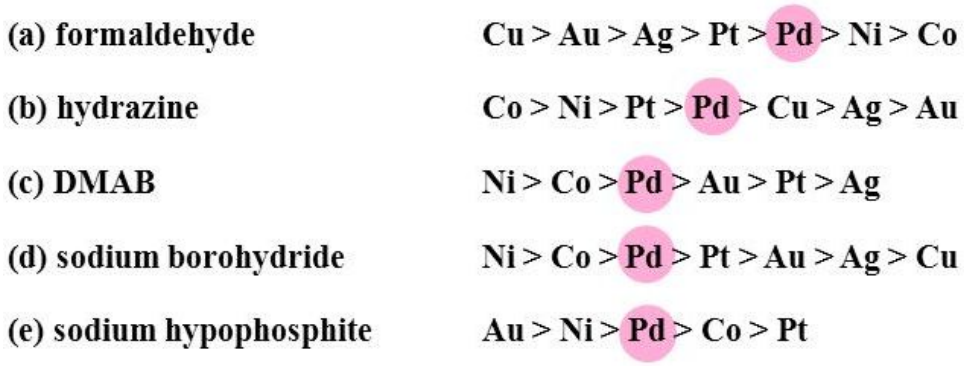

Fig. 1.2. Catalytic activities of metals for oxidation of reducing agents. (a) formaldehyde, (b) hydrazine, (c) DMAB, (d) sodium borohydride, and (e) sodium hypophosphite.[13]

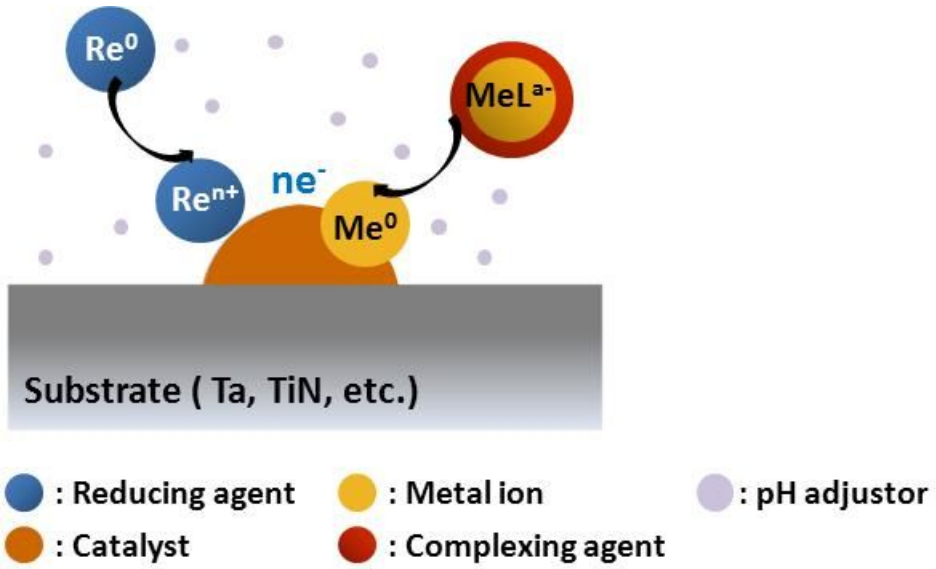

Fig. 1.3 Schematic diagram of reactions in electroless deposition.

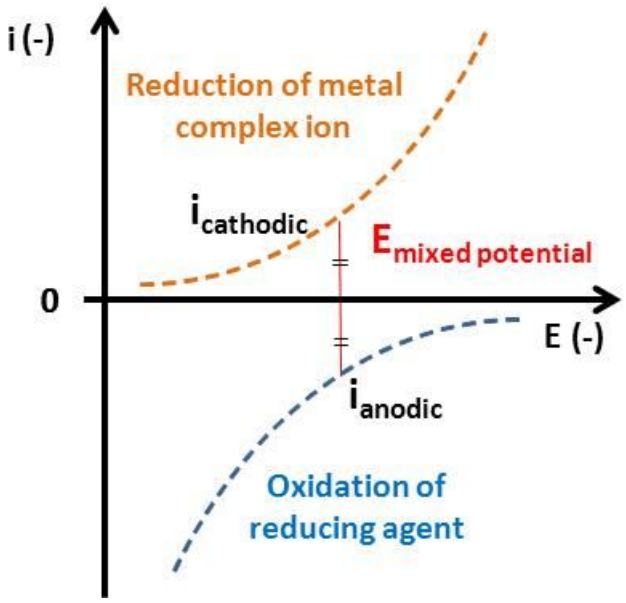

Fig. 1.4. Current-potential profiles of partial reactions in electroless deposition.

1-2. Cu ELD

Among various elements, Cu ELD has been widely investigated due to its potentials of several applications because it has low resistivity and is easily achieved owing to its abundance. It also follows generally three steps as explained in chapter 1-1. At the first step of the surface treatment, the substrate is treated to remove the organic contaminations or make hydrophilic surface for improving the wettability in following catalyzation step. For example, the surface of Ta is cleaned by hydrofluoric acid (HF) and nitric acid (HNO_3) solution for etching the native oxide.[8] As the second step, metallic catalyst such as Pd, Pt, or Au, should be formed on the substrate to initiate the deposition, which is called by activation. There are several activation methods like one-step activation, two step activation, substrate-oxidation, and adsorption of nanoparticles.[8, 15-23] Fig. 1.5 describes each activation method with Pd. Two-step activation shown in Fig. 1.5 (a) consists of Sn sensitization and Pd activation. Once Sn ions adsorb on the substrate by Sn sensitization step, Pd nuclei are formed by the displacement reaction due to the difference of reduction potential between Sn^{4+}/Sn^{2+} and Pd^{2+}/Pd since the reduction potential of Pd^{2+}/Pd is more positive than that of Sn^{4+}/Sn^{2+}. Pd displacement spontaneously takes place. One-step activation means the combination of those two processes in two-step activation as depicted in Fig. 1.5 (b), as a result, SnPd colloid containing metallic Pd or Sn/Pd alloy is formed. Because there are Sn^{4+} ions on perimeter of colloids, it needs further elimination step. Another

activation method, substrate-oxidation, intends simultaneous two reactions; the oxidation of substrate and the reduction of Pd ions. Recently, the application of Pd nanoparticles in activation displayed in Fig. 1.5 (c) has been widely researched because it enabled to reduce the catalyst size compared to aforementioned methods. Synthesized Pd nanoparticles can be directly loaded on the substrate or self-assembled monolayer aids the attachment. In addition, introduction of this method improves the adhesion strength of Cu film and enables the selective deposition.

After catalyzation process, Cu ELD started on Pd catalysts. Cu ELD solution is composed of four elements including Cu sulfate as explained chapter 1-1. As a complexing agent, ethylenediaminetetraacetic acid (EDTA) is usually used to prevent homogenous precipitation by cheating with freely existed Cu ions. Electrons are supplied by oxidation of formaldehyde (HCHO), the reducing agent. pH of solution is adjusted by potassium hydroxide (KOH) not to make undesirable precipitates such as CuO, CuO_2, or $Cu(OH)_2$. Stable solution undergoes Cu deposition via cathodic and anodic reactions with several steps as follows.

The overall reaction of Cu ELD with EDTA and HCHO can be written as Eqs. 1-D and 1-E, and it depends on the types of catalyst.[2,24]

$$CuEDTA^{2-} + HCHO + 3OH^- \rightarrow Cu + 2H_2O + HCOO^- + EDTA^{4-} \text{ (Pt, Pd, Rh)} \quad \text{(Eq. 1-D)}$$

$$CuEDTA^{2-} + 2HCHO + 4OH^- \rightarrow Cu + H_2 + 2H_2O + 2HCOO^- + EDTA^{4-} \text{ (Ag, Cu, Au)} \quad \text{(Eq. 1-E)}$$

In cathodic reaction, complexed Cu ions reduced to Cu metal.

$CuEDTA^{2-} \rightarrow CuEDTA^{2-}_{ads}$ (Eq. 1-F)

$CuEDTA^{2-}_{ads} + e^{-} \rightarrow CuEDTA^{3-}_{ads}$ (Eq. 1-G)

$CuEDTA^{3-}_{ads} + e^{-} \rightarrow CuEDTA^{4-}_{ads}$ (Eq. 1-H)

$CuEDTA^{4-}_{ads} \rightarrow Cu^{0} + EDTA^{4-}_{ads}$ (Eq. 1-I)

$2Cu^{2+} + 5OH^{-} + HCHO \rightarrow Cu_2O + HCOO^{-} + 3H_2O$ (Eq. 1-J)

Although Cu_2O also transited to Cu^0 by the disproportion reaction, Cu ions can be reduced to Cu_2O by formaldehyde with undesirable reaction of Eq.1-J, The reaction related to the formation of Cu_2O results in the decomposition of solution since it is non-catalytic reaction.

In anodic reaction under alkaline conditions, formaldehyde is oxidized with generating of electron. Methylene glycol, hydrated from of formaldehyde, is principal factor. The oxidation reactions can be expressed as follows.

$HCHO + H_2O \rightarrow CH_2(OH)_2$ (Eq. 1-K)

$CH_2(OH)_2 \rightarrow CH_2(OH)O^{-} + H^{+}$ or (Eq. 1-L)

$CH_2(OH)_2 + OH^{-} \rightarrow CH_2(OH)O^{-} + H_2O$ (Eq. 1-M)

$CH_2(OH)O^{-} \rightarrow CH(OH)O^{-}_{ads} + H_{ads}$ (Eq. I-N)

$CH(OH)O^-_{ads} + OH^- \rightarrow HCOO^- + H_2O + e^-$ (Eq.1-O)

$H_{ads} + OH^- \rightarrow H_2O + e^-$ (Pt, Pd, Rh) (Eq.1-P)

$2H_{ads} \rightarrow H_2$ (Ag, Cu, Au) (Eq.1-Q)

Throughout those reactions, Cu film is made by repetition of nucleation, growth, and coalescence. Growth mode is determined by the interactions between metals and substrate. According to the binding energy (E_B), there are three growth modes in metal formation as exhibited in Fig. 1.6.[25] Especially, on the highly resistive substrate like Ta or TiN, Volmer-Weber growth that represents three-dimensional growth (3-D) appears. Especially, in the presence of Pd catalyst on the substrate, initial Cu growth is governed by 3-D growth mode. When small Cu nuclei on Pd are agglomerated, make clusters, and finally form continuous film, growth obeys two-dimensional (2-D) by the surface diffusion and experienced coalescence to reduce boundary energy.[19, 26-29] As a result, perfectly crystallized Cu film built up as described in Fig. 1.7. In addition, it is important to obtain Pd catalyst that has high density, uniformity on substrate, and small size, since more initiation site of Pd provides the formation of thin and smooth Cu film by fast transition to 2-D growth.[30-31]

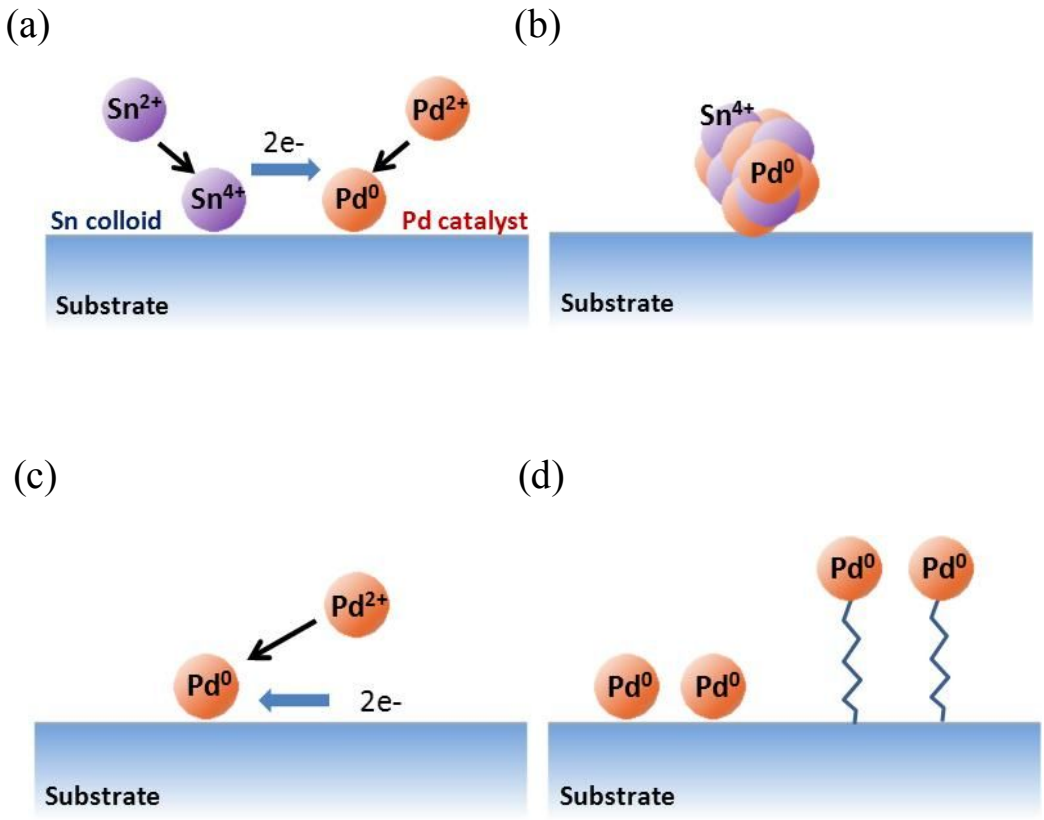

Fig. 1.5. Methods for the surface activation with Pd catalyst by (a) two-step activation, (b) one-step activation, (c) substrate-oxidation, and (d) Pd nanoparticles.

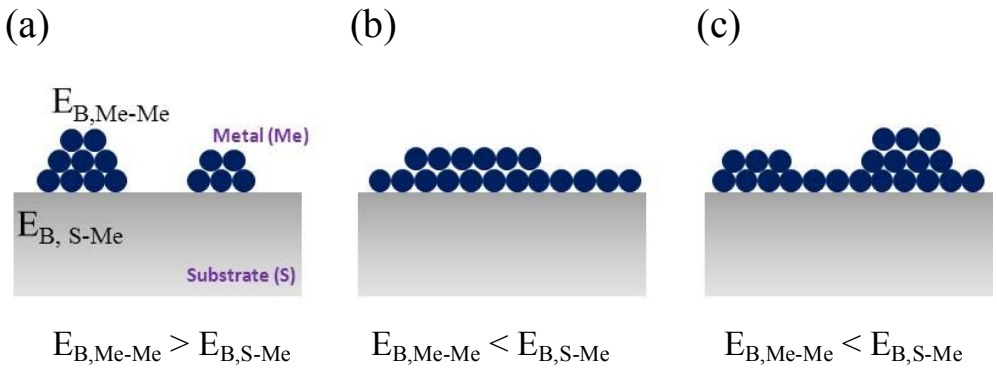

Fig. 1.6. Growth modes of metal film on the substrate depending on the binding energy. (a) Volmer-Weber growth (3-D growth), (b) Frank-van der Merwe growth (2-D growth), and (c) Stranski-Krastanov growth (2-D layer and 3-D islands).

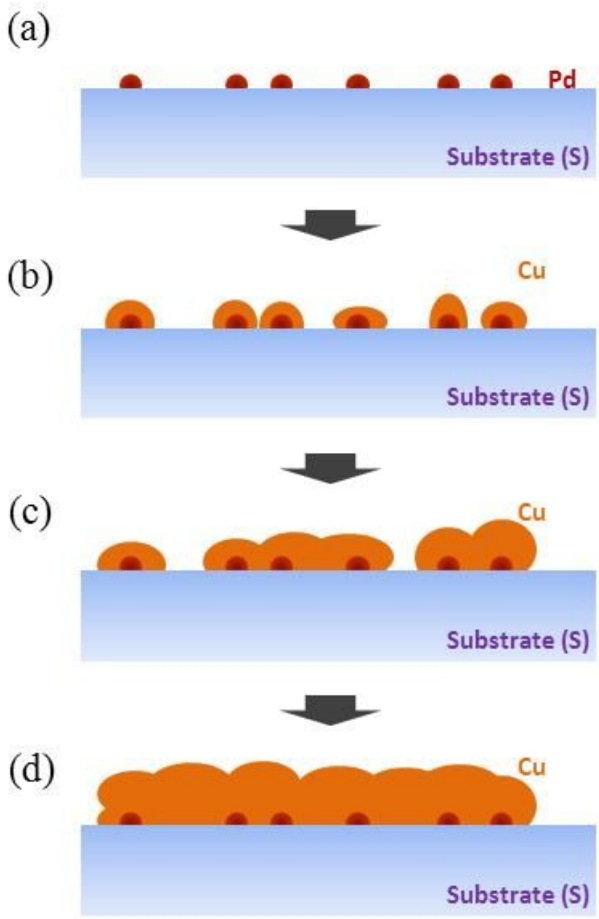

Fig. 1.7. Schematic diagram of Cu growth on the substrate. (a) Pd activation, 3-D evolution for (b) formation of Cu nuclei on Pd and (c) Cu growth and coalescence, and (d) Cu film formation by 2-D growth.

1-3. Material properties of Cu film

It is important to obtain Cu film with desirable material properties. Among various properties of Cu film, the electrical resistivity is the most important in the field of metal interconnection fabrication. As the line width is shrinking to below tens of nanometers, controlling the electrical resistivity of Cu to have under 5 μΩ·cm has been on the rise.[33] Moreover, high electrical resistivity of Cu seed layer causes the non-uniform deposition between the center and the side of the wafer.[34] It is known that the electrical resistivity is governed by phonons, the concentration of impurities, grain boundary, and surface roughness. The phonon scattering is the intrinsic characteristic according to the metals and is affected by temperature so that its effect could be omitted when the same metal is considered. In terms of impurities, if Cu ELD was conducted with organic additives, some organics would be incorporated in Cu film. In case, it is not negligible in sulfur-containing additives to affect the electrical resistivity. The scattering at the grain boundary is one of the important factors. If the thickness of Cu film is decreased to mean free path of Cu, 39 nm, its importance would be enlarged because thin Cu film is accompanied with the decrease in the grain size. Mayadas-Shatzkes proposed the model that indicates relationship between the grain size and the resistivity shown in equation (1-R).[34-35]

$$\rho_g = \rho_b \left\{3\left[\frac{1}{3} - \frac{1}{2}\alpha + \alpha^2 - \ln\left(1 + \frac{1}{\alpha}\right)\right]\right\}^{-1} \quad \text{where} \quad \alpha = \frac{\lambda}{d}\frac{R}{1-R} \tag{1-R}$$

Where ρ_g is resistivity of film considered with grain boundary scattering, ρ_b is bulk resistivity, and λ represents the mean free path of electrons in bulk film, d is the grain size, and R represents the grain boundary scattering coefficient of electrons. It clearly indicates the small grain size of film increased the electrical resistivity.

The last factor that affects the electrical resistivity is the surface roughness that has to be considered at thinner film. Rougher surface induced more surface scattering, as a result, it leads the increase in the electrical resistivity. Many researchers such as Fuch-Sondheimer, Namba, or S. M. Rossnagel introduced the relationship between the surface roughness and the electrical resistivity.[35-36] Especially, S. M. Rossnagel *et al.* suggested the combined equation that considers both the grain size and the surface roughness which affect the electrical resistivity written in (1-S).

$$\rho = \rho_b \left(1 + 0.375(1-p)\frac{S\lambda}{t} + 1.5\frac{R}{1-R}\frac{\lambda}{d}\right) \tag{1-S}$$

where ρ is resistivity of film considered with grain boundary scattering and surface roughness, t means the thickness of film, p represents the scattering parameter ($0 < p < 1$), and S means the roughness factor. Therefore, it is obvious that the grain size and the surface roughness are main

factors to be controlled.

In Cu ELD, those characteristics are influenced by the substrate. ELD on non-conductive substrate surely needs catalyzing process with Pd. Cu film grown on Pd catalyst has fine grain size because the reaction should be started on only densely distributed Pd.[13, 37] Despite of the evolution to the columnar structure in further development of microstructure, it might be severe problem in thin Cu film. The other thing that functions in structure evolution is the organic additives during ELD. In addition that the organic additives changes the deposition rate, they facilitate the control of the grain size and the surface by lowering surface energy or inhibiting coalescence.[38] Therefore, the properties of electrolessly deposited Cu film should be investigated with carefully considering each influences of variables as stated above.

1-4. Applications of Cu ELD in ULSI

Cu ELD has wide applications not only as interconnection techniques of ultra large-scale integration (ULSI) circuits, 3-D packaging but also for preparing electrocatalyst in fuel-cell and seed layer for synthesis of thin films of copper indium selenide and copper indium gallium selenide (CIGS) films in solar cells.[39-43]

In recent decades, Cu filling without defects in the damascene process has been actively investigated.[2] Damascene process is summarized with simplification in Fig. 1.8 (a)~(f). It makes the trenches by photolithography (Fig. 1.8 (a) and (b)), and diffusion barriers such as Ta/TaN or TiN are deposited to prevent the diffusion of Cu to silicon (Si) or silicon dioxide (SiO_2), which is a cause of device failure (Fig. 1.8 (c)). After that, Cu seed layer, which is a conductive layer to amicable pass of electrons in further step, is deposited (Fig. 1.8 (d)). Inside of trench is filled by Cu electrodeposition (ED) (Fig. 1.8 (e)), then, over-deposited Cu is polished by chemical mechanical planarization (CMP) to make multi-level interconnection. In damascene process, ED and ELD have been had the limelight, and ELD can be applicable to formation of seed layer and Cu filling.

ED process reduced the Cu ions to metal by externally supplied electrons, and the deposition features can be controlled by current, potential, organic additives, or deposition mode like direct, pulse, or pulse-reverse deposition.[44-47] There has been many attempts and reports to

get void-free filling. However, it always needs the seed layer, the electron pathway.

ELD is another wet process which can get electrons itself by chemical reaction in bath. Films deposited by ELD without organic additives have good step coverage in order that it is applicable to make conformal Cu seed layer. In the presence of organic additives, the bottom-up filling is also possible even on seedless trench[49]. There are three cases of deposition in the trench; subconformal, conformal, and superconformal as described in Fig. 1.9. When the Cu is forced to deposit intensively at the corner of the top (Fig. 1.9 (a)), further Cu deposition brings out the formation of voids at the center of the trench. If the film is uniformly deposited at all directions, conformal Cu film would be obtained that has the same thickness at the top, side, and the bottom as shown in Fig. 1.9 (b). In other case, there is superconformal deposition that induces the defect-free fillings. It fills the trench from the bottom inhibiting the deposition at the top, so called as bottom-up filling, which is required character in Cu interconnection for excellent reliability and speed. Deposited Cu has the unique feature, the bump, the evidence of defect-free filling (Fig. 1.8 (e)).

C. H. Lee *et al.*, achieved the bottom-up filling on Ta/TaN substrate without Cu seed layer[49]. On Pd catalyst, the trench was filled with simultaneous formation of Cu seed layer. As the width of trench is shrinking to tens of nanometer, formation of diffusion barriers and seed layer were subject to restriction in the thickness. In order to solve those problems, thinner seed layer is required or new barrier materials that do not need seed layer are needed. Formation of

thinner seed layer by conventional method of PVD can lead to some discontinuity, which can be easily complemented through the repairing by Cu ELD.[49] Developed new barrier materials, such as Ru or Co alloys, can act as catalytic layers in ED and ELD so that direct Cu filling is possible.[50-54] Therefore, ELD is concerned as a promising process in next generation to solve the significant problems of voids or seams and thickness limitations. In addition, the role of organic additives has a momentous importance to obtain desirable profile of Cu deposits.

In addition to trench filling, the importance of the formation of through silicon vias (TSVs) for high-density 3-D integration of chips has been reported in numerous literature.[55-57] There are two types of vias on the basis of the preparation process, the Bosch and the non-Bosch vias.[58-59] As the TSV is similar to submicron scale Damascene Cu in structure, it has been regarded as an extension of Cu superfilling. To achieve an efficient and defect-free Cu filling, it is important to control the continuity and conformality of the Cu seed layer, which functions as a conductive path of electrons for electrodeposition (ED).[60]

In general, physical vapor deposition (PVD) is used for seed layer formation. However, there are several problems in applying this to the TSVs. As the flux of Cu atoms traveling to the bottom is decreased in micro-scale of deep and high aspect ratio of via, it reduced the Cu deposits at the sidewall and the bottom. To improve the film continuity, ionized metal plasma (IMP) or hollow cathode magnetron (HCM) methods that enhance the directionality and controllability of the metal ions have been adopted to the collimated sputtering system of

PVD.[58,61-62]

Especially in the non-Bosch via, to overcome structural disadvantages such as the overhang that causes severe discontinuity of films by interrupting the flux of the Cu atoms headed into the hole, additional etching of the overhang and sidewalls or wider and tilted openings were suggested.[63-64] Despite these efforts, there is still a possibility of voids getting trapped near the bottom after ED because of the discontinuity of the seed layer.

Owing to its excellent step coverage, the electroless deposition (ELD) has a high potential for application in forming the seed layer as explained.[62] However, there have been no considerations about the geometry effect of the via on the catalyzing. There is difficulty in managing the electrolyte flow inside a deep via or trench because relatively slow flow makes it difficult to transport the reactants through the via.[65-67] On that account, there have been many efforts to enhance the mass transfer by agitation, acoustic streaming, or buoyancy-driven convection.[68-70]

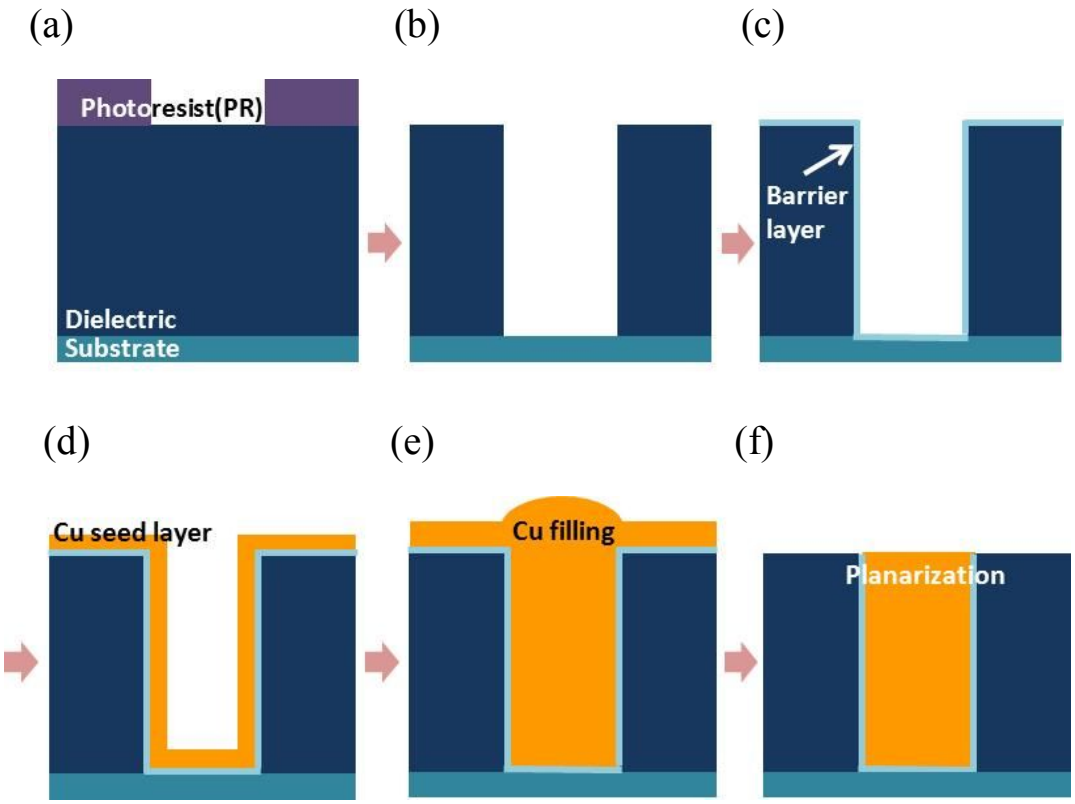

Fig. 1.8. Damascene process in USLI metallization; (a) and (b) patterning by PR coating and etching, (c) barrier layer deposition, (d) Cu seed layer deposition, (e) Cu filling, (f) planarization by CMP.

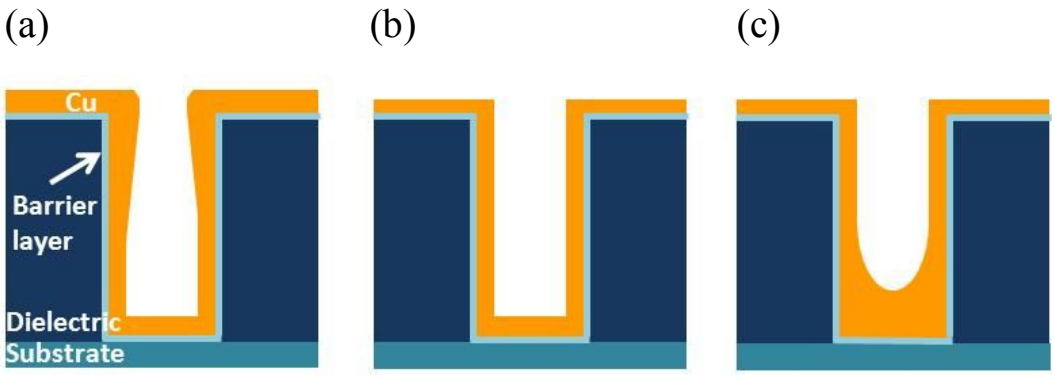

Fig. 1.9. Profiles of Cu deposits in trench; (a) sub-conformal, (b) conformal, and superconformal deposition.

2-2. Organic additives

It is important to figure out the role of organic additives in Cu ELD according to their purposes. In ELD, they can be classified into three types with their usages; stabilizer, suppressor, and accelerator, and the representative additives are listed in Table 1.2 and Table 2.3. The solutions for Cu ELD have inherent problem of decomposition toward homogeneous metallic neucleation since they contain both reductant and oxidant. Those problems can be solved by controlling the pH of solution or the bath composition such as types and concentrations of complexing agent and reducing agent. Complexing agent that minimizes the freely existent Cu ions or reducing agent that has suitable reactivity should be selected. In addition, the adoption of stabilizer is one of the methods to control the stability and the reactivity of bath. 2,2'-dipyridyl, thiourea (TU) and 2-mercaptobenzothiazole are commonly used as stabilizers, which competitively adsorb on the active site to avert from the adsorption of reducing agent or make strong complex with Cu (I), intermediate state.[72-73] Those can also act like suppressors, thereby concentration control is necessary.

The adoption of suppressor and accelerator is material to realize the desirable deposits of bottom-up filling or pillar-to-pillar bonding as introduced in previous chapter. Fig. 1.10 indicates the schematic diagram of bottom-up filling in the presence of both accelerator and suppressor. Accelerator promotes the deposition rate, which has disulfide bonds (-S-S-) or

mercapto group (-S-H). Although there is lack of study on the exact mechanism of acceleration in Cu ELD, the mechanism is usually explained with referring to Cu ED. Accelerator facilitates speeding up by expediting the rate determining reaction that Cu (II) reduces to Cu (I), that is, delocalized π-electron bond eases the reduction by breakage of Cu-complex.[74-75] However, when the high concentration of accelerator is added, additives function as a suppressor. It is because large amount of additives on the surface shield the adsorption of reducing agent by strong adsorption of additives and their dimer or byproducts. For this reason, many of accelerator acts both as an accelerator and a suppressor, and their roles are rely on the concentration. Those additives can be solely used as an application in trench and TSV filling. C. H. Lee *et al*. reported that the bottom-up filling of the sub-microscale of trenches using bis-(3-sulfopropyl)-disulfide (SPS), 3-N,N-dimethylaminodithiocarba moyl-1-propanesulfonic acid (DPS), or 2-Mercapto-5-benzimidazolesulfonic acid sodium salt dihydrate (MBIS).[48,74-76] Zenglin Wang *et al*. achieved the hole filling with only SPS, the suppressor.[77-78] The concentration gradient happened between the top and the bottom along the trench or hole by difference in diffusion flux, which makes high concentration of additive at the top and relatively low concentration at the bottom. Therefore, Cu deposition inhibited at the top whereas more Cu deposits with high deposition rate can be obtained at the bottom.

Poly(ethylene glycol) (PEG) and its derivatives such as poly ether (PE) or poly(ethylene glycol)-poly(propylene glycol) (PEG-PPG) block copolymer are the representative suppressor

both in ELD and ED.[79-81] It is known that, in Cu ELD, it retards the deposition rate by means of prevention of the adsorption of active materials, especially the reducing agent.[79] Its adsorption and inhibition strength are dependent on the molecular weight.[80] Like polymeric suppressor, mercapto alkyl carboxylic acid (MACA) such as 3-mercapto-propinonic acid, 11-mercapto-undercanoic acid, and 16-mercapto-hexadecanoic acid (16-MHA) can efficiently impede the deposition.[82] In addition, there are many researches of application in Cu filling using only suppressor. Madoka Hasegawa *et al.* adopted PEG and Zhifeng Yang *et al.* used PEG-PPG tri copolymer to achieve the void-free filling.[83-84] Bottom-up filling can be obtained by the concentration difference of suppressor between top and the bottom so that the deposition is rarely interfered at the bottom whereas it shows powerful inhibition at the top. Smaller diffusion coefficient with long chain leads stronger inhibition. In addition, the combination of accelerators and suppressors is one of the Cu filling method to make synergetic effect, which results in the acceleration at the bottom and the effective inhibition at the trench opening. For instance, combinations of SPS-PEG, TU-guanidine hydrochloride, 2-mercaptobenzothiazole (2-MBT)-PE 3650, and Janus Green B-triblock copolymer PEP-3100 are investigated.[81, 85-87]

Table 1.2. Representative Organic Additives in Cu ELD

Organic additives	**Structure**	**Molecular weight (g/mol)**
2,2'-dipyridyl	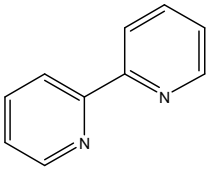	156.18
Thiourea (TU)	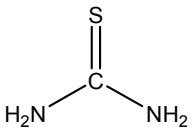	76.12
Bis-(3-sulfopropyl)-disulfide disodium salt (SPS)	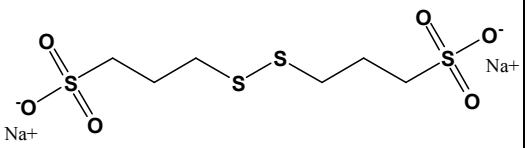	354.40
Poly(ethylene glycol) (PEG)	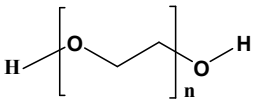	Variable depends on n

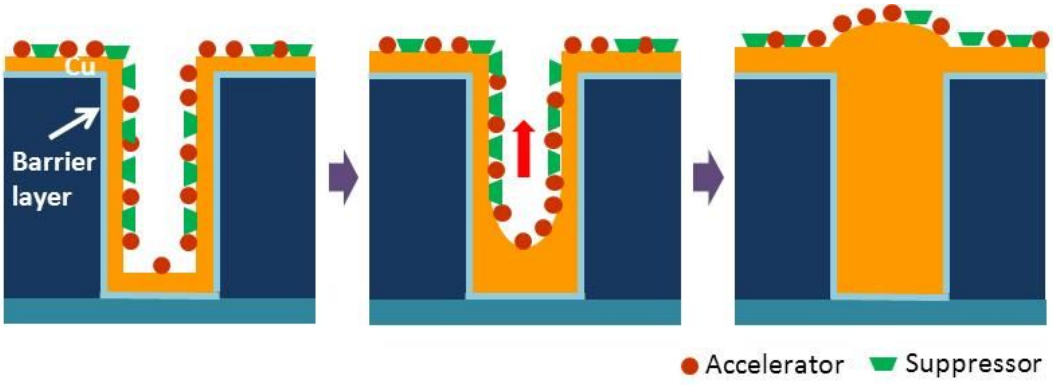

Fig. 1.10. Schematic diagram of bottom-up filling process with accelerator and suppressor.

1-6. Evaluation of Cu ELD solution

ELD solution is basically composed of metal sources, complexing agents that stabilize the solution by chelation with metal ions, reducing agents that supply electrons to reduce the metal ions, and pH adjustor. ELD solution contains the reactants so that the nucleation in homogeneous phase according to the kinetic characteristics can cause the inherent instability problem of solution. The control of the stability is usually achieved by changing the bath composition, the addition of the stabilizing agents, and the optimization of the plating condition such as temperature and agitation, or a continuous circulation and filtration of bath during the operation. However, those trials usually accompany the retarded reactivity. For practical applications, the deposition rate should be high enough, which means that the balance between stability and reactivity is essential for the formulation of the bath composition. Accordingly, the evaluation of solution nature is important with easy and accurate tool.

The tools for monitoring of the solution performance have been investigated for decades. Generally, stability, the endurance time that maintains its stability without homogeneous reaction, was monitored by naked-eyes[88]. Recently, F. Inoue *et al*. reported the control method of bath stability by combination of UV-VIS spectroscopy, pH and mixed potential measurement that represents the Cu-EDTA complex properties.[89] Especially, adjusting of pH induced the formation of void-free Cu seed layer. In the aspect of reactivity, many researches to evaluate the

reactivity have been extensively studied. Monitoring methods can be classified into *ex-situ* and *in-situ* based on the point of time to analyze. *Ex-situ* methods can involve scanning electron microscopy (SEM)[90], atomic force microscopy (AFM)[91], gravimetric techniques[89], or oxidative stripping[91]. Most conventional *ex-situ* method is SEM analysis of deposited film on substrate. After the thickness of deposited film is measured, deposition rate can be calculated by dividing with the deposition time. The surface morphology that features roughness or aggregates from SEM images gives information about reactivity as well. AFM imaging is also applicable to measuring the thickness by the difference of height between as-prepared and deposited substrate. Gravimetric techniques that provide the gained weight of metal deposits and oxidative stripping of deposited film can make the estimation of reactivity. However, these methods are some limitations. Deposited samples should be destructed and much time consumes because preparation experiments are essential. Their experiments always need the substrate to deposit.

In contrast, *in-situ* methods can continuously keep track on the status of solution during the reactions. Many electrochemical analyses have been applied to evaluate the solution performance such as linear sweep voltammetry (LSV)[92-93], cyclic voltammetry (CV)[92], open circuit potential (OCP)[94] or electrochemical quartz crystal microgravimetry (EQCM)[95-96]. In LSV and CV analyses, the most conventional *in-situ* methods, reactivity can be evaluated by measurement of cathodic or anodic current with half-cell reaction. Observation of the cathodic or anodic potentials also suggests the thermodynamic favors. Meanwhile, electrochemical

analyses have limitations, for example they cannot reflect the real reaction environment and there are lots of reports about the contradictory results between half-cell reaction and actual electroless deposition. Monitoring of OCP changes also gives the data to figure out the progress of reaction without the effects of overpotential on the electrode. Although EQCM is similar in the viewpoint of analysis of deposits, it can represent the weight of deposits in real-time. Recently, the verification of Cu ELD mechanism was reported by the combination of OCP and QCM measurements focusing on the adsorption of chemicals in Cu ELD solution.[r] However, in current status, there is restriction regarding the substrate materials. Cu is served as the substrate in the majority of cases, though Pd is common catalyst in Cu ELD. Therefore, the characterization of reaction behavior on Pd is insufficient.

In this study, powerful *in-situ* monitoring method was proposed using relationship between laser transmittance and its scattering according to the solution state. In following chapter III, it will cover the introduction of in situ transmittance measurement and the characterization of Cu ELD solutions. First chapter 3.1 will describe the construction of equipment for *in-situ* transmittance measurement. In chapter 3.2 ~ 3.5, it will deal with the comprehension of transmittance curve with reference Cu ELD solution. In addition, it will be done to examine the effects of components, such as complexing agent, reducing agent, and organic additives, with respect to the stability and the reactivity of solution. As one of the application, the changes in properties of Cu film with organic additives with transmittance measurement results are

introduced in chapter IV. Furthermore, chapter V addresses the application of CU ELD on seed layer formation for TSV filling as a second application.

CHAPTER II

Experimental

2-1. *in-situ* transmittance measurement

The *in-situ* monitoring of the relative transmittance was performed by a home-made transmittance analysis system. This system was constructed with He-Ne laser (632. 8 nm), photodiodes, a beam splitter, and a temperature-control system as described in Fig. 3.1.

All of the experiments were carried out in a glass vial, loaded into an alumina holder, and the temperature of the solution was maintained at 70℃ by the circulation of heated water through the inside of the aluminum holder connected to the thermostat. The temperature of the solution was stabilized to 70℃ from room temperature within 300 sec. In addition, pH of solution was adjusted to 13.0 by KOH.[97] All of the transmittance measurements were recalculated based on the fixed intensity of deionized water to be unity. The intensity of transmittance could be decreased because the natural color of Cu ions in aqueous solution easily absorbs the incident laser of 632.8 nm wavelength. Some additives were necessary to monitor the growth procedures of Cu particles in each step by ceasing further growth of Cu on the particles. The mixture of 3-amino-1,2,4-triazole and 1-decanethiol was adopted as a stopping

agent, which prevented further growth of particles and also inhibited the agglomeration between particles by adsorption on the Cu surface. Stopping agents should not affect to the intrinsic transmittance value. For example, when stopping agents were injected as soon as the transmittance was significantly decreased, there was no change in transmittance value as shown in Fig. 2.1. It meant that the Cu ELD was surely inhibited by stopping agent. Once the stopping-additives were injected during the reaction, Cu particles were sampled in 20 sec after the injection, then rinsed, and put on bare wafer for further analysis, in sequence.

SnPd colloid solution was concocted by mixing and dilution of Sn solution (0.04 M $SnCl_2$ + 0.67 M HCl) and Pd solution (0.56 mM $PdCl_2$ + 0.03 M HCl) to provide the active sites for Cu reduction with the Pd catalysts $4.5 \times 10^{10}/cm^2$(the number of Pd catalyst in square centimeter) population which has standard deviation about 10 % was obtained on Ta substrate.[97] The density of Pd catalyst was derived from the SEM images after Pd activation. Data capture of the surface images, counting the number of Pd particles in defined area, and recalculation based on square centimeter were carried out in sequence. This process was repeated three times and average value was presented.

Cu ELD solution consists of four elements; Cu source, pH adjustor, reducing agent, and complexing agent. Each solutions contained basically 0.025 M $CuSO_4 \cdot 5H_2O$, 0.481 M potassium hydroxide (KOH) and complexing agents and reducing agents. In case, some organic additives could be added to solutions. In this study, various kinds of complexing agents,

reducing agents, and organic additives were measured. Five complexing agents were selected as follows; KNa tartrate tetrahydrate, triethanolamine (TEA), ethylenediaminetetraacetic acid (EDTA), hydroxyethyl ethlenediamine-N,N',N'-triacetic acid (HEDTA), and trans-1,2-Diaminocyclohexane-N,N,N′,N′-tetraacetic acid monohydrate (CDTA). The former three kinds of complexing agent are commonly used in ELD, while the latter two have a little different structure with EDTA. The detail properties are listed in Table 2.1. The concentration of complexing agents were used from 0.054 M to 0.162 M. As reducing agents, 0.097 M paraformaldehyde ($(HCHO)_n$), 0.033 M glyoxylic acid, 0.033 M hydrazine (NH_2NH_2), and 0.065 M DMAB were checked as shown in Table 2.2. Especially, in the case of hydrazine, each components of solution were diluted by 1/7 based on HCHO solution. When the DMAB-based solution was prepared, 0.045 M 4, 5, 8, 12-tetraazadodecane (2,3,2-tet) and 0.3 M triethanolamine (TEA) were used. In addition, organic additives that were usually adopted in Cu ELD were examined. PEG having different molecular weight from 1500 to 10000 and SPS, DPS, MBIS as described in Table 2.3 were evaluated. To determine the *in-situ* transmittance behavior, the ELD solution was chosen with 0.054 M of EDTA and 0.097 M $(HCHO)_n$ which had an approximately 0.3 nm/sec deposition rate at 70℃.[97] The size and the surface morphology of Cu particles and thickness of Cu film were characterized by field emission scanning electron microscopy FESEM, HITACH S-4800). For analysis of crystallinity, X-ray diffractometer (XRD) was used. (Bruker, New D8 advance).

Table 2.1 Various Kinds of Complexing Agents and Their Properties

Complexing agent	**Structure**	**Formation constant (pK_f)**	**Monohydroxy complex (%)**
KNa tartrate tetrahydrate	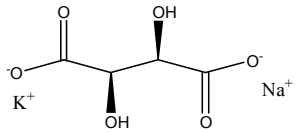	3.9	-
Triethanolamine (TEA)	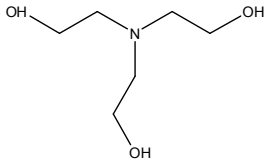	3.2	-
Ethylenediaminetetra acetic acid (EDTA)	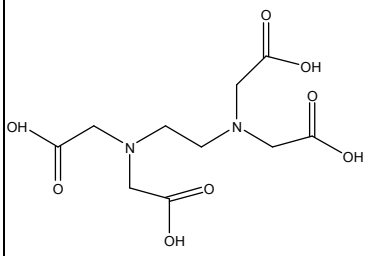	21.1	65
Hydroxyethylethlene diamine-N,N',N'-triacetic acid (HEDTA)	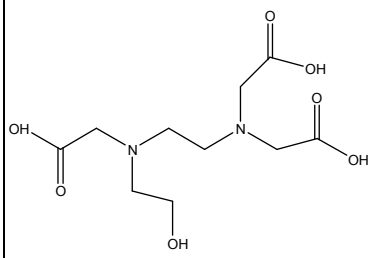	19.7	31
Trans-1,2-Diaminocyclohexane-N,N,N',N'-tetraacetic acid monohydrate (CDTA)	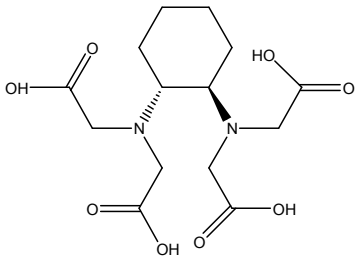	23.2	65

Table 2.2 Various Kinds of Reducing Agents

Reducing agents	**Structure**
Paraformaldehyde ($(HCHO)_n$)	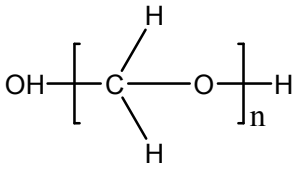
Glyoxylic acid	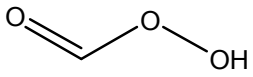
Hydrazine (NH_2NH_2)	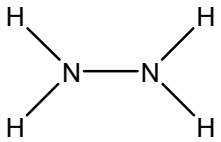
Dimethylaminoborane (DMAB)	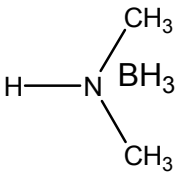

Table 2.3 Various Kinds of Organic Additives

Organic additives	**Structure**	**Molecular weight (g/mol)**
Poly(ethylene glycol) (PEG)	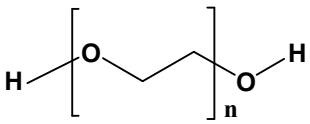	1500, 8000, 20000, 100000
Bis-(3-sulfopropyl)-disulfide disodium salt (SPS)	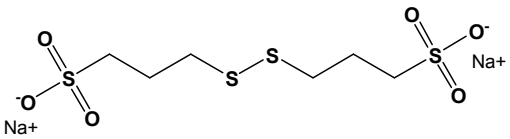	354.40
3-N,N-dimethylaminodithiocarbamoyl-1-propanesulfonic acid (DPS)	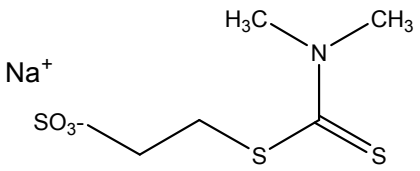	264.43
2-Mercapto-5-benzimidazolesulfonic acid sodium salt dihydrate (MBIS)	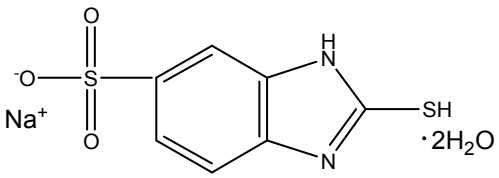	252.52

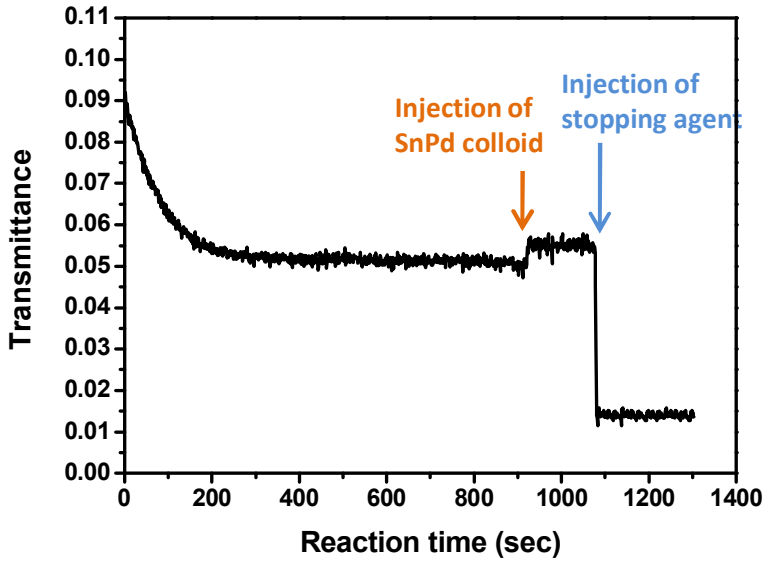

Fig. 2.1. Effect of stopping agent on the reaction of Cu ELD and transmittance value.

2-2. Cu film deposition

Cu ELD was performed on substrate to make Cu film and prove the validity of *in-situ* transmittance measurement on the evaluations of stability and reactivity of various Cu solutions. Also, Cu film was deposited to characterize the film properties according to the organic additives.

Basically, all experiments were carried out with the exact same conditions in *in-situ* transmittance measurements except using the Ta substrate. Substrate has a structure of three layers including barrier layers; Ta (15 nm) by PVD and TaN (15 nm) by PVD on Si. There needs several pretreatment steps before Cu ELD. As a removal of native oxide on Ta, each substrate was treated with 0.57 M HF and 0.31M HNO_3 for 10 min. On cleaned surface, Pd catalysts were prepared by two step activation composed of Sn sensitization and Pd activation. Sn sensitization was conducted for 2 min with 0.04 M $SnCl_2$ and 0.67M HCl, and Pd activation for 20 sec was performed with 0.56 mM $PdCl_2$ and 0.03 M HCl. Subsequently, Cu ELD was carried out at 70℃ with various complexing agents, and reducing agents as listed in Table 2.1~2. In case, organic additives such as SPS, DPS, MBIS, PEG (Mw 1500, 8000, 20000, 100000) were added described in Table 2.3.

Each deposition rate was calculated by dividing the thickness of Cu film with the deposition time, 30 sec. Based on the calculated deposition rate, the thickness of Cu was controlled to be

constant to investigate the properties. The film thickness and surface morphology of Cu were analyzed checked by field emission scanning electron microscopy FESEM, HITACH S-4800). Surface roughness of film was measured by atomic force spectroscopy (AFM, Agilent 5100). Crystallinity of film was analyzed by X-ray diffractometer (XRD, Bruker, New D8 advance).

2-3. Seed layer formation in through silicon vias (TSVs)

A non-Bosch TSV with 5 μm diameter, 50 μm depth, and tapered to 96° at the bottom was made using the reactive ion etching (RIE). The overhang existed at a point 10% from the top. A 30 nm Ta layer was deposited by PVD onto a 15 nm Si_3N_4 by atomic layer deposition (ALD). The profile of the Cu seed layer was inspected by observing both the sidewalls and the cross-sectional morphology as shown in Fig. 2.2. Each coupon wafer was dipped in a solution of 0.57 M HF and 0.31M HNO_3 to remove the Ta native oxide. After this, Sn sensitization with 0.04 M $SnCl_2$ and 0.67M HCl and Pd activation with 0.56 mM $PdCl_2$ and 0.03 M HCl were sequentially performed. Cu ELD was carried out at 70°C with solution containing 0.025 M $CuSO_4 \cdot 5H_2O$, 0.054 M ethylenediaminetetraacetic acid (EDTA), 0.481 M KOH, and 0.097 M HCHO (pH = 12.9)[31,97] with 0.64 mM 2,2′-dipyridyl and 1.0 ml/L solution of 3% diluted RE-610 (RHODAFAC®) as additives. In part of this study, a homemade Teflon® holder was introduced as the rotation system described in Fig. 2.3.

After the formation of the seed layer, ED was performed with an electrolyte composed of 0.25 M $CuSO_4$, 1.0 M H_2SO_4, 88 μM poly(ethylene glycol) (PEG; MW 3400), 1 mM Cl^-, 5 μM bis(3-sulfopropyl) disulfide (SPS), and 20 μM Janus Green B (JGB). Cu filling was done using the pulse reverse ED for 2 h with 4.2 mA/cm^2 average current density.

The cross section and surface of the seed layer were analyzed using field emission scanning electron microscopy (FESEM; HITACHI, S4800). The cross section of the Cu-filled TSV was observed using the focused ion beam (FIB; SII NanoTechnology Inc., SMI3050SE) technique.

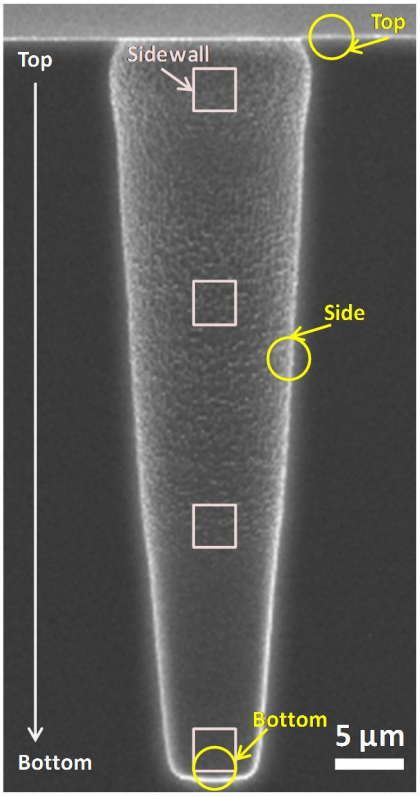

Fig. 2.2. Profile of as-prepared non-Bosch via and denoted positions for analysis.

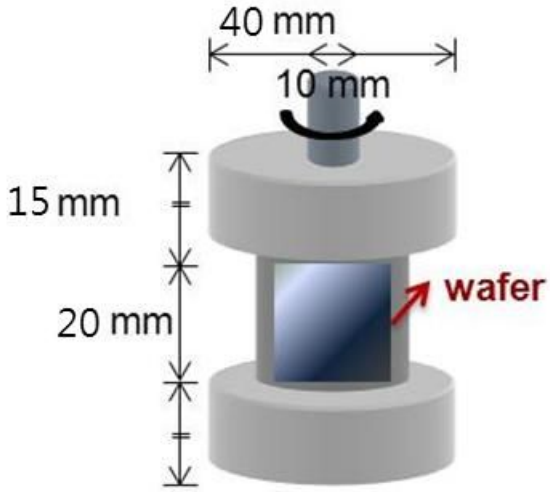

Fig. 2.3. Schematic diagram of Homemade Teflon holder.

CHAPTER III

in-situ transmittance measurement in Cu ELD

3-1. Equipment of *in-situ* transmittance measurement

The equipment was fabricated to measure the scattering level of solution with recording the transmittance changes. It made it possible to monitor the formation of particles in the solution with real-time. Fig. 3.1 (a) illustrates the schematic diagram of equipment. It was organized with two parts. First part is related to the monitoring of the chemical reaction with four subparts of ⓐ~ⓓ, He-Ne laser (melles Griot, 05-LLR-811-230), cube beam splitter (UniNanoTech Co., Ltd., 15mmx15mmx15mm), alumina holder, and photodiode. Second part is associated with data processing of obtained signals from first part, consisting of amplifying circuit, data acquisition (DAQ) board (National instruments, USB type, Part No 194710D04L), and LabVIEW™ program in PC.

He-Ne laser beam with 632.8 nm wavelength was split by a cube beam splitter, and two beams indicating transmittance were detected by photodiodes. One of the beams that passed through the solution reflected the state of solution. The other one that was directly detected meant the signal of original beam. One thing noticeable is the control of light intensity from two diodes. He-Ne laser used in this study has unstable and weak output intensity. To overcome

these, variable resistances (10kohm) and operational amplifiers (LM741) were connected to the lines from two photodiodes in amplifying circuit. Schematic diagram of photocurrent amplifier using an operational amplifier (op amp) was shown in Fig. 3 (b), in which AC-DC converter was used for power supply (POWER PLASA, FSD10-1515). It also led the low noise level, the weak dark current, and hundreds of thousands times higher output voltages which is linear to the light intensities. Converted and amplified voltage signal could be adjustable with the regulation of variable resistance (R_1), thereby it complemented unsteady intensities for secured measurement.

Solution was contained in temperature-controllable aluminum holder, inside which particles could be formed by homogeneous or heterogeneous reaction according to the solution characteristics. Formation of particles over the wavelength of irradiated laser resulted in the significant scattering, thereby the intensity loss occurred. The photodiodes perceived the light intensity and converted it to the electrical signal via op amp, in such signal was transferred to computer via DAQ board which is the convertor from the analog to digital. Finally, LabVIEW™ facilitated the data processing including filtering and calculating the relative transmittance. Final values were presented by graph according to the time in monitor and saved to text file with the extensions “txt”. Finally, the relative transmittance (ratio of solution signal to reference signal) was recorded on-time during the reaction through LabVIEW™.

(a)

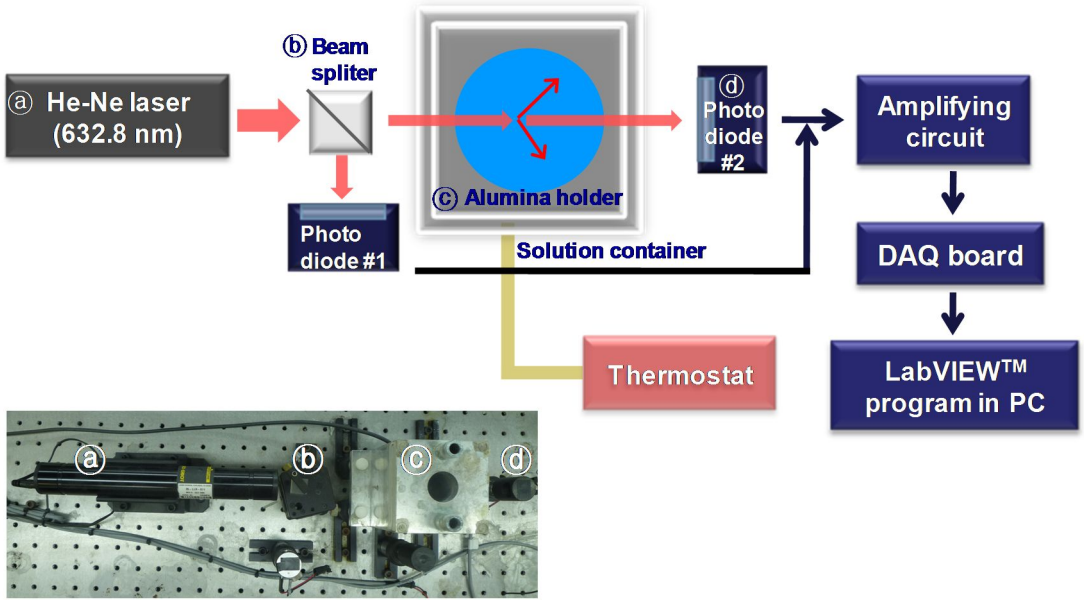

(b)

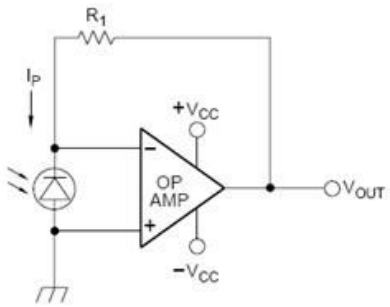

Fig. 3.1. (a) Schematic diagram of equipment for *in- situ* transmittance measurement, and (b) Photocurrent amplifier without bias.

3-2. Basic understanding of transmittance curve

The reactivity of the electroless deposition solution induces the formation of small nuclei in the solution that may grow further to the larger particles. The intensity of the laser through the ELD solution could be attenuated by three cases: 1) absorption by the chemical components of Cu source and a complexing agent by UV-VIS absorption, 2) scattering by small nuclei formed in the solution (smaller than wavelength), and 3) blocking of the beam pathway by larger particles. The absorbance of the UV-VIS spectroscopy of the Cu electroless plating solution including EDTA was shown in Fig.3.2 (a). At the wavelength of 632.8 nm, its absorbance by the electrolyte itself was found to be considerable. Once the temperature of solution was maintained to 70℃ there was no significant change in the absorbance throughout the process as shown in Fig. 3.2 (b). That shows that the transmittance of reference solution decreased to 0.05 by UV-VIS absorption, and maintained its value. The scattering of the light due to the small size particles suspended in a solution could be interpreted by Mie scattering[98]. However, scattering by the particles was ignored because its portion was too small compared to the laser passed through the solution. The most important factor was blocking by the cluster of large particles, which were comparable in size with the wavelength. The formation of Cu particles by homogeneous reduction onto SnPd colloids led to the catalytically active Cu particles in the solution, and they could precede continuous growth, turning the solution opaque until the

precipitation. At this stage, the size of the agglomerated particle (a secondary particle) clusters usually exceeds the wavelength of the laser, and the transmittance showed stiff declining. Therefore, the final intensity of the light would be just the function of free cross-section where the clusters did not block the beam path.

The transmittance of the reference solution based on $CuSO_4 \cdot 5H_2O$, KOH, EDTA and HCHO was measured to investigate the behaviors of transmittance change during Cu ELD. Also, growth of Cu particles during reaction was maintained by the addition of the stopping agent at a certain time. Fig. 3.3.(a) represents the change of transmittance as a function of time, which can be clearly divided by five stages in the graph, (A) ~ (E). In stage (A), transmittance gradually decreased as the solution temperature increased to 70℃ owing to the difference of solution absorbance, then steady transmittance was observed in stage (B) with constant value about 0.05. Without the addition of SnPd colloids into the solution, the transmittance value could be sustained for several hours. SnPd colloids that could offer active sites for the initiation of Cu growth were injected into the solution, which initiated stage (C). The SnPd colloids had a diameter of approximately 110 nm, which was confirmed by a particle size analyzer. Slight increase of the transmittance at the moment of injection of the colloids was due to the decoloring of solution in consequence of the increase of solution volume by 5%. Since the addition of HCl solution with same pH to colloidal solution had no effect on the transmittance, the change of the pH of the solution did not play any role in increasing the transmittance at this

stage. It was due to the decoloring of solution in consequence of the increase of solution volume by 5%. From stage (C), both particle growth and agglomeration of Cu occurred by going through the incubation time which generally happens in ELD. As a certain time elapsed, a significant drop of transmittance and severe hydrogen evolution were observed in stage (D). Starting with vigorous initialization of reduction on Pd in the former stage, subsequent growth and agglomeration of Cu particle actively proceeded. In stage (D), the size of Cu particles increased as the reaction progressed, leading to the abrupt decrease of transmittance owing to the active light scattering in the solution. In this stage, particle formation and growth were observed in each step as shown in Fig. 3.3 (b). Particle size was approximately 124 nm which was a similar size with injected SnPd catalyst at the initial stage of reaction, however it became larger about 245 nm in the middle of the reaction as both active growth and agglomeration occurred. As the reaction continued, the particle size reached to 276 nm. Since the deposition rate was found to be a few nm/sec in case the ELD solution was applied to a flat source, the particle sizes at this stage were well matched with time elapsed. Finally, in stage (E), transmittance increased again, resulting from the consumption of Cu ions by the ELD and the precipitation of the reduced particles. After all reactions ceased, the estimated average size of precipitated Cu particles was about 340 nm. However, at this moment the particles coagulated with each other, forming a chain-like structure. As shown in Fig. 3.3 (c), there was little difference in size as compared to that in former stages with consideration of standard deviation,

which denoted that most of the reaction occurred in (C) and (D) stages. As a result, steps of (C) and (D) can be regarded as a reaction determining stage, and the duration of steps (C) and (D) are used in this study to evaluate the reactivity of solution. In other words, reaction time is termed as a length of period summed (C) and (D) steps. The length of (C) and (D)steps means the time until the Cu grown on the SnPd colloids is large enough to be precipitated, and the particle size is not large enough to cause scattering of the laser, the drop of the intensity and the precipitation would be induced by the formation of big clusters of the particles. The probability of the coalescence of the particles to form a complex cluster is a product of the particle density and size. Therefore, it is a function of the deposition rate from each bath, which could be used as a quantitative indicator of the reactivity of the bath. Simply, the degree of stability would come from the time until the transmittance value dropped. Based on these results, the effects of components in Cu ELD solution, such as complexing agents, reducing agents, organic additives, and their concentrations on stability or reactivity were contemplated.

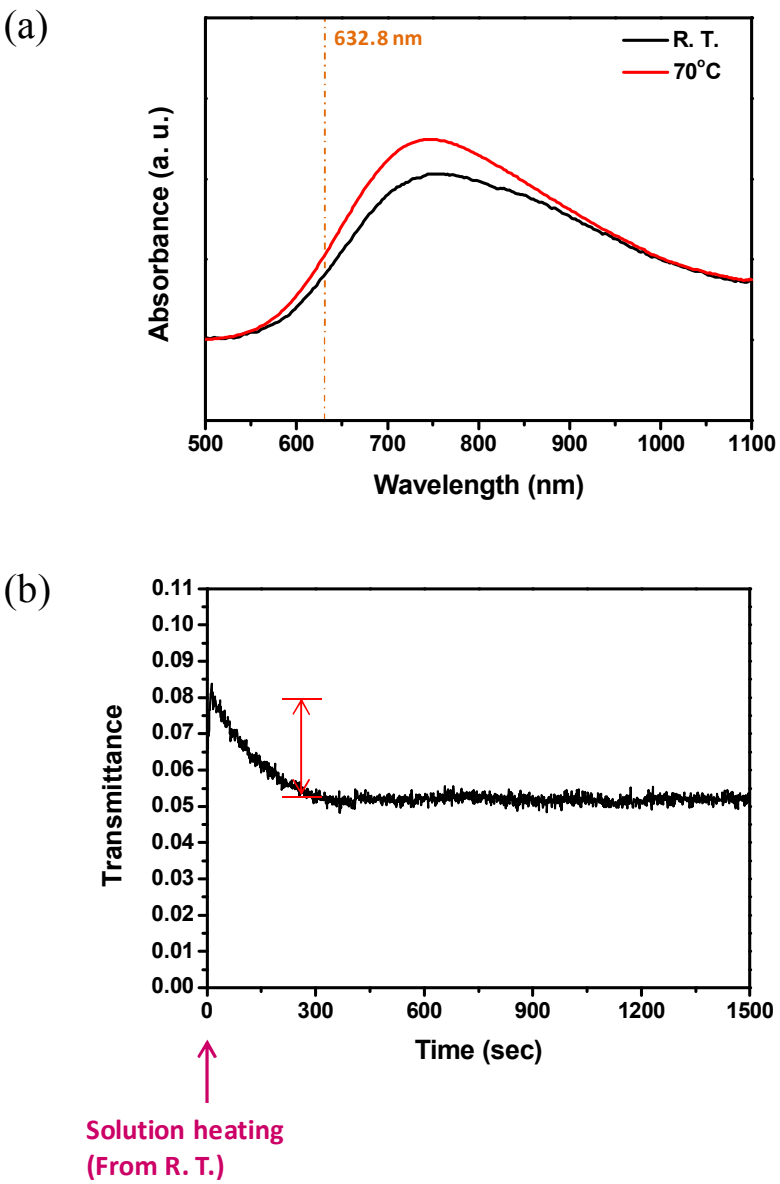

Fig. 3.2. (a) Absorbance change of Cu ELD solution according to the temperature and (b) transmittance change of reference solution with heating.

(a)

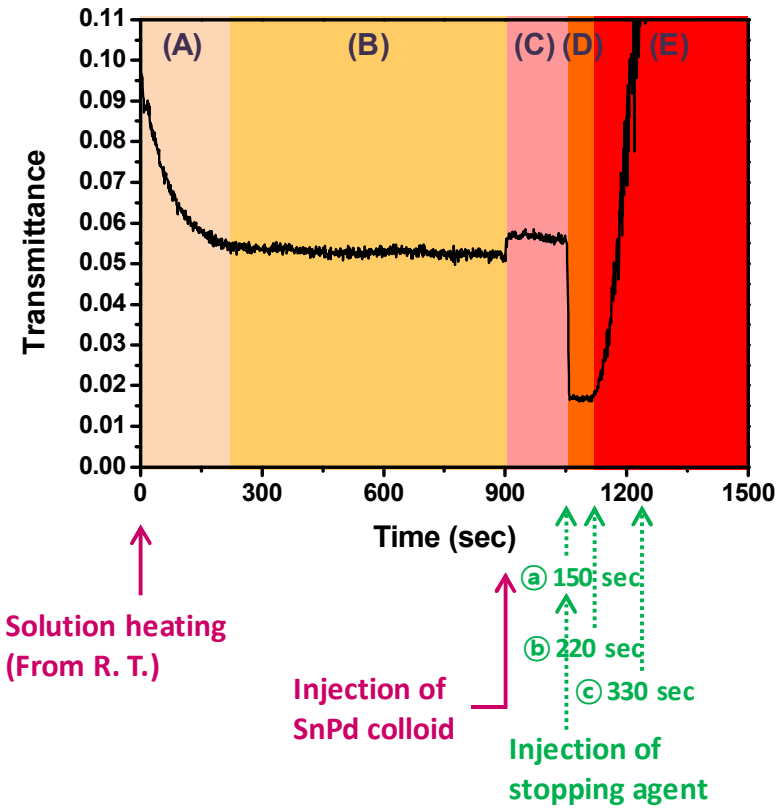
(A)
(B)
(C)
(D)
(E)
Transmittance
0.11
0.10
0.09
0.08
0.07
0.06
0.05
0.04
0.03
0.02
0.01
0.00
0
300
600
900
1200
1500
Time (sec)
Solution heating
(From R. T.)
Injection of
SnPd colloid
ⓐ 150 sec
ⓑ 220 sec
ⓒ 330 sec
Injection of
stopping agent

(b)

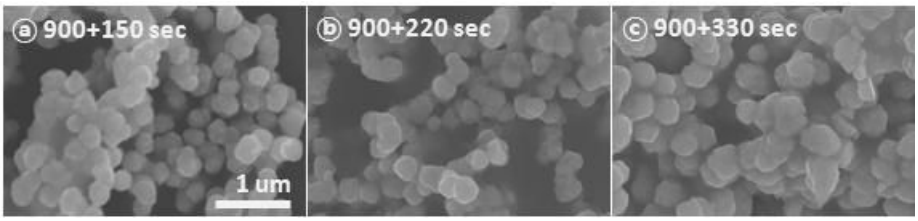
ⓐ 900+150 sec
1 um
ⓑ 900+220 sec
ⓒ 900+330 sec

(c)

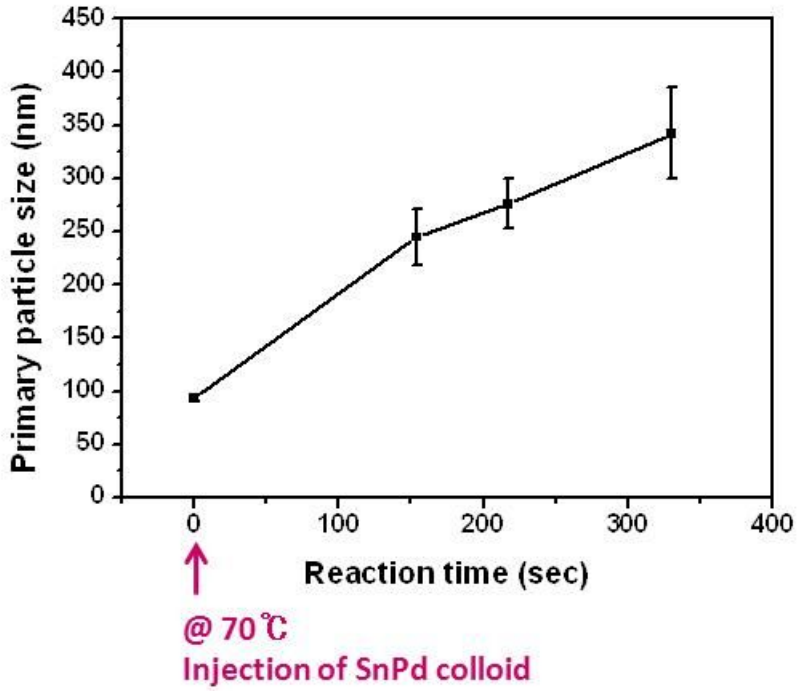

Fig. 3.3. (a) Transmittance changes of solution with injection of SnPd colloid, (b) SEM images of Cu particles at each step after the reaction began, and (c) Cu growth as a function of reaction time.(Each reaction time in green allows of Fig. 3.3 (a) corresponds the times of injection of stopping agents in Fig. 3.3 (b) and (c).)

3-3. Effects of complexing agent

Complexing agents which chelate with Cu ions are key factors that determine the stability and reactivity of the solution. It is meaningful to consider the effect of complexing agents according to types and concentration to control the solution performance because chelating has two influences. The shift of the reduction potential of Cu to negative value causes the decrease in the deposition rate, and improves stability of solution by prevention of Cu oxide, Cu hydroxide, or homogeneously generated Cu metal formation.

Fig. 3.4.shows the results of the stability test with five complexing agents in absence of SnPd colloid injection. Each solution has a different transmittance value at the initial measurement, contributed by the individual color. In KNa tartrate tetrahydrate and TEA cases as appearing in Fig. 3.4. (a) and (b), transmittance were decreased by homogeneous particle formation and finally increased as the consumption of Cu ion and the precipitation of Cu particles even at high concentration of complexing agents. In particular, in the case of TEA, transmittance changed at the initial stage of heating and the stage of particle formation was not observed. Since the TEA-containing solution absorbed more light due to absorbance characteristics, the change of transmittance was shielded. In contrast, stable values of transmittance of the solutions that included HEDTA, EDTA, and CDTA were observed even after the temperature of solutions were adjusted to 70℃ as shown in Fig. 3.4(b).The later three

complexing agents showed excellent stability compared to others at minimum concentration, as expected from their huge formation constants (Table 2.1).

Based on these results, the reactivity test was carried out with stability-confirmed complexing agents of HEDTA, EDTA, and CDTA. As mentioned above, SnPd colloid was injected at 70℃, and variation in the length of the rate determining stage was observed. As depicted in Fig. 3.5, reaction time of the baths decreased in the order of HEDTA, EDTA and CDTA, which meant the reactivity increased in reverse order. As the concentration of HEDTA and EDTA increased, reactivity degraded due to stabilization by the complexing agent. However, CDTA did not show strong dependence on its concentration. In all cases, reaction time was saturated over 0.081 M, 3.2 times larger than the concentration of Cu(II) ion. The length of reaction stages matched with the reverse order of stability constant (pK_f), that may be explained by exertion of intermediate Cu_2O during copper reduction from monohydroxy complexes $CuLOH^{1-n}$ (L: ligand) as described below[96].

$$2CuLOH^{1-n} + e^- \rightarrow Cu_2O + 2L^{-n} + H_2O \quad (3\text{-A})$$

$$Cu_2O + H_2O + 2e^- \rightarrow 2Cu^* + 2OH^- \quad (3\text{-B})$$

$$Cu^* \rightarrow Cu \quad (3\text{-C})$$

$$Cu^* + CuLOH^{1-n} + OH^- \rightarrow Cu_2O + L^{-n} + H_2O \quad (3\text{-C'})$$

From this reaction mechanism, it is clear that reactivity depends on how the homogeneous formation of Cu_2O is effectively suppressed. R. Pauliukaite*et al*., measured the ratio of monohydroxy complexes of some complexing agents (Table 2.1), which showed that the lowest ratio in HEDTA showed retarded reactivity. However, inverse tendency of reaction time in EDTA and CDTA cases was found despite the same ratio of monohydroxy complexes and higher pK_f value of CDTA. It is suggested that kinetic activity due to the complex structure and charge transfer rate on the substrate had more importance in the explanation of the reactivity of the bath according to the complexing agent[96]. As shown in Fig. 3.6, the same order of reactivity was obtained when the complexing agents were applied to Cu ELD on Ta substrate, which confirmed that the measured reactivity from *in-situ* transmittance could be a practical indicator of the solution reactivity.

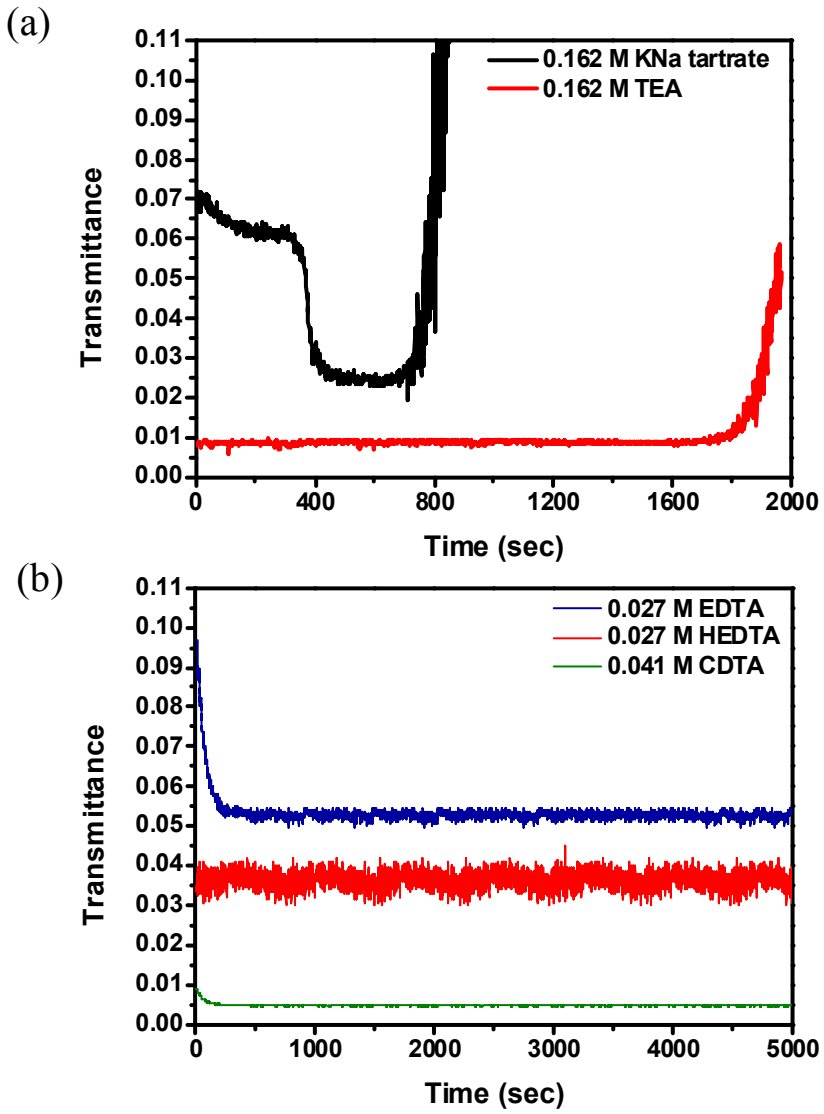

Fig. 3.4. Stability test of Cu ELD solution with (a) KNa tartrate tetrahydrate and TEA, and (b) EDTA,HEDTA, and CDTA as complexing agents.

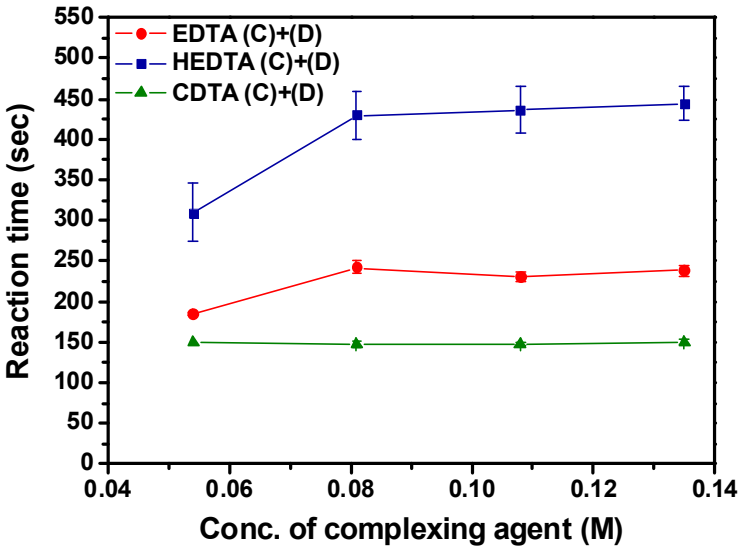

Fig. 3.5. Change of reaction time ((C)+(D)) with various complexing agents as a function of concentrations.

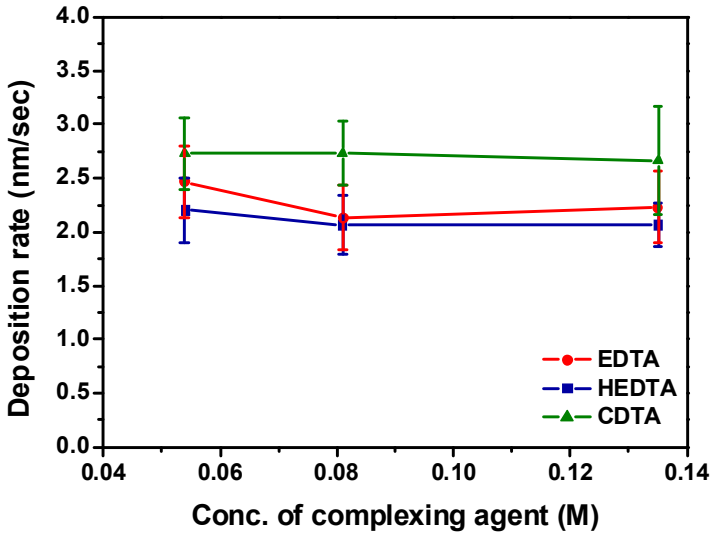

Fig. 3.6. Deposition rate of EDTA, HEDTA and CDTA as a function of concentrations.

3-4. Effects of reducing agent

Reducing agents that generate the electrons by oxidation to reduce the metal have different thermodynamic and kinetic characteristics depending on their types and kinds of catalysts. Along with complexing agents, the selection of reducing agents carries an important meaning to determine the stability and the reactivity of solution. In this chapter, four kinds of reducing agents were examined, formaldehyde, glyoxylic acid, hydrazine, and dimethylamine borane (DMAB). Their detail compositions were described in experimental section. Exceptionally, hydrazine-based solution was composed of low concentration by 1/7 as respect to the Cu ion and EDTA so as to retain the fundamental stability problem caused by the immediate decomposition.

The changes in the stability according to the reducing agents were investigated in the absence of SnPd colloid for 2000 sec, and the solution temperature was elevated from room temperature to 70℃ during the measurement. The transmittance curves are presented in Fig. 3.7. The initial values of transmittance were not identical because of the changes in the temperature as similar to previous results with formaldehyde. Those values soon stabilized and maintained during recording implying no spontaneous formation of precipitate in the solution. Hence, it can be concluded that the stability of these four solutions was confirmed. There was a disparity in the transmittance values at the start points from 0.95 to 0.04, hydrazine, glyoxylic acid,

formaldehyde, and DMAB-based solution, with a descending order. It could be explained by the characteristic colors by Cu-complex as comparison in Fig.3.8. In UV-VIS analysis of solutions, all solutions excluding hydrazine case were diluted by 1/7 to adjust the concentration of Cu ion that makes a big impact on the absorbance. Formaldehyde, glyoxylic acid, and hydrazine-based solution have similar peak position at around 730 because these solutions identically contained EDTA as the complexing agent. In contrast, DMAB-based solution with 2,3,2,-tet as a complexing agent showed a peak absorbance at around 530 nm, indicating the change in the complexing form compared to EDTA cases. It was confirmed that the peak was dominated by the complex with the Cu ions and complexing agents. The important thing to determine the transmittance of solution is the absorbance at 632.8 nm, which is the wavelength of irradiated laser. Given the wavelength marked with orange line in Fig. 3.8 and actual Cu concentrations in each solution, they could be arranged in sequence of absorbance increment; hydrazine, glyoxylic acid, formaldehyde, and DMAB. As a result, the transmittance value was shown with the inverse order of absorbance. Therefore, it was confirmed that this *in-situ* monitoring could measure various solutions with reflection of their characters from Cu-complex.

The reactivity of these solutions was investigated with the injection of SnPd colloids, and the results are displayed in Fig. 3.9. In each case, SnPd colloid was injected at 900 sec when the solution temperature reached to 70℃. As compared to Fig. 3.9 (a) and (b), reducing agents that have aldehyde functional group, formaldehyde and glyoxylic acid, indicated the similar

behaviors of transmittance curve with the accompaniment of the region (A) to (E) as similar to previous results in chapter 3.2. The relation between 1/Reaction time ((C)+(D)) and the deposition rate by film deposition was drawn in Fig. 3.10. It was found that the reactivity of glyoxylic-based solution also could be predicted by the reaction time ((C)+(D)). Comparing the surface morphologies of Cu film and Cu powders shown in Fig 3.11 (a), (b), (d), and (e), there was no noticeable differences. Instead, it seemed that the size of Cu power was strongly related to the reaction rate. For example, the reduction in size of Cu powder prepared in glyoxylic acid-based solution might be ascribed to the slow reaction rate. It will be discussed in following chapter. Meanwhile, the other two reducing agents, hydrazine and DMAB, depicted the different transmittance curves as drawn in Fig. 3.9 (c) and (d). In the case of hydrazine, the trend of transmittance change and the shape of Cu powder shown in Fig. 3.11 (f) were similar to that of the formaldehyde. However, it was hard to distinguish the region like (D) and (E) because of its low reactivity so that the direct estimation of solution was intricate. In the aspect of film deposition with hydrazine, Cu film could not be obtained because Pd catalyst on Ta was apt to be desorbed during deposition. Hence, it was impossible to estimate the solution reactivity by film deposition. Given this limitation, *in-situ* transmittance measurement has the advantage that it can elicit the relative comparison of reactivity without the concerning of Pd detachment on substrate. In terms of DMAB, transmittance value was low about 0.004 at the beginning of the measurement because of significant absorption as described in Fig 3.8. It obscured the

observation of transmittance change even Cu reduction reaction and severe hydrogen evolution happened. After 2000 sec, the increasing transmittance was only observed as the solution became transparent. Therefore, it is difficult to distinguish the regions according to the changes of the solution by reaction. It is expected that the adoption of infrared laser emitting longer wavelength than 700 nm overcomes this limitation and makes accurate analysis, for example, neodymium-doped yttrium aluminum garnet (Nd:YAG), neodymium doped yttrium orthovanadate (Nd:YVO_4), nedodymium doped yttrium lithium fluoride (Nd:YLF), and Ytterbium doped yttrium aluminum garnet (Yb:YAG). Considering the surface morphologies and cross-sectional images of deposits, hedgehog-like morphology of Cu film was observed in Fig. 3.11. (c) and (h). Cu powder morphology shown in Fig. 3.11. (g) also presented the spiky rough surface. Through the measurements with reducing agents, it can be deduced that *in-situ* transmittance measurement is applicable to confirm the stability and predict the reactivity with aldehyde-containing solution. Other reducing agents have limitations to forecast the reactivity. However, it is anticipated that the relative reactivity of solutions made of same reducing agent would be compared based on reference solution, and it have place to improve its detection by equipment modification.

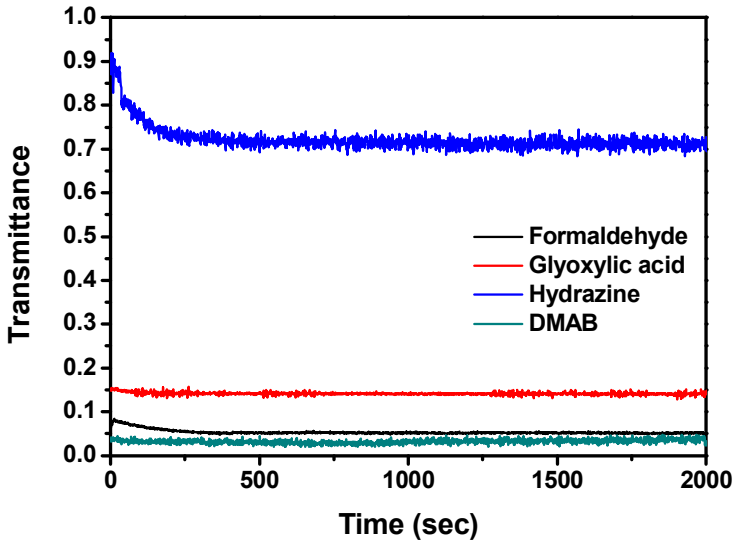

Fig. 3.7. Stability test of Cu ELD solutions consisting of four different reducing agents; formaldehyde, glyoxylic acid, hydrazine, and DMAB without any addition of SnPd colloid.

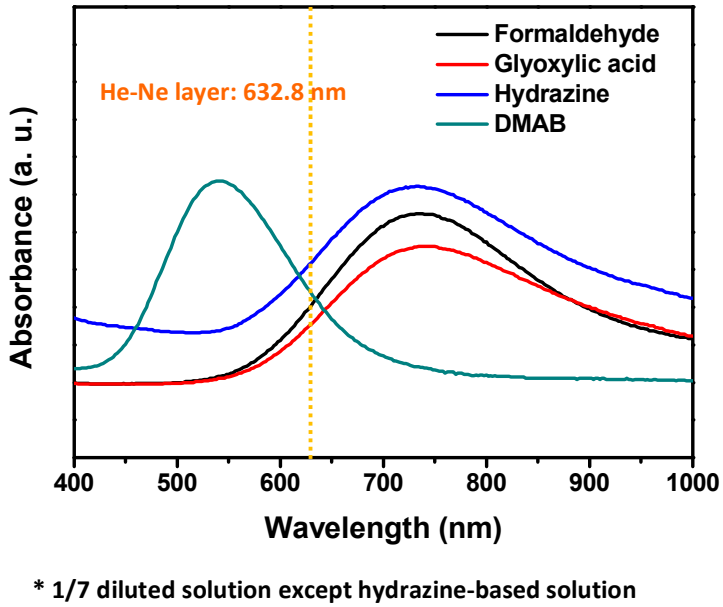

Fig. 3.8. UV-VIS absorbance of Cu ELD solutions according to the reducing agents containing same concentration of Cu-complex.

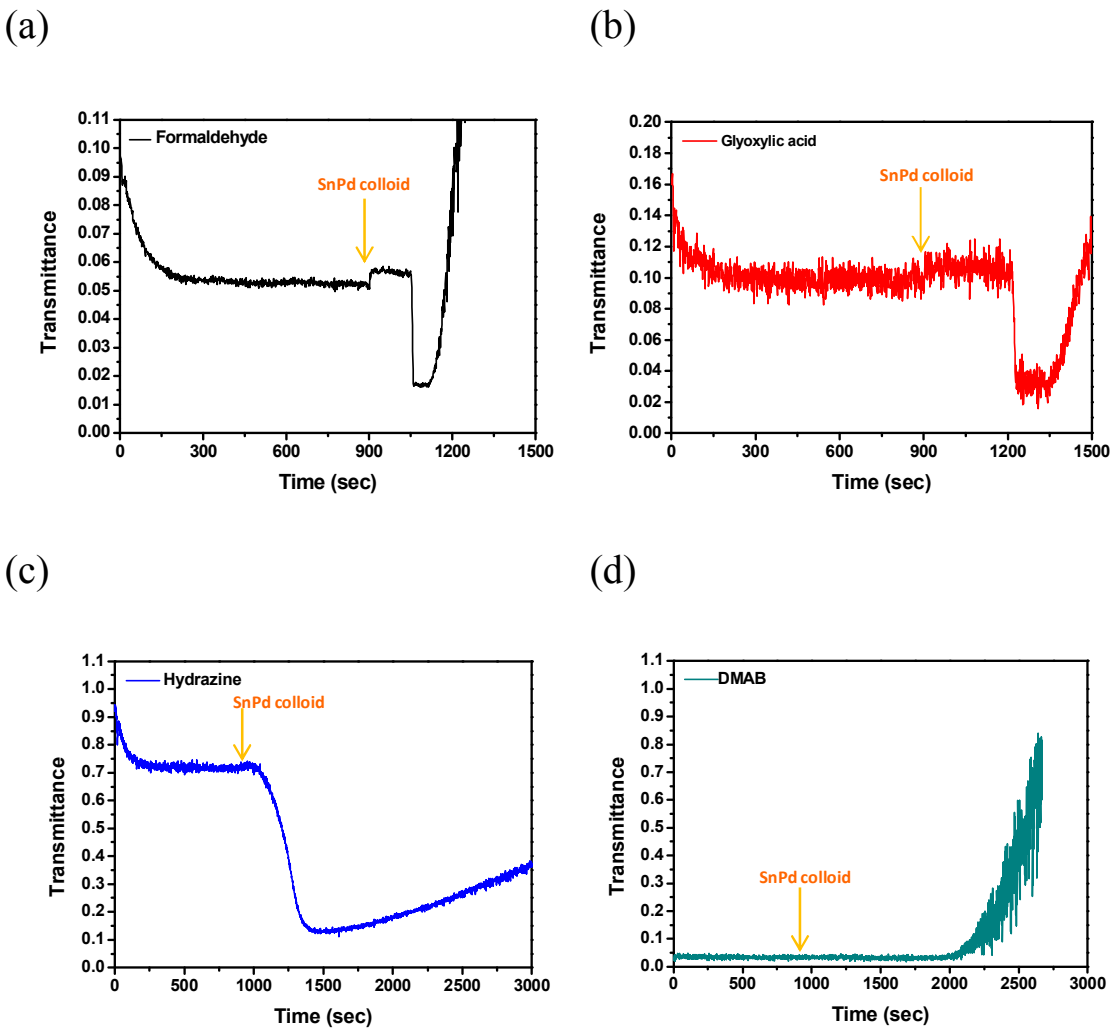

Fig. 3.9. Reactivity test of Cu ELD solutions containing four kinds of reducing agents with injection of SnPd colloid at 900 sec; (a) formaldehyde, (b) glyoxylic acid, (c) hydrazine, and (d) DMAB.

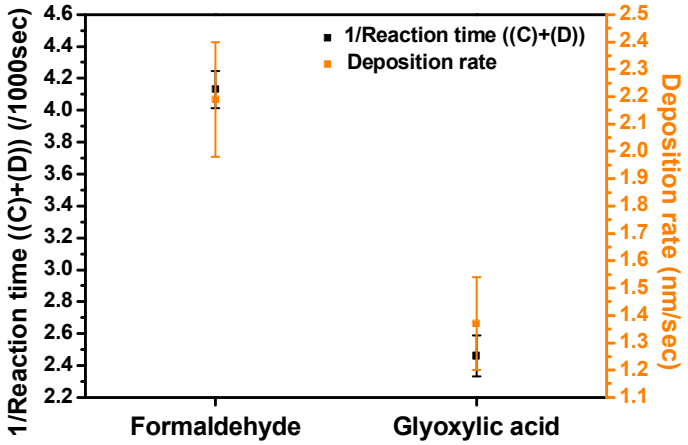

Fig. 3.10. Relation of 1/Reaction time ((C)+(D)) and the deposition rate with reducing agent of formaldehyde and glyoxylic acid.

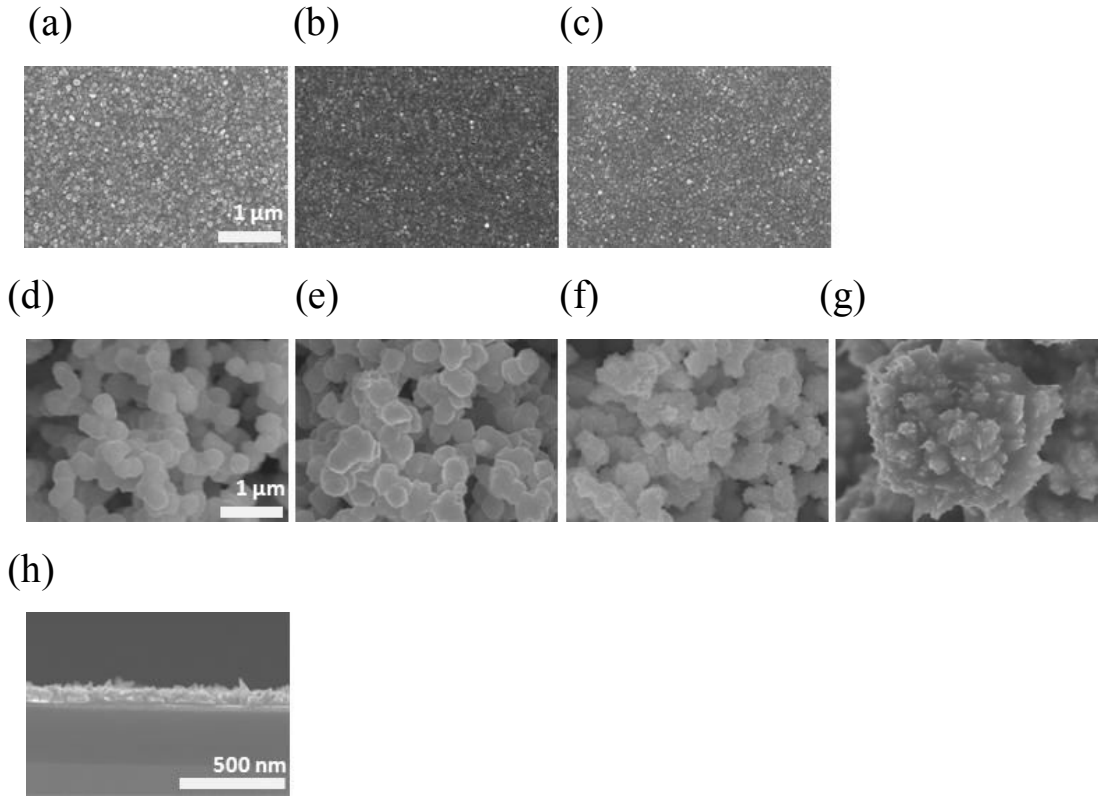

Fig. 3.11. FE-SEM images of surface morphology of Cu film and Cu powder (a) ~ (g); (a) and (d) formaldehyde, (b) and (e) glyoxylic acid, (f) hydrazine, (d) and (g) DMAB, (h) cross-sectional image of Cu film obtained by DMAB-based solution.

CHAPTER IV

Organic additives in Cu ELD

4-1. Effects of organic additives

Organic additives in Cu ELD can be broadly classified into stabilizer, suppressor and accelerator according to their influences on the deposition rate. Among them, the investigation of the suppressors and the accelerators were focused. Generally, sulfur-containing additives such as SPS, DPS, MBIS or polymer additives like PEG are used as described in chapter I. In this study, the characteristics of organic additives affecting to the reactivity and Cu deposits were examined by *in-situ* transmittance measurement and Cu powder.

PEG is generally used as a suppressor in bottom-up filling or an antifoaming agent in thin film formation in Cu ELD, and the changes in the bottom-up performance and the reactivity according to the molecular weight and concentration have been reported. Hence, the effects of PEG having various molecular weights on reactivity were to be clarified with *in-situ* transmittance measurement. At first, the behaviors of PEG-8000 (Mw 8000) were contemplated. Fig. 4.1 presents the relation between the reaction time ((C)+(D)) and the deposition rate in the presence of PEG-8000. The reaction time ((C)+(D)) was measured by *in-situ* measurement and the deposition rate was calculated from the Cu film deposition for 30 sec on Ta substrate. As

higher concentration of PEG-8000 was added, the deposition rate was decreased from 2.19 to 1.61 nm/sec indicating strong suppression, and it was saturated over 0.56 μM. Similarly, the reaction time ((C)+(D)) became prolonged so that its inverse was changed from 0.00413/sec to 0.00237/sec. It was found that the variation of the inverse of reaction time ((C)+(D)) followed the same trends with deposition rate. The changes in size and surface of Cu powder presented in Fig. 4.2 (a) and (b) provided the information on the effects of PEG. Each of size of primary particle was obtained by the assumption that there was an assumption that Cu particles had sphere shape. The diameters of fifty particles in three SEM images captured with 30000 magnifications were measured and calculated the average. The size of primary Cu particles without additives was about 355 nm, however, it became decreased to 265 nm as the concentration of PEG increased to 1.12 μM. Those results could be explained by following reasons. Once SnPd colloid was added, they were apt to be aggregated in solution. However, the adsorption of PEG-8000 prevent the aggregation of SnPd colloid by steric hindrance. It result in the smaller and higher numbers of initial active site of SnPd colloid with compared to additive-free solution. In the aspect of reaction rate, Cu reduction reaction was started on Pd surface with retarded reaction rate because the pre-adsorption of PEG on SnPd colloid impeded the adsorption of formaldehyde, electron supplement reagent, to the active site.[79] Therefore, it was verified Cu particles having small primary particle size was ascribed to the suppression effect of PEG-8000.

In the consideration of the surface of particles, each particle seemed to be experienced agglomeration with smooth surface as the concentration of PEG-8000 increased. It means that the addition of PEG-8000 was contributed to not only the deposition rate but also the characters of Cu growth. During Cu growth, PEG can act as a surfactant with its hydrophilic characteristic, in turn, boundaries between Cu particles were ambiguous and Cu particles grew with smooth surface. As compared to the surface from the Cu film in Fig. 4.3, the surface morphology was changed by the addition of PEG-8000, and boundaries of Cu became blurring with smoothed surface as identical to Cu powder. All these effects were converged over 0.56 μM due to the saturated adsorption coverage of PEG-8000.[79] On the basis of these results, the *in-situ* transmittance measurement and obtained Cu powder during the measurement could represent the reactivity of solution as well as give the information on the surface morphology of Cu film.

Based on these results, the reaction trends and the characters of Cu deposits according to the molecular weight of PEG were considered. Reactivity test was proceeded with 0.56 μM of PEG which has 1500, 8000, 20000, 100000 of molecular weight. Fig. 4.4 depicts the relation between the inverse of reaction time ((C)+(D)) and the deposition rate. The deposition rate was decreased from 2.19 to 1.06 nm/sec with the increase in the molecular weight, and the inverse of reaction time ((C)+(D)) has the same tendency with varying from 0.00413/sec to 0.00141/sec. It implies that the inhibition effect of PEG was increased with higher molecular weight.[79,99-100] Although higher molecular weight of PEG has slower diffusion rate than smaller ones, its large

size can effectively hinder the adsorption site of HCHO by steric hindrance despite the lower number of molecules at same concentration.[79] As explained previously with PEG-8000 case, the size and the morphology of Cu powder showed similar results. Cu particle shown in Fig. 4.5 (a) and (b) was definitely decreased in primary size Cu from 355 to 212 nm and more connected Cu particles were observed according to the molecular weight of PEG. Taking the changes of surface morphology of Cu film into account as depicted in Fig. 4.6, Cu surface seemed to be reduced protrusions as predicted from the features of Cu powder. Therefore, it could be deduced that the inhibition effect by PEG caused the decrease in the size of primary Cu powder as well as the reduction in the surface roughness.

The sulfur-containing organic additives such as SPS, DPS, and MBIS were evaluated. It was reported that the influences of those additives on the deposition rate depended on their concentration. Those additives are known that they work as accelerator and suppressor in Cu ELD, and both effects are dependent on their concentrations.[74-76] In the case of SPS, it decomposes to MPSA by virtue of the protons and the electrons from the oxidation of reducing agent. MPSA reduces Cu^{2+} to Cu^{+}, which is the rate determining step in Cu reduction, therefore, it leads to the acceleration of deposition rate. This effect can be seen with relatively low concentration of SPS. On the other hand, when high concentration of SPS was added, it rather functions as suppressor because numbers of SPS, which do not convert to MPSA, hindered the active site.[74-75] The trends in Fig. 4.7 explained those two effects throughout the deposition rate

and the reciprocal reaction time ((C)+(D)). When 0.07 μM of SPS was added, the reciprocal of reaction time ((C)+(D)) was ascended from 0.00413 to 0.00422 and the deposition rate also increased from 2.19 to 2.36 nm/sec, in the same manner. It means that SPS acted as accelerator with low concentration. In contrast, over 0.14 μM, SPS inhibited the Cu deposition indicating the continuous descent in the reciprocal of reaction time ((C)+(D)) to 0.0026 and the deposition rate to 1.51 nm/sec. It inferred that *in-situ* transmittance measurement was useful to predict both of accelerated and suppressed reactivity with additive-containing solutions. The surface morphology of Cu power according to SPS concentration is revealed in Fig. 4.8. The primary size of Cu particle was 358 nm at 0.07 μM, the similar value with the additive-free case. However, over 0.14 μM, the sizes of Cu particle became increased up to 979 nm with large standard deviation. Although SPS showed suppressor effect like PEG, its influence to the growth of Cu powders was different. Considering the surface and size of Cu powder and the slowed deposition rate, it could be inferred that the suppressor of SPS inhibited reaction and gave enough chance to Cu particles to be aggregated. The surface morphology in Fig..4.9 showed more rough surface with protrusions at the concentrations showed suppression effect as compared to results with PEG. Therefore, the changes in the surface of Cu film could be inferred by the observation of the surface of Cu Powder. Consequently, it was found that the effect of SPS on the reactivity and Cu deposits could be observed with Cu powder from *in-situ* transmittance measurement.

As the same way, DPS and MBIS were examined. Fig. 4.10 exhibited the effect of DPS on reactivity of solution by means of 1/Reaction time ((C)+(D)) and the deposition rate calculated from the film thickness and deposition time. Like the behaviors of SPS, both of acceleration and suppression were observed. When 0.14 ~ 0.28 μM of DPS was added, it functioned as accelerator showing the increase in 1/Reaction time ((C)+(D)) from 0.00413 to 0.00514 and in deposition rate from 2.19 to 2.38 nm. Over 0.56 μM, DPS acted as suppressor due to its interruption of reduction reaction. The trends of particle size and the morphology were followed as obtained by SPS addition as shown in Fig. 4.10 (a) and (b). The size of Cu particles decreased in the range of 330 nm to 345 nm at low concentrations, and it increased at high concentrations up to 760 nm. Enhanced deposition rate led the fast nucleation and growth, which contributed to the relatively small size of powder. In contrast, large particle size was observed on account of inhibited reactivity that provided Cu particles to experience more agglomeration as explained above. However, in the surface morphology of Cu powder in Fig. 4.11 (a), it seemed to have rougher surface at 1.12 μM as compared to the result from SPS. In addition, the surface morphology of Cu film in Fig. 4.12 exhibited more protrusions. It was thought that it might be from the faster deposition rate with DPS as compared to that with SPS, because the fast deposition rate resulted in loosely deposited Cu and rough surface.

MBIS also had similar additive effect such as SPS and DPS. In Fig. 4.13, the reactivity was improved with the addition of 0.14 ~ 0.28 μM of MBIS, and suppressed over 0.56 μM. The

trends of both 1/Reaction time ((C)+(D)) and the deposition rate were similar. Acceleration effect was observed with 0.00487 of 1/Reaction time ((C)+(D)) and 2.4 nm/sec of maximum deposition rate at 0.28 μM. In the cases of more than 0.56 μM, the deposition rate was decreased to 1.84 nm/sec with 0.00277 of 1/Reaction time ((C)+(D)). The deposition rate with MBIS was similar with the case of DPS. In regard to features of Cu particles, MBIS affected the growth of Cu particles as similar with SPS and DPS as measured in Fig. 4.14 (a) and (b). The particle size was varied by the addition of MBIS. When the accelerating effect appeared, the size decreased to 340 nm at 0.28 μM. In the case of suppression effect, the primary Cu particle was grown to 1156 nm. Despite the similar the deposition rates with MBIS and DPS according to their concentrations, relatively smooth surface of Cu powder at the concentration range of suppression was observed with MBIS. It seemed to have connection with the surface morphology of Fig. 4.15 showing not remarkable changes, which might be related to the characteristic of MBIS. It needs to further study of characterization of Cu film with deposited by various kinds of S-containing additives.

From the contemplation of organic additives in Cu ELD, it was possible to predict the reactivity by means of *in-situ* transmittance measurement considering the inverse of reaction time ((C)+(D)). Furthermore, the particle size and its surface gave information about the reactivity, and the surface morphology in Cu film that could infer their characters.

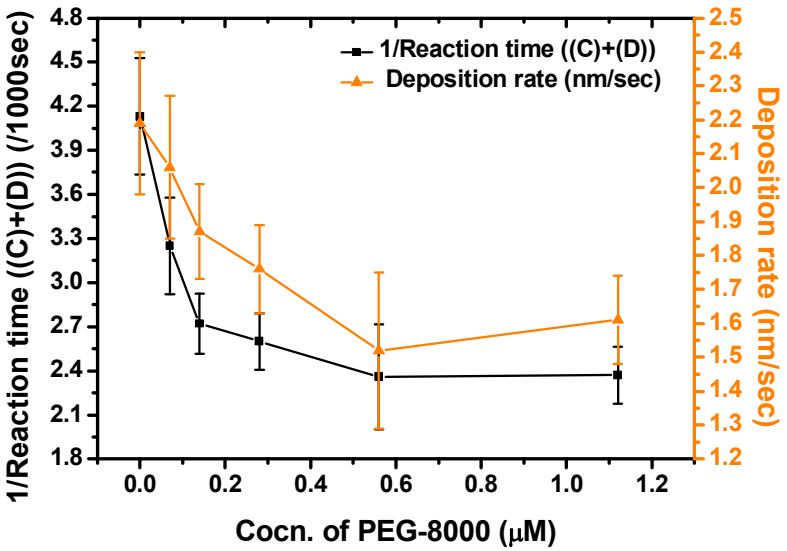

Fig. 4.1. 1/Reaction time ((C)+(D)) and the deposition rate as a function of the concentration of PEG-8000.

(a)

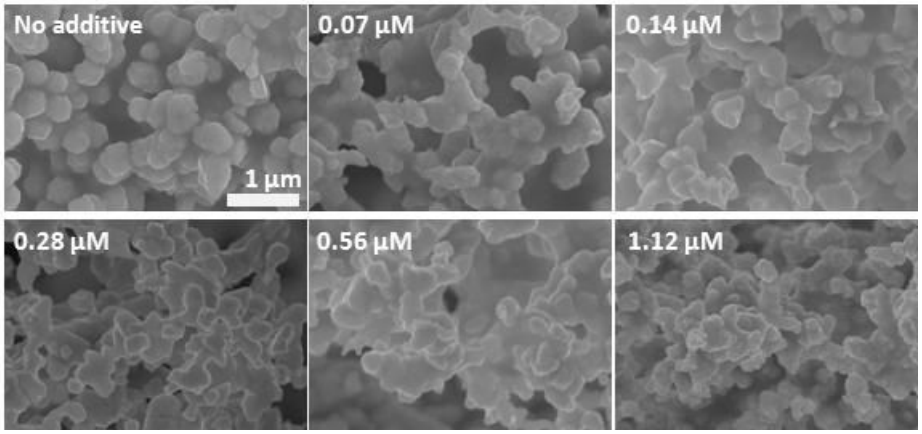

(b)

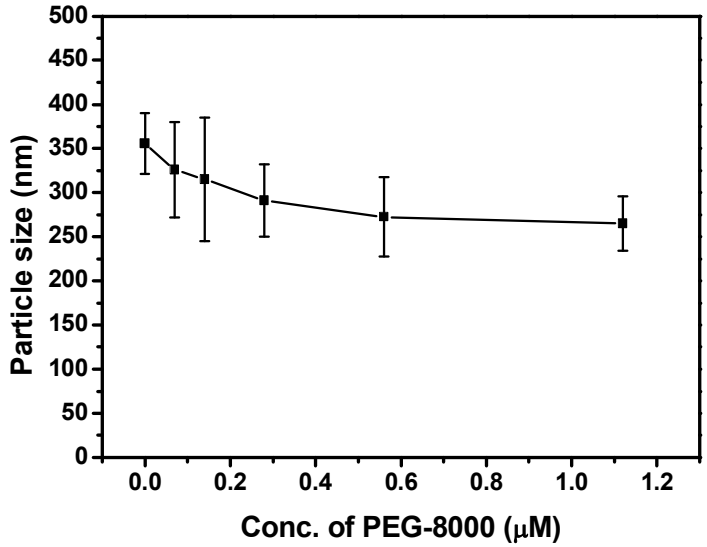

Fig. 4.2. (a) The shape of Cu powder prepared with various concentrations of PEG-8000, and (b) the sizes of Cu particles.

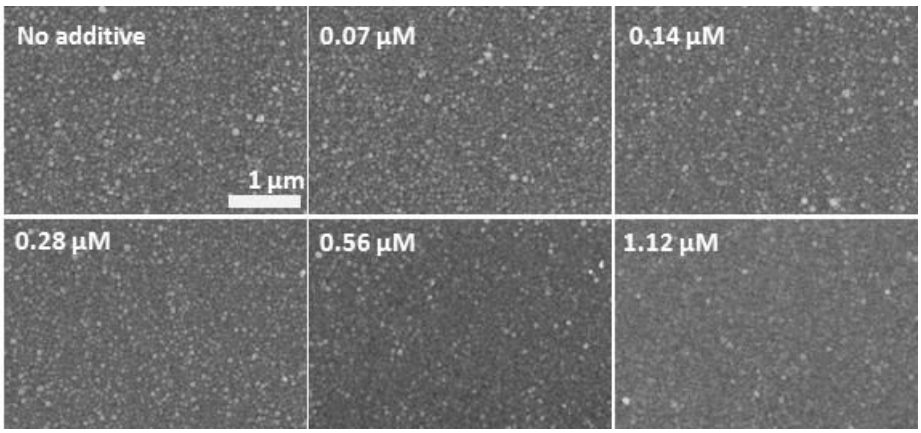

Fig. 4.3. The changes of surface morphology of Cu films deposited with various concentrations of PEG-8000.

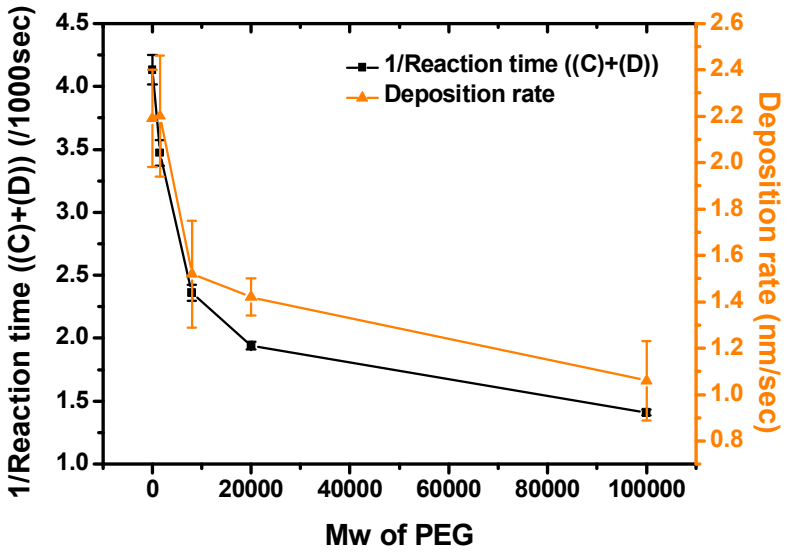

Fig. 4.4. 1/Reaction time ((C)+(D)) and the deposition rate according to the molecular weight of PEG.

(a)

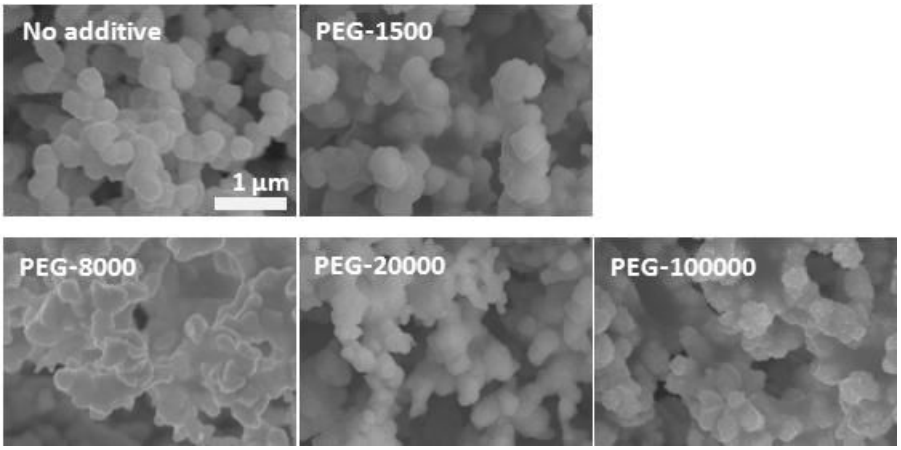

(b)

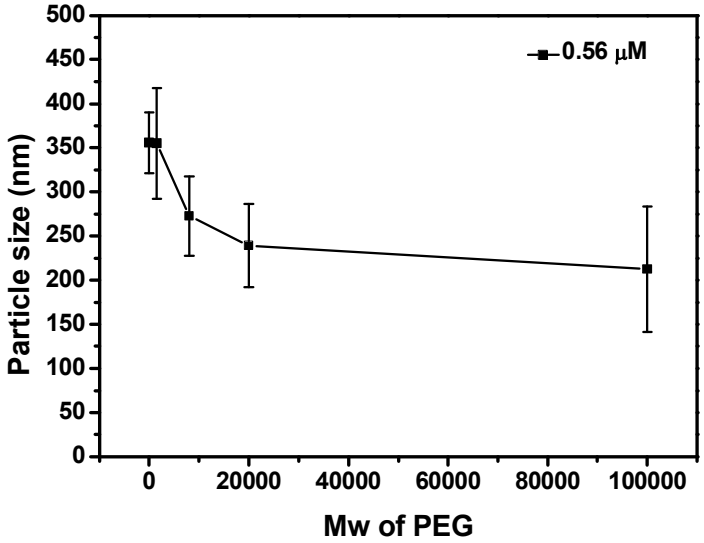

Fig. 4.5. (a) The shape of Cu powder prepared with various molecular weight of PEG, and (b) the sizes of Cu particles.

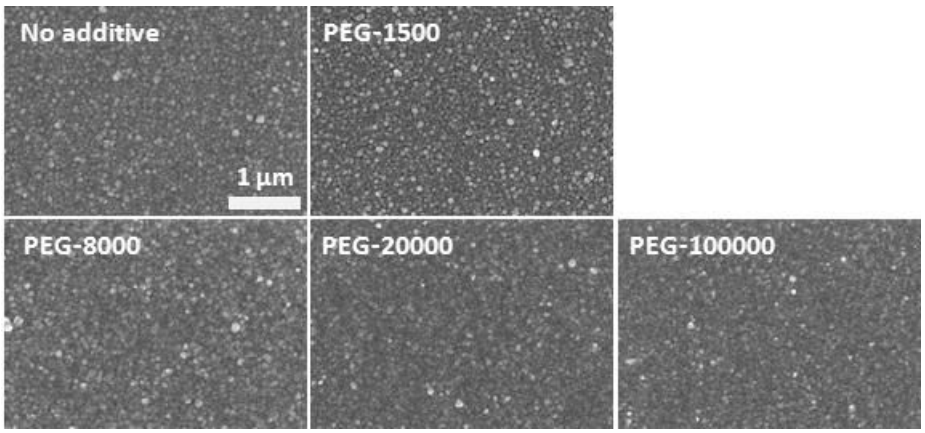

Fig. 4.6. The changes of surface morphology of Cu films deposited with various molecular weights of PEG.

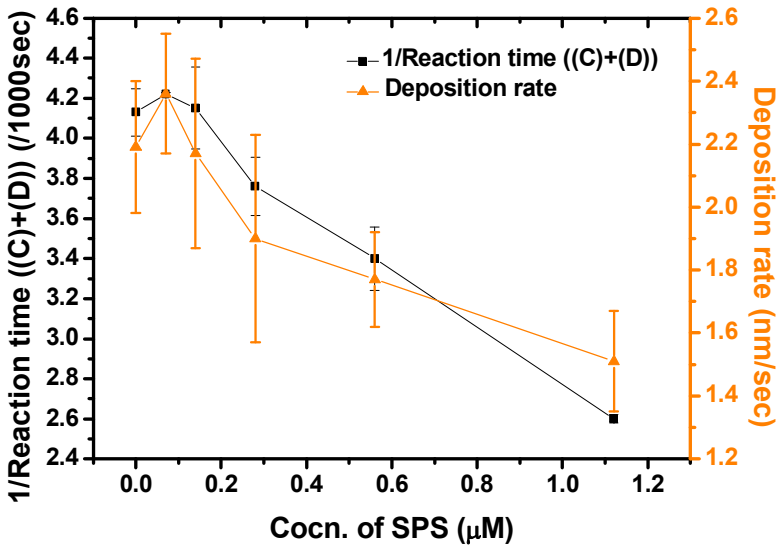

Fig. 4.7. 1/Reaction time ((C)+(D)) and the deposition rate according to the concentration of SPS.

(a)

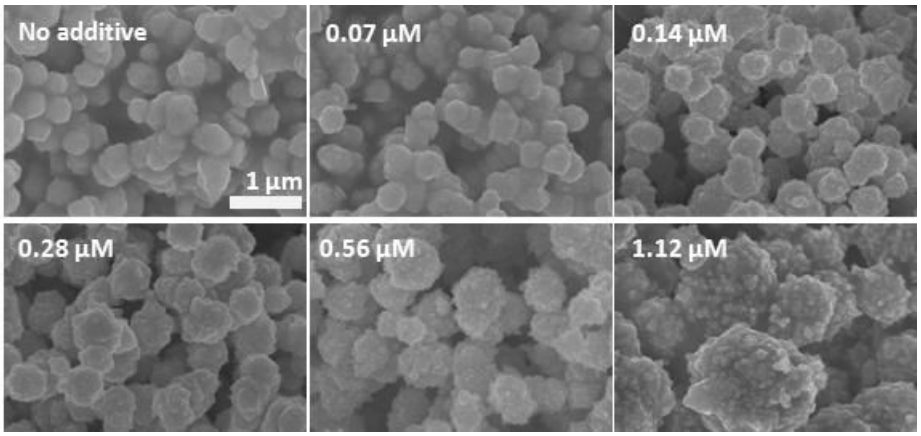

(b)

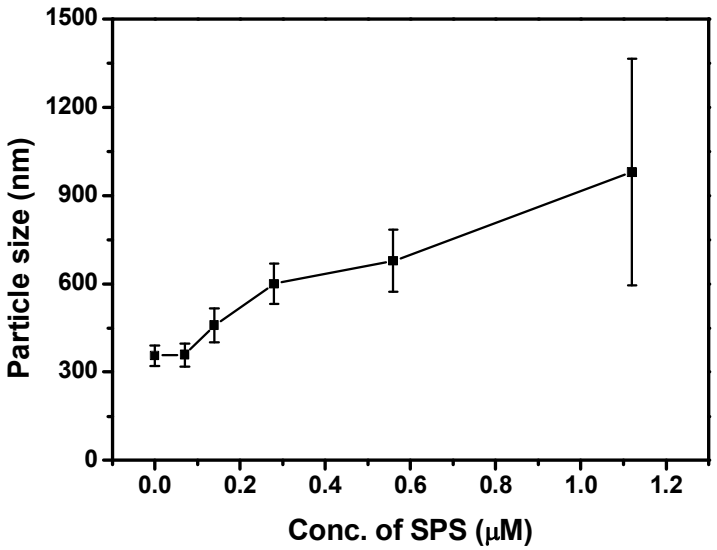

Fig. 4.8. (a) The shape of Cu powder prepared with various concentrations of SPS, and (b) the sizes of Cu particles.

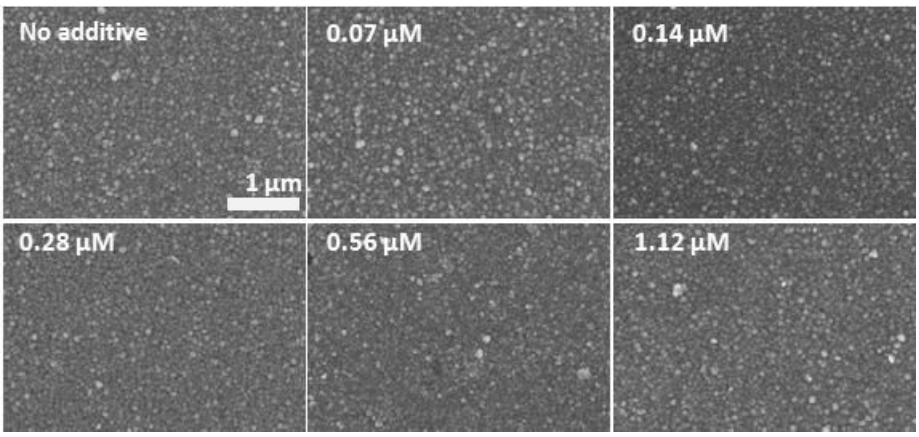

Fig. 4.9. The changes of surface morphology of of Cu films deposited with various concentrations of SPS.

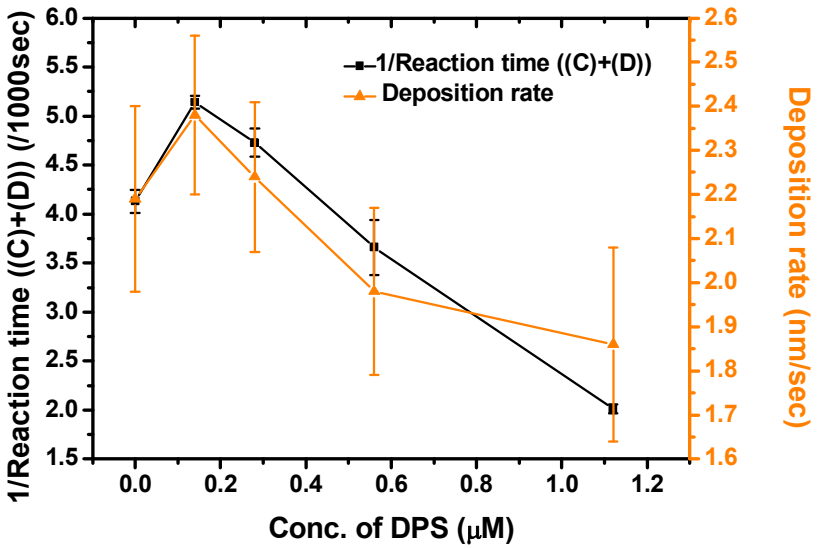

Fig. 4.10. 1/Reaction time ((C)+(D)) and the deposition rate according to the concentration of DPS.

(a)

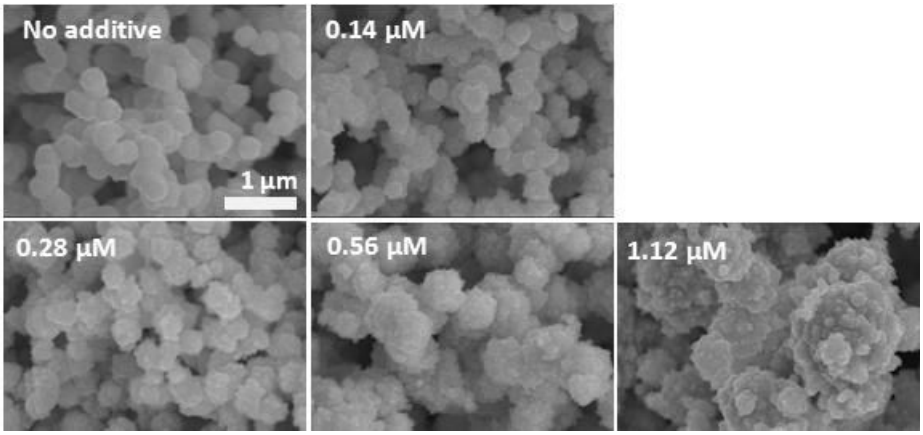

(b)

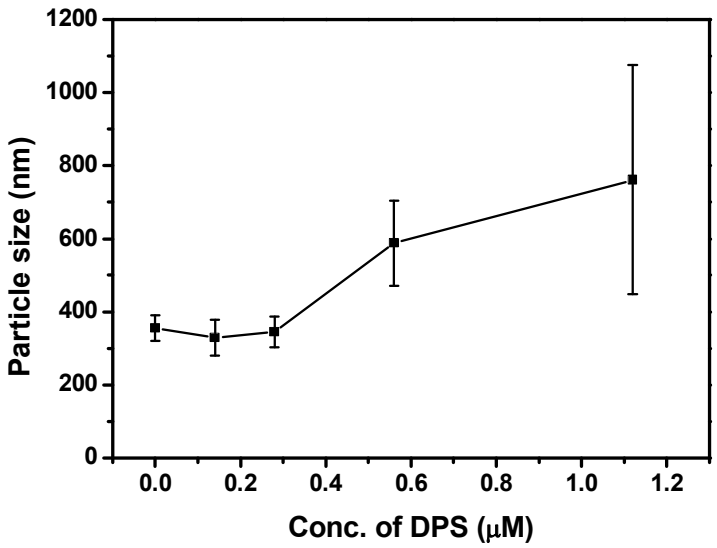

Fig. 4.11. (a) The shape of Cu powder prepared with various concentrations of DPS, and (b) the sizes of Cu particles.

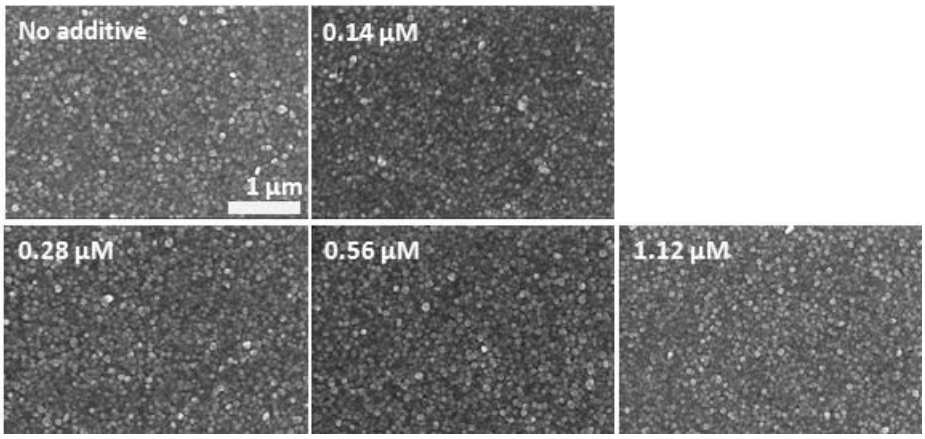

Fig. 4.12. The changes of surface morphology of Cu films deposited with various concentrations of DPS.

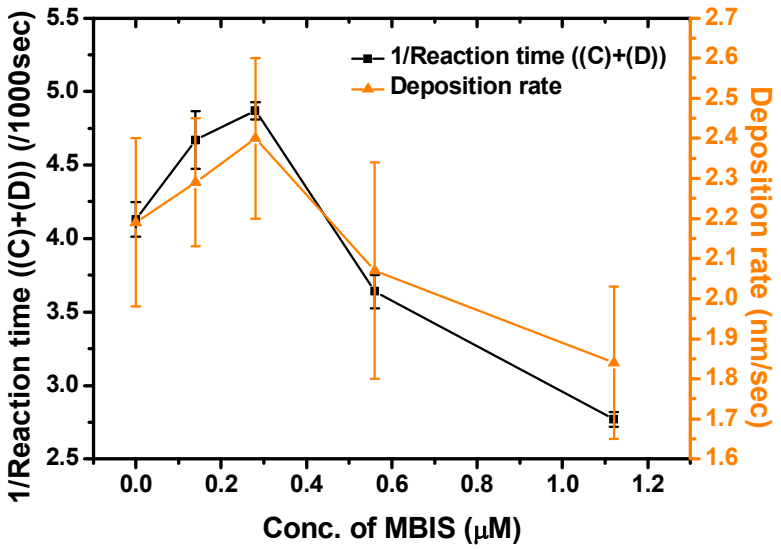

Fig. 4.13. 1/Reaction time ((C)+(D)) and the deposition rate according to the concentration of MBIS.

(a)

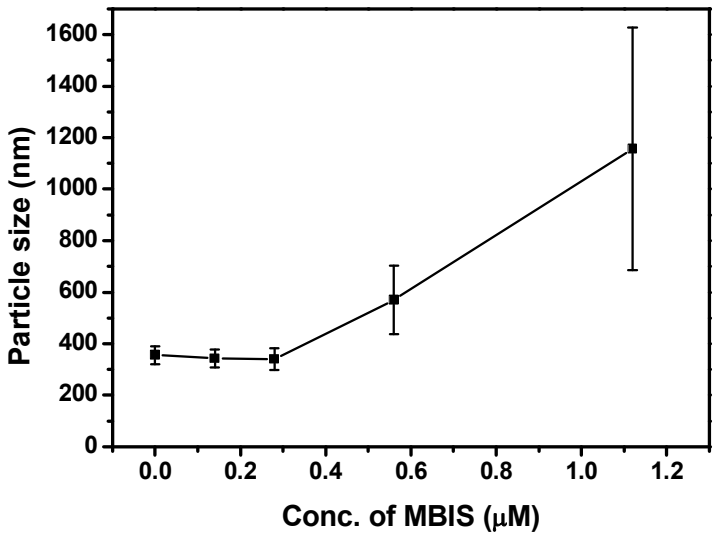

(b)

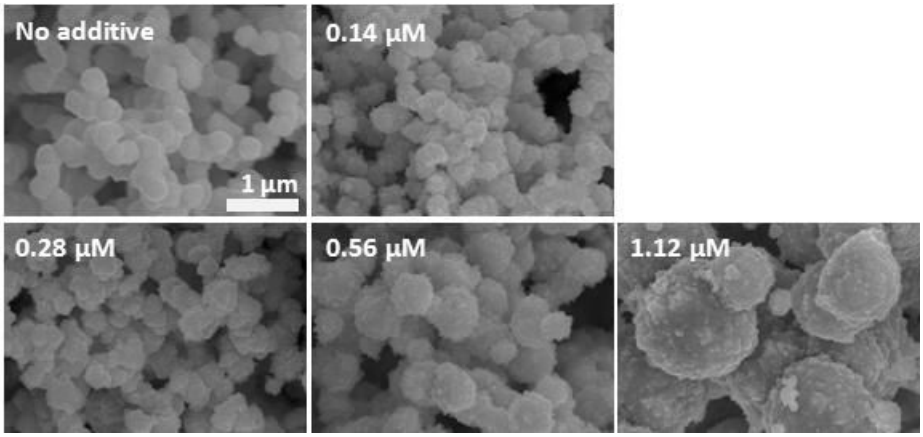

Fig. 4.14. (a) The shape of Cu powder prepared with various concentrations of MBIS, and (b) the sizes of Cu particles.

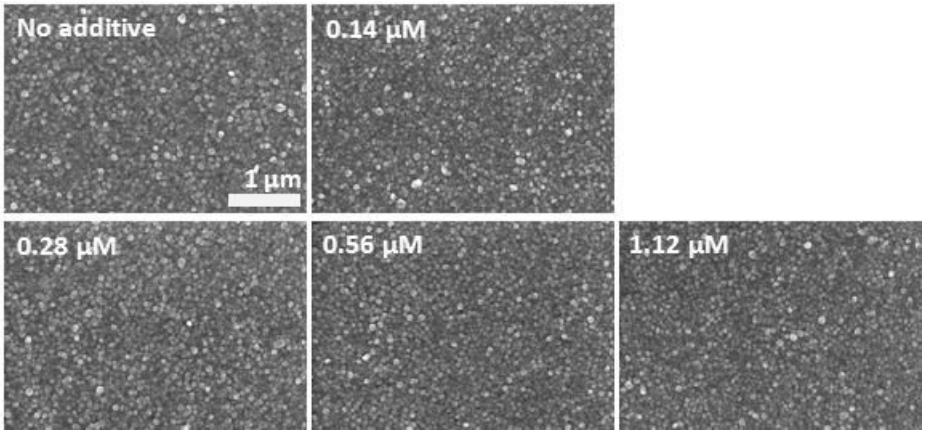

Fig. 4.15. The changes of surface morphology of Cu films deposited with various concentrations of MBIS.

4-2. Characterization of material properties with organic additives

The electrical resistivity of Cu film has a leading role in Cu interconnection application in reduced device size. To reduce the electrical resistivity, the grain size and the surface roughness of Cu film should be controlled. Substrate, deposition rate, and the organic additives can affect the film properties as mentioned in introduction. The effect of substrate can be ignored in this study because the conditions of substrate for deposition were same. Therefore, the roles of organic additives such as PEG with various molecular weights and SPS were focused. The grain size was calculated from Cu (111) peak obtained by XRD by using Scherrer's equation. The properties of Cu film were compared to those of Cu powder prepared during in-situ transmittance measurement. In all cases, 1.12 μM of additives were supplied and the thickness of Cu film was precisely controlled to have 60 nm.

The changes of the grain size in Cu film were observed according to the molecular weight of PEG from 1500 to 100000. As Fig. 4.16 (a) exhibits, the grain size calculated from Cu (111) peak was decreased as higher molecular weight of PEG added. In the absence of additive, the grain size was about 35 nm, whereas it decreased down to 25 nm as the molecular weight of PEG was increased, then saturated with PEG having the molecular weight more than 8000. It was reported that the PEG impeded the adsorption of HCHO by pre-adsorption on the active site. Adsorbed PEG on reactive surface such as Pd or Cu inhibited the growth to larger columnar

structure, which resulted in the decrease of the grain size. In general, PEG with high molecular weight has small diffusion coefficient and shows stronger suppression ability by large steric hindrance. However, it seemed that the grain size did not reflect the inhibition strength. It is thought that limited adsorption site made the suppression effect saturated even with high molecular weight of PEG that has low number of molecules at same concentration. When it compared to the results of Cu powder that obtained by *in-situ* transmittance measurement with same conditions, decrease in the grain size was confirmed as depicts in Fig. 4.16 (b). It was impossible to compare the results in the cases of PEG-20000 and 100000, because of the excellent wetting properties of PEG made Cu powder stick to the membrane filter used for rinsing and collecting powder, which disabled the sampling of Cu powder. Though there was limitation for comparison, it was found that *in-situ* transmittance measurement allowed not only to estimate the solution performances but also to predict the change of the grain size, one of the material properties.

The changes in the surface roughness of Cu film according to the molecular weights of PEG were displayed in Fig. 4.17, indicating that the addition of PEG made the surface smoother. The surface roughness was decreased and saturated to about 7 nm. The additives that have hydrophilic characteristics like 5-aminotetrazole (ATRA) or PEG are easy to adsorb on the surface. They facilitates the connection between spaces by reducing the total surface energy, which helps to curb the formation of high-resistive groove and develops low-resistive groove.[38]

Finally, small portion of protrusion brought about the decrease in the surface roughness. In the case of PEG-1500, it did not exhibit effective smoothing, whereas higher molecular weight of PEG over 8000 considerably reduced the surface roughness. In the observation of Cu powder in Fig. 4.2 (a) and Fig. 4.5 (a), smooth surface could be observed with the addition of PEG. Although it was hard to analyze the surface roughness of Cu powder with quantitative consideration, the changing trends in the roughness could be contemplated.

The electrical resistivity of Cu film was calculated from the sheet resistance and thickness, and the results are exhibited in Fig. 4.18. It was gradually saturated from 7.67 to 5.5 μΩ·cm by 27% of reduction as PEG molecular weight increased. Decrease in the grain size provides more grain boundaries where electron scattering happens, while the decrease in the surface roughness leads to low electrical resistivity.[34,37] Given that the 28% decrease in both the grain size and the 50% of improved surface roughness, it could be concluded that the decrease in the surface roughness by PEG addition dominantly contributed to lowering the electrical resistivity.

Cu film properties deposited with 1.12 μM of SPS was also investigated. At this condition, it was confirmed that SPS acted as a suppressor in previous chapter. Fig. 4.19 presented the grain size of Cu film deposited without additives, with PEG-8000, and with SPS. PEG-8000 was selected to compare the properties because its deposition rate like 1.6 nm/sec was similar to that of SPS. In the presence of SPS, the grain size was changed with 5% of increment, and the result of Cu powder supported it. It is counter to some reports that the addition of organic additives

reduced the grain size in ED of film deposited on Cu by ED.[47] Actually, the exact mechanism of organic additives in ELD has not been clarified yet because of the complexity of ELD solution containing lot of chemicals. Therefore, these results could be explained by following hypotheses. First one is that the adsorption of SPS interrupted the nucleation of Cu, which caused the Cu growth rather than the nucleation so that the grain size became large. Considering the morphology of Cu powder shown in Fig. 4.8 (a) that the size of Cu particles was increased the addition of SPS, the preference in Cu growth. Second one is originated from the complex chemistry in Cu ELD solution. Solution has four chemical species at least, and there might be interactions among the chemicals and organic additives that are unknown. If components of solution related to minify the grain size are blocked to be adsorbed due to the adsorption of SPS, the grain size would be rather increased. However, they need to further study about these hypotheses. In the aspect of the surface roughness, there was 8% of decrease as described in Fig. 4.20. Inhibited deposition rate mainly contributed to the surface smoothing. As a result, 17% of reduction in the electrical resistivity was achieved by aid of both large the grain size and smooth surface.

From these results, it was found that Cu film properties were altered by the addition of organic additives. Even though both PEG and SPS worked as suppressor, those effects were dependent on the characteristics of them. Moreover, Cu powder from *in-situ* transmittance

measurement could represent the grain size of Cu film and provide the prediction of the surface roughness, which assured the feasibility of this method for characterization of properties.

(a)

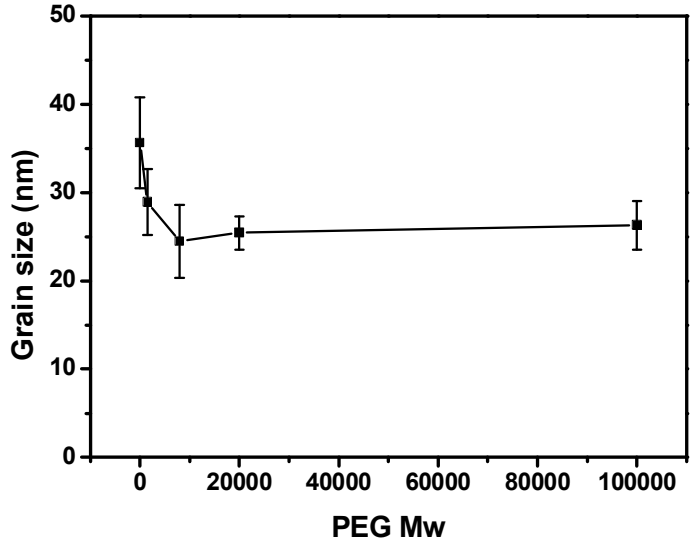

(b)

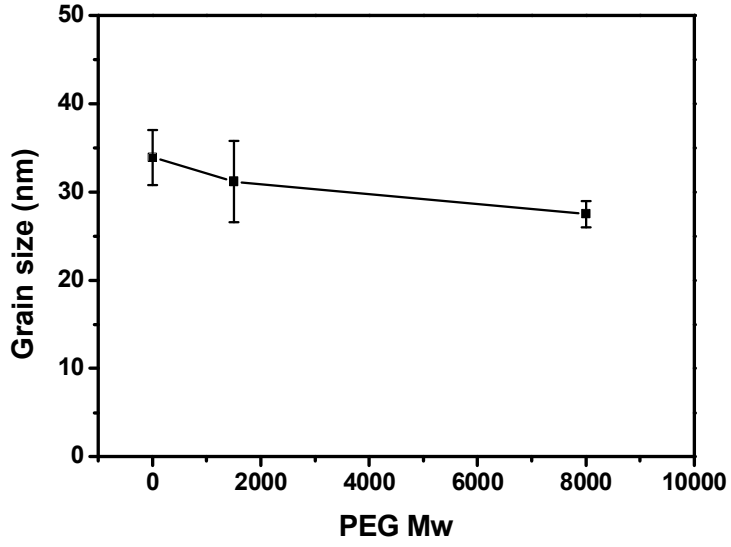

Fig. 4.16. The changes in the grain sizes according to the molecular weight of PEG; (a) Cu film (b) Cu powder.

(a)

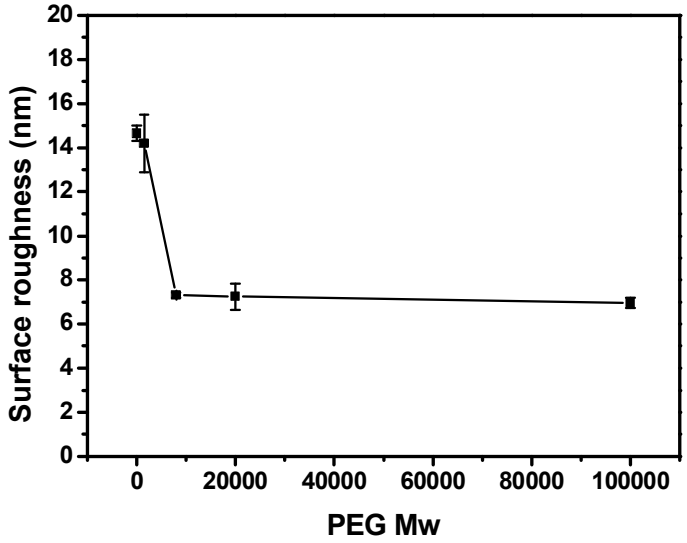

(b)

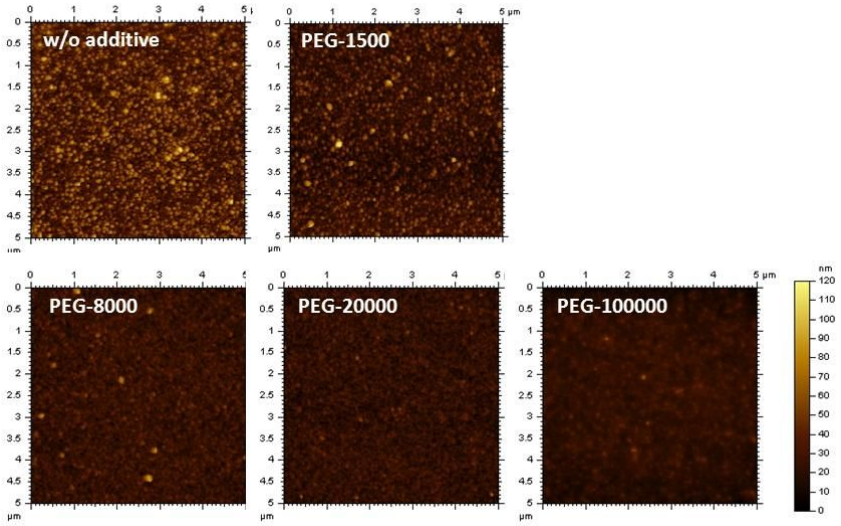

Fig. 4.17. (a) The change in surface roughness of Cu film according to the molecular weight of PEG and (b) their AFM images.

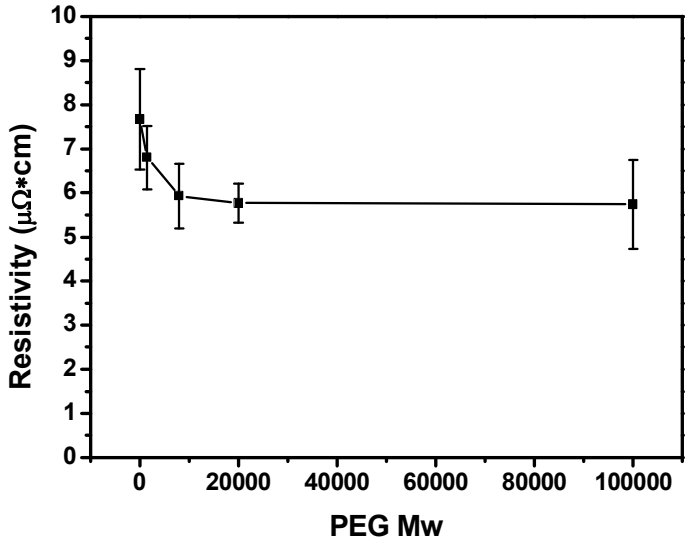

Fig. 4.18. The changes in resistivity of Cu film according to the molecular weight of PEG

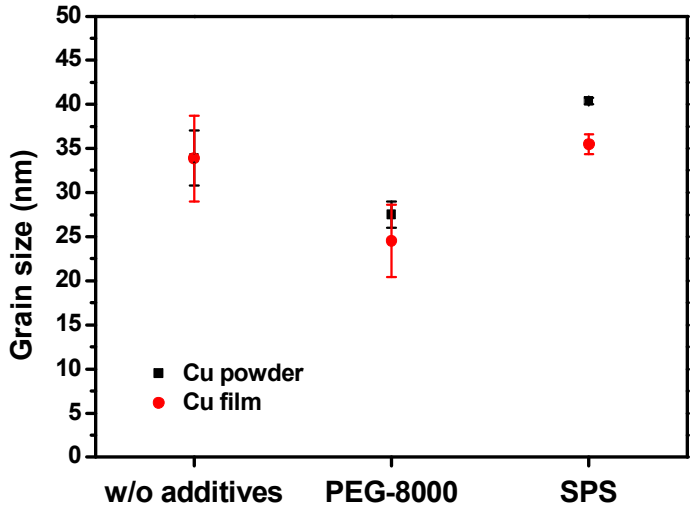

Fig. 4.19. Comparison of the grain sizes from Cu powder and Cu films prepared without additives and with 1.2 μM of PEG-8000 and SPS.

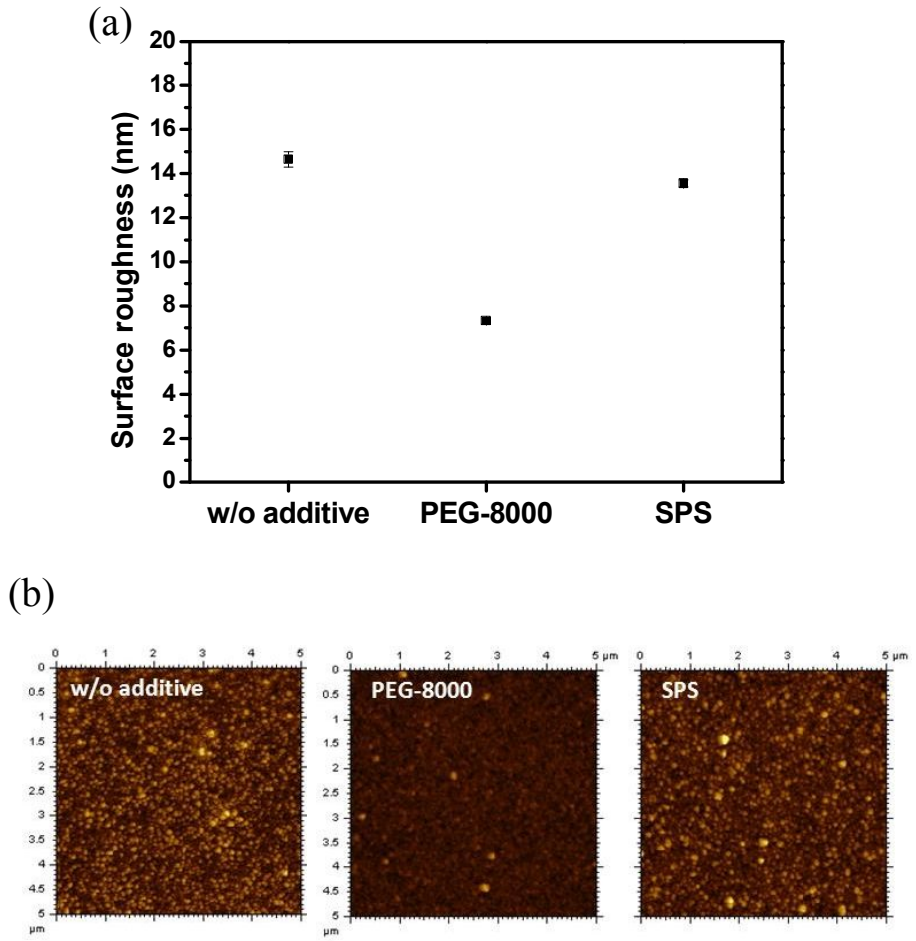

Fig. 4.20. (a) The changes in surface roughness of Cu films deposited without additives and with 1.2 μM of PEG-8000 and SPS, and (b) their AFM images.

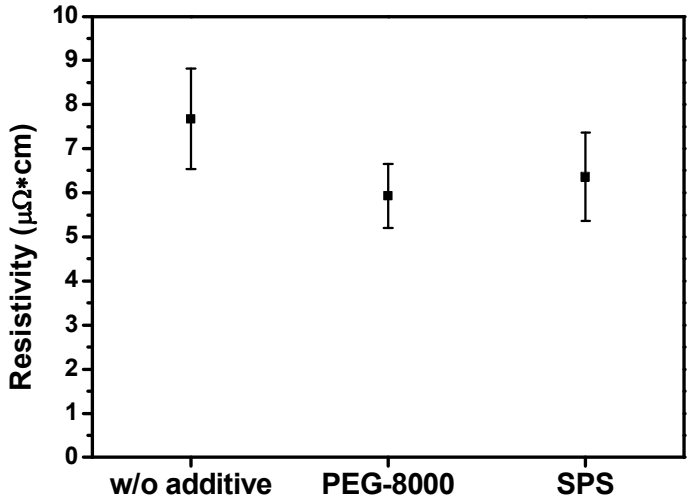

Fig. 4.21. The resistivity of Cu films deposited without additives and with 1.2 μM of PEG-8000 and SPS.

CHAPTER V

Seed layer formation in through silicon via (TSV)

As a result of transmittance measurement, the combination of EDTA-HCHO was estimated to be one of the optimums both in that the stability and the reactivity. EDTA-HCHO-based solution was applied to the formation of Cu seed layer in high aspect ratio TSV. To enhance the adhesion of Cu film, the deposition rate was controlled to be slowed by the addition of 2,2'-dipyridyl and RE-610®. Besides, further optimization and modification in process were demanded.

On inspecting the Cu seed layer formed in the stationary condition, only Cu islands were observed at the near-bottom of the via, whereas continuous Cu film was deposited at the top (S/W 1) as shown in Fig. 5.1 (a). The high aspect ratio and overhang of the via resulted in decrease in the metal ion flux by interfering with the diffusion through the hole, thereby leading to the depletion of metal ions. The poor quality of the seed layer may be caused by low density of the Pd catalyst or by poor nucleation and growth of Cu. To solve these problems, a convection force was induced in the Pd activation step using the rotating system that applied a convective force parallel to the direction of the chip. A 300 rpm rotation speed was equivalent

to approximately 0.76 m/s linear velocity. Fig. 5.1 (b)–(d) show the FESEM images of the Cu films from the top to the bottom for varying rotation speeds in the Pd activation step. The images in Fig. 5.1 depict the improved deposition profile after the Cu ELD. However, at the bottom, only Cu nuclei are observed. Among the different rotation speeds considered, the 300 rpm case exhibited notable improvement in film continuity with the smoothest and most continuous surface near the top and a relatively uniform and denser Cu nuclei near the bottom of the via. Therefore, optimization of pretreatment conditions are required to enhance the density of the Pd catalyst, which is one of the key factors that aid in obtaining a smooth and continuous film.[8,31]

The optimization in pretreatment time was achieved by changing the processing time in the 300 rpm case in the Pd activation. Prior to experiment on patterned wafer, the optimized time was tried on non-patterned via same experimental conditions. Experiments on non-patterned wafer offered the direct information of Pd density so as to analogize Pd density in the via since it is hard to observe Pd catalysts in the via. As shown in Fig 5.2 (a) when the sensitization time with fixed Pd activation time was increased from 2 to 10 min, the density of the Cu nuclei diminished. As Sn ions were immediately oxidized once exposed to air or water, the active sites for displacement of Pd decreased, which in turn resulted in the relatively low number of Cu nuclei. Fig. 5.2 (b) display the effect of Pd activation time on film continuity with a constant Sn sensitization time of 2 min. In earlier research,[101] it has been reported that the formation of Pd

catalyst consists of three steps: growth, secondary nucleation, and ripening according to the activation time, which is in good agreement with the experimental results from this study. When the activation time was increased to 50 sec, Pd density was increased up to $11x10^{10}/cm^2$ by the enough nucleation and growth time. However, for a longer activation time of 100 sec, Pd density was dramatically decreased, because of agglomeration through van der Waals' interaction and Oswald ripening, and the dissolution due to the longer exposure to the alkaline bath.[102] Based on these results, Cu ELD was conducted with patterned wafer with same conditions of pretreatment time and the bottom of the via was observed as shown in Fig. 5.3. Longer Sn sensitization time made Pd density decreased, as a result, Cu nuclei at the bottom also decreased (Fig. 5.3 (a)~(c)). When Pd activation time was increased to 50 sec, nearly continuous film was formed at the bottom because of the dense Pd catalyst as Fig. 5.4 (d) depicts. However, with 100 sec of Pd activation, there are some voids in Fig. 5.4 (e) due to the diminishing Pd density. From these results, 2 min of Sn sensitization and 50 sec of Pd activation were found to be the optimized conditions.

The rotation speed, which induced the convective motion inside trench, was the second parameter to be optimized in the range of 200 to 1000 rpm as shown in Fig. 5.4. At 200 rpm rotating speed, the decreased Cu film thickness along the depth led to conformality of 0.88 for the seed layer. Fig. 5.5 shows the conformality, which is the ratio of the thickness at the bottom to at the sides, versus the rotation speed. The voids between the Cu nuclei at the sidewalls

signify insufficient flow by the concentration gradient in the via, which contributed to the deposition of the relatively thin film at the bottom. However, when a 300 rpm rotation was applied, a continuous seed layer with conformality of 0.98 and a ratio of 0.88 film thickness between the side and the top was obtained. This implied the possibility to form conformal seed layer by reducing the concentration gradient of Cu ions through the via. Although conformality of 0.96 was obtained with a rotation speed of 600 rpm, the surface has rough morphology with small grains at the sidewalls. In high-speed rotation of 1000 rpm, it was impossible to calculate the conformality because of the detachment of the film and trapping of some voids at the sides. In addition, at rotation speeds higher than 600 rpm, surface coverage at the flat surface of wafer was dramatically decreased because the Pd catalysts were easily detached by a strong drag force during the rotation in the Cu ELD step. The continuity of the seed layer at the top and flat regions for electrical contact has to be considered for following Cu ED. Therefore, a 300 rpm rotation speed in the Cu ELD step is the optimal condition for the formation of conformal Cu seed layer. Based on the optimized conditions in the pretreatment and Cu ELD steps, Cu seed layer with good conformality and adhesion was achieved as presented in Fig. 5.6 (a).

The Cu ED with pulse reverse mode was proceeded with organic additives to fill the via on the prepared seed layer by Cu ELD for 120 min. As shown in Fig. 5.6 (b) and (c), void-free filling of the via was achieved, which profile indicated V-shape that is the evidence of feature filling. It was ascribed to the concentration gradient of leveler, JGB, and its convection

dependent adsorption, which led the stronger suppression effect at the top due to the robust convection that at the bottom. Therefore, the application of *in-situ* monitoring was confirmed that conformal Cu seed layer was formed by ELD that conducted using stability and reactivity estimated solution, with optimization of process.

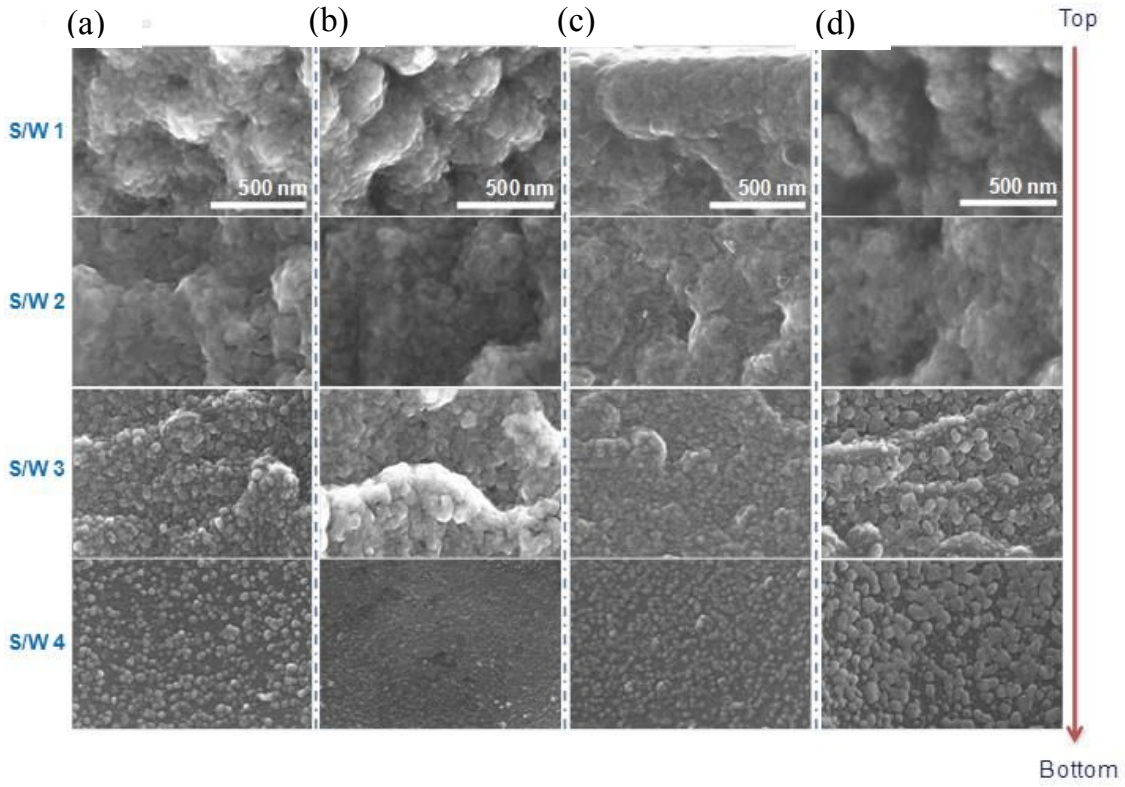

Fig. 5.1. Profiles of sidewalls (SW) of the via from the top to the bottom after Cu seed layer formation for varying rotation speeds in the Pd activation step: (a) without rotation, (b) 200 rpm, (c) 300 rpm, and (d) 600 rpm.

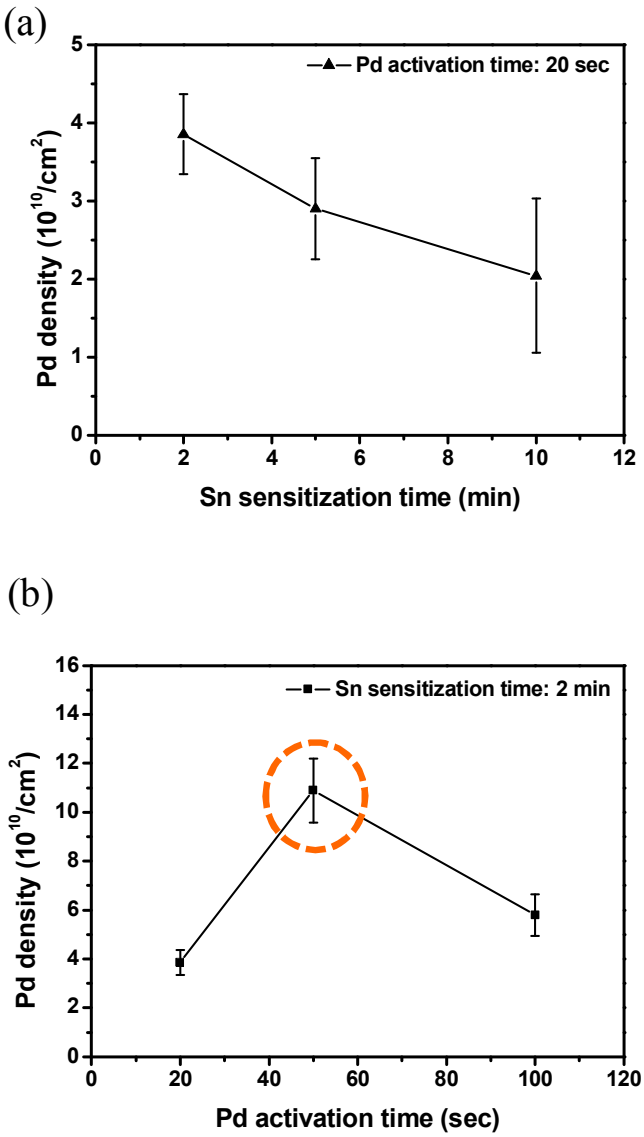

Fig. 5.2. Variation of Pd density (a) as a function of the Sn sensitization time with 20 sec of Pd activation and (b) as a function of the Pd activation time with 2 min of Sn sensitization.

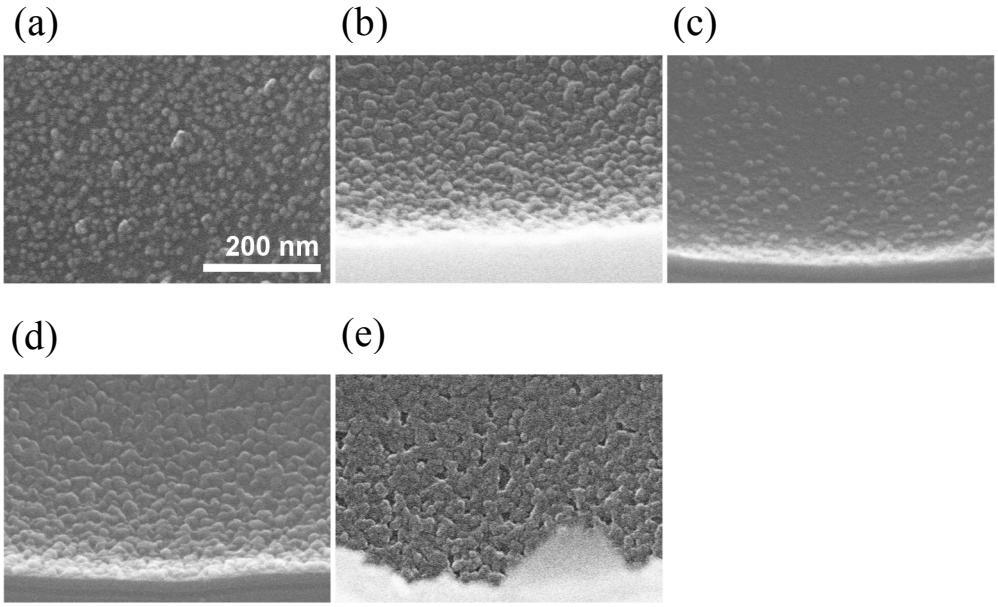

Fig. 5.3. Bottom of the via after Cu seed layer formation with varying pretreatment time (Sn sensitization/Pd activation time); (a) 2 min/20 sec, (b) 5 min/20 sec, (c) 10 min/20 sec, (d) 2 min/50 sec, and (e) 2 min/100 sec.

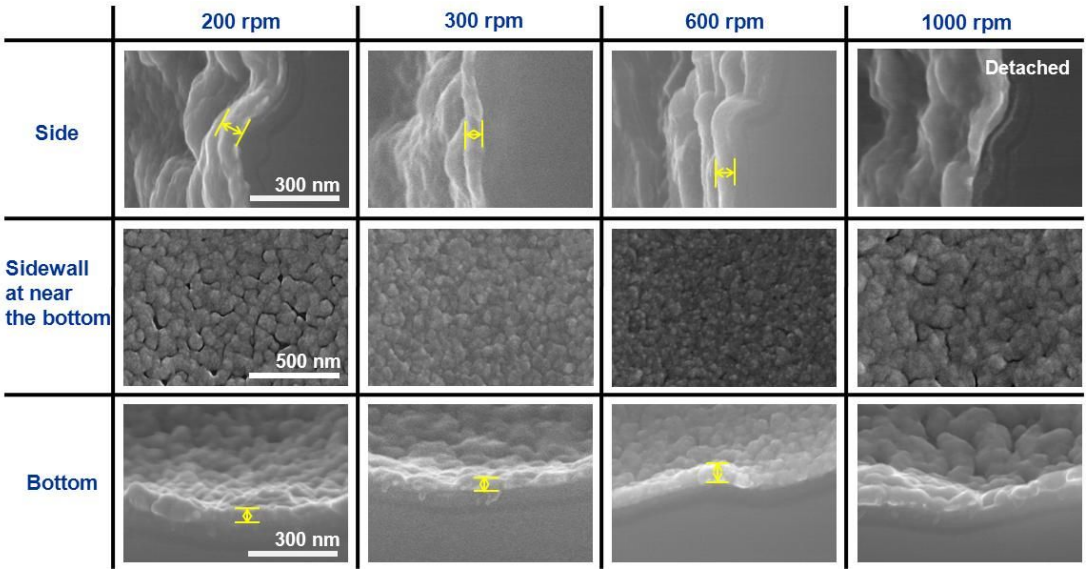

Fig. 5.4. Deposition profiles of the Cu seed layer according to the positions of via as a function of rotation speed in the Cu ELD step.

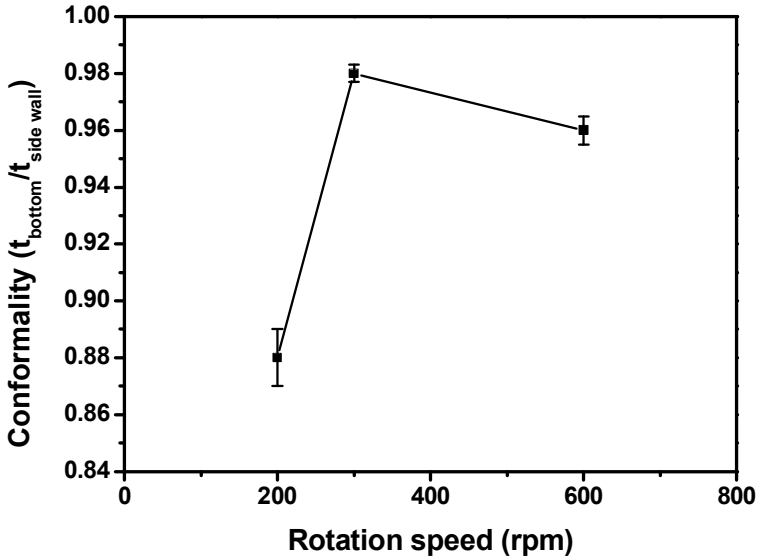

Fig. 5.5 . Conformality of the seed layer versus the rotation speed during the Cu ELD.

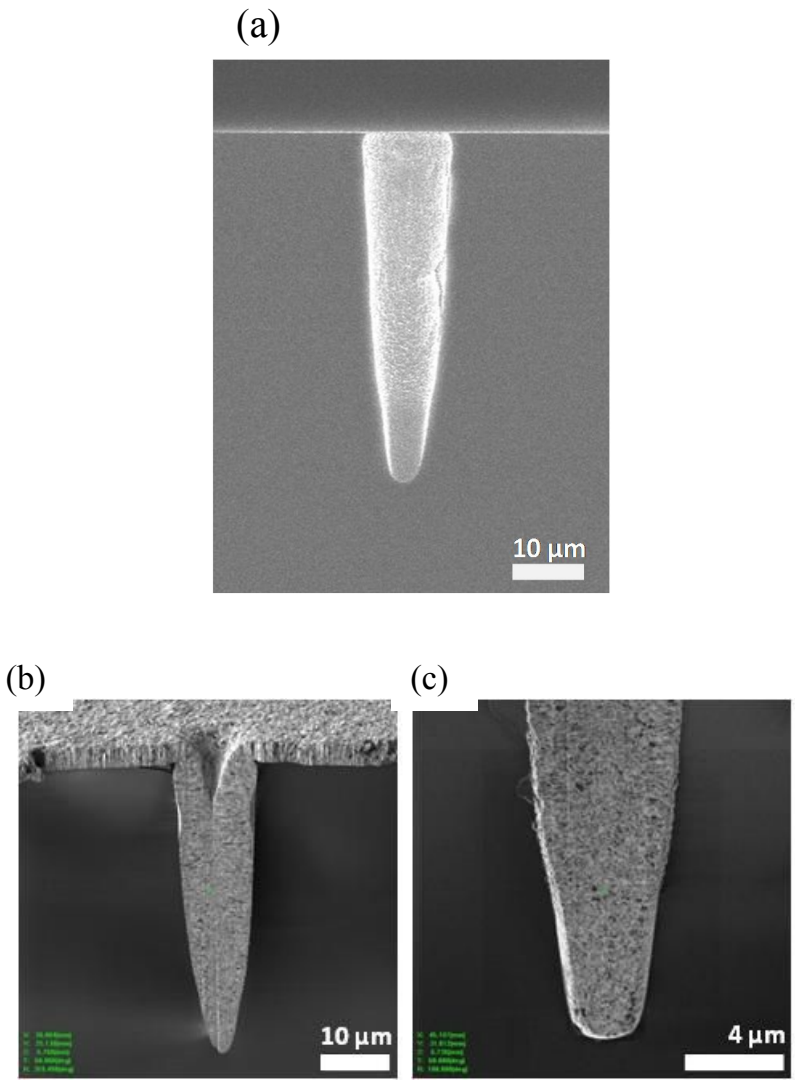

Fig. 5.6. (a) FESEM image of the Cu seed layer–deposited via with optimized conditions, and FIB images of Cu filled via by ED (b) whole via and (c) magnified via at the bottom.

CHAPTER VI

Conclusions

in-situ transmittance measurement was introduced for evaluation of solution performance of CU ELD solution. It gave the information about the situation of solution by means of real-time monitoring of the intensity loss owing to the Mie scattering, expressed by transmittance. Behaviors of transmittance change in each stage were interpreted with EDTA-HCHO based reference solution. It was verified that the transmittance change was highly related to particle formation by homogeneous or heterogeneous reactions, which could indicate the status of solution. Based on these understanding, effects of complexing agents, reducing agents, and organic additives that compose of solution were verified.

In the stability test with complexing agents, it was observed that complexing agents with lower formation constant (pK_f) led to the decomposition of solution at 70℃, whereas complexing agents with higher pK_f showed stable state. In reactivity test, the reaction time to Cu reduction with SnPd colloid was increased in the order of pK_f values. Also, the feasibility of this *in-situ* monitoring method was confirmed by comparison with the results from real deposition on Ta substrate.

In the evaluation with reducing agents, the stability of solutions could be proved despite of the different intensity due to the characteristic absorption of them. The reactivity test with

aldehyde-based formaldehyde and glyoxylic acid showed similar characters in transmittance curve and Cu powder, which inferred the reactivity of solutions. However, it was hard for hydrazine-based solution that has low deposition rate to distinguish the reaction section. Instead, the fact that the solution is reactive on Pd was assured, in contrast it was impossible in film deposition due to desorption of Pd on substrate. Besides, the small output intensity of DMAB-based solution showed the limitation in measurement. The problem related to absorption would be solved with the adoption of appropriate incident laser.

Effects of organic additives such as PEG with various molecular weights and sulfur-containing SPS, DPS and MBIS were demonstrated by *in-situ* monitoring. As expected and confirmed by film deposition, the acceleration and the suppression effects were clearly observed. In addition, it was found that the size and the surface features of Cu powder could help the prediction of the reactivity and the surface morphology of Cu film. Furthermore, the material properties of Cu powder and Cu film with PEG and SPS was analyzed and compared. Organic additives affected the grain size and the surface roughness, whose effects were observed both in Cu powder and Cu film. The trends which were obtained through Cu powder were reconfirmed on the non-patterned flat substrate.

From *in-situ* transmittance analyses, the optimal compositions of the solutions that have the stability and the reactivity were confirmed. Among them, EDTA-HCHO based solution was selected for the application of Cu seed layer formation on non-Bosch via. By additional efforts

to afford continuous Cu film like applying rotation during the Pd activation and the Cu ELD steps, the concentration gradient of reactants between the top and bottom of the via could be moderated. In addition, by optimizing the pretreatment time, a high density and uniform Pd catalyst at the bottom of the via was achieved. Finally, a seed layer with a smooth surface and good conformality was obtained. A void-free Cu filling was accomplished by ED, thereby elucidating the suitability of ELD to deposit conformal Cu seed layer.

In conclusion, this study introduced *in-situ* transmittance measurement to evaluate the performance of Cu ELD solution, the stability and the reactivity. The validity of real-time monitoring method was proved by figuring out the roles and the effects of solution components such as complexing agent, reducing agents and organic additives, and comparing their results with those of Cu film deposition. Moreover, it was applicable to predict the surface morphology and material properties. It is expected that this method can be easily adopted to verify the characteristics of other solutions.

References

1. P. -L. Pai, and C. H. Ting, IEEE Elect. Dev. Lett., **10**, 423 (1989)

2. Y. S. -Diamand, Valery Dubin, Matthew Angyal, Thin solid films, **262**, 93 (1995)

3. R. L. Jackson, J. Electrochem. Soc., Accelerated brief communication, 3172 (1988)

4. A. Bauer, J. Ganz, K. Hesse, and K. Kohler, Appl. Surf. Sci., **154**, D182 (2007)

5. I. Choi, S. H. Ahn, J. J. Kim, and O. J. Kwon, Appl. Catal. B: Environ., **101**, 608 (2011)

6. Z. J. Yu, E. T. Kang, and K. G Neoh, **43**, 4137 (2002)

7. S. J. Cho, T. Nquyen, and J. H. Boo, J. Nanosci. Nanotechnol.11, 5328 (2011)

8. C. H. Lee, S. H. Cha, A. R. Kim, J. -H. Hong, and J. J. Kim, J. Electrochem. Soc., **154,** D182 (2007)

9. J. J. Kim and S. H. Cha, Jpn. J. Appl. Phys., **40**, 7151 (2001)

10. Y. -M. Lin and S. -C. Yen, Appl. Surf. Sci., **178**, 116 (2001)

11. J. Li and P. A. Kohl, Plat. Surf. Finshing, 1 (2004)

12. L. Paunovic, J. Electrochem. Soc., **124**, 349 (1977)

13. G. O. Mallory and H. B. Hajde, Electroless Plating: Fundamentals and Applications, American Electroplaters and Surface Finishers Society, Orlando (1990)

14. H. Honma and T. Kobayashi, J. Electrochem. Soc., **141**, 730 (1994)

15. E. Natividad, E. Lataste, M. Lahaye, J. M. Heintz, and J. F. Sivain, Surf. Sci., **557**, 129 (2004)

16. H. P. Fong, Y. Wu, Y. Y. Wang, and C. C. Wan, J. Elect. Mater., **32**, 9 (2003)

17. W. L Goh, K. T. Tan, M. S. Tse, K. Y. Liu, Inter. J. Mod. Phys. B, **16**, 197 (2002)

18. C. -L. Lee, Y. -C. Huang, C. -C. Wan, Y. -Y. Wang, Y. -Jen, Ju, L. -C. Kuo, and J. -C. Oung, J. Electrochem. Soc., **152**, C520 (2005)

19. S. -Y. Chang, C. -J. Hsu, R. -H. Fang, and S. -J. Lin, J. Electrochem. Soc., **150**, C603 (2003)

20. F. Wang, Y. Li, Y. Wang, and Z. Cao, Nano. Res. Lett., **6**, 483 (2011)

21. D. Aldakov, Y. Bonnassieux, B. Geffroy, and S. Palacin, Appl. Mater and Interfaces, **1**, 584 (2009)

22. C. -L. Lee, C. -C. Wan, and Y. -Y. Wang, J. Electrochem. Soc., **150**, C125 (2003)

23. V. M. Dubin and Y. S. Diamand, J. Electrochem. Soc., **144**, 898 (1997)

24. R. Schumacher, J. J. Pesek, and O. R. Melroy, J. Phys. Chem., **89**, 4338 (1985)

25. E. Budevski, G. Staikov, and W. J. Lorenz, Electrochemical phase formation and growth-an introduction to the initial stages of metal deposition, VCH Verlagsgesellschaft mbH (1996)

26. X. Cui, D. A. Hutt, and P. P. Conway, Thin solid films, **520**, 6095 (2012)

27. Y. -C. Sung, C. -H. Lai, S. -J. Lin, and S. -Y. Chang, Electrochem. and Solid-State Lett., **9**, C85 (2006)

28. R. Sard, J. Electrochem. Soc., **117**, 864 (1970)

29. H. -H. Hsu, J. -W. Yeh, and S. -J. Lin, J. Electrochem. Soc., **150**, C813 (2003)

30. T. Lim, H. -C. Koo, K. J. Park, M. J. Kim, S. -K. Kim, and J. J. Kim, J. Electrochem. Soc., **159**, D142 (2010)

31. C. H. Lee and J. J. Kim, J. Vac. Sci. Technol. B, **23**, 475 (2005)

32. Interconnection, ITRS roadmap (On-line document), 2007 edition, International Technology Roadmap for Semiconductors (2007)

33. L. Yang, T. Atanasova, A. Radisic, J. Deconinck, A. C. West, and P. Vereecken, Electrochim. Acta, **104**, 2428 (2013)

34. T. Sun, B. Yao, A. P. Warren, K. Barmak, M. F. Toney, R. E. Peale, and K. R. Coffey, Phys. Rev. B, **81**, 155454 (2010)

35. H. -D. Liu, Y. -P. Zhao, G. Ramanath, S. P. Murarka, G. -C. Wang, Thin solid films, **384**, 151 (2001)

36. S. M. Rossnagel and T. S. Kuan, J. Vac. Sci. Technol. B, **22**, 240 (2004).

37. C. V. Thompson, R. Carel, Mater. Sci. Eng. B, **32**, 211 (1995)

38. H. -C. Koo and J. J. Kim, J. Electrochem. Soc., **155**, D176 (2008)

39. Y. C. Ee, Z. Chen, L. Chan, A. K. H. See, S. B. Law, K. C. Tee, K. Y. Zeng, and L. Shen, Thin solid films, **462-463**, 197 (2004)

40. R. N. Bhattacharya, W. Batchelor, and R. N. Noufi, Electrochem. and Solid-State Lett., **2**, 222 (1999)

41. P. Mani, R. Srivastava, and P. Strasser, J. Phys. Chem. C, **112**, 2770 (2008)

42. H. -C. Koo, R. Saha, and P. A. Kohl, J. Electrochem. Soc., **159**, D319 (2012)

43. T. Osborn, N. Galiba, and P. A. Kohl, J. Electrochem. Soc., **156**, D226 (2009)

44. M. J. Kim, S. K. Cho, H. -C. Koo, T. Lim, K. J. Park, J. J. Kim, J. Electrochem. Soc., **157**, D564 (2010)

45. M. S. Kang, S. -K. Kim, K. Kim, and J. J. Kim, Thin solid films, **516**, 3761 (2008)

46. M. J. Kim, T. Lim, K. J. Park, S. K. Cho, S. -K. Kim, and J. J. Kim, J. Electrochem. Soc., **159**, D538 (2012)

47. M. J. Kim, T. Lim, K. J. Park, O. J. Kwon, S. -K. Kim, and J. J. Kim, J. Electrochem. Soc., **159**, D544 (2012)

48. C. H. Lee, A. R. Kim, S. -K. Kim, H. -C. Koo, S. K. Cho, and J. J. Kim, Electrochem. and Solid-State Lett., **11**, D18 (2008)

49. S. K. Cho, M. J. Kim, T. Lim, O. J. Kwon, and J. J. Kim, J. Vac. Sci. Technol. B, **29**, 1017 (2011)

50. T. -K. Eom, W. Sari, T. Cheon, S. -H. Kim, W. K. Kim, Thin solid films, **521**, 73 (2012)

51. T. P. Moffat and D. Josell, in Semiconductor FabTech 27th Edition, 133 (2005)

52. T. Iatabashi, H. Nakano, and H. Akahoshi, Prodeedings of the IEEE 2002 International, 285 (2002)

53. M. Paunovic, P. J. Bailey, R. G. Schad, and D. A. Smith, J. Electrochem. Soc., **141,** 1843 (1994)

54. H. -C. Pan and T. -E. Hsieh, J. Electrochem. Soc., **158**, P123 (2011)

55. A. C. West, C.- C. Cheng, and B. C. Baker, J. Electrochem. Soc., **145**, 3070 (1998)

56. A. C. West, J. Electrochem. Soc., 147, 227 (2000)

57. O. Luhn, C. Van Hoof, W. Ruythooren, and J. –P. Celis, Electrochim. Acta, 54, 2504 (2009)

58. R. Nagarajan, K. Prasad, L. Ebin and B. Narayanan, *Sensors and Actuators A*, **139**, 323 (2007)

59. K. W. Kok, W. J. Yoo, K. Sooriakumar and P. J. Sheng, *J. Vac. Sci. Technol. B* **20**, 1878 (2002)

60. J. Reid, Jpn. J. Appl. Phys., **40**, 2650 (2001)

61. S. M. Rossnagel and J. Hopwood, J. Vac. Sci. Technol. B, **12**, 449 (1994)

62. V. Vyas and M. J. Kushner, J. Vac. Sci. Technol. A, **24**, 1955 (2006)

63. R. Beica, C. Sharbono, and T. Ritzdorf, 58th Electronic Components and Technology Conference, **577** (2008)

64. Z. Wang, O. Yaegashi, H. Sakaue, T. Takahagi, and S. Shingubara, J. Electrochem. Soc., **151**, C781 (2004)

65. F. Inoue, Y. Harada, M. Koyanagi, T. Fukushima, K. Yamanoto, S. Tanaka, Z. Wang, S. Shingubara, Electrochem.Solid-State Lett., **12**, H381 (2009)

66. R. H. Nilson, and S. K. Griffiths, J. Electrochem. Soc., **150**, C401 (2003)

67. K. G. Jordan, and C. W. Tobias, J. Electrochem. Soc., **138**, 1933 (1991)

68. J. G. Kaufmann, M. P. Y. Desmulliez, Y. Tian, D. Price, M. Hoghes, N. Strusevich, C. Bailey, C. Liu, and D. Hutt, Microsyst. Technol., **15**, 1245 (2009)

69. K. M. Takahashi and M. E. Gross, J. Electrochem. Soc., **146**, 4499 (1999)

70. R. H. Nilson, and S. K. Griffiths, J. Electrochem. Soc., **149**, G286 (2002)

71. K. Kondo, K. Kojima, N. Ishido, and M. Irie, J. Electrochem. Soc., **140**, 1598-1600 (1993)

72. Aina Hung, J. electrochem. Soc., 132, **5** (1985), 1047-1049

73. F. Hanna, Z. A. Hamid, and A. A. Aal, Mater. Lett., **58**, 104-109 (2003)

74. C. H. Lee, S. C. Lee, and J. J. Kim, Electrochem. and Solid-State Lett., **8,** C110-C113 (2005)

75. C. H. Lee, S. C. Lee, and J. J. Kim, Electrochimica Acta, **50**, 3563-3568 (2005)

76. C. H. Lee, A. R. Kim, H. -C. Koo, J. J. Kim, J. Electrochem. Soc., **156**, D207-D210 (2009)

77. Z. Wang, O. Yaegashi, H. Sakaue, T. Takahagi, S. Shingubara, Jpn. J. Appl. Phys., **43**, 7000-7001 (2004)

78. Z. Wang, O. Yaegashi, H. Sakaue, T. Takahagi, S. Shingubara, J. Electrochem. Soc., **151,** C781-C785 (2004)

79. T. Lim, K. J. Park, M. J. Kim, H. -C. Koo, K. H. Kim, S. Choe, Y. -S. Lee, and J. J. Kim, J. Electrochem. Soc., **160**, D3015-D3020 (2013)

80. S. -L. Ko, J. -Y. Lin, Y. -Y. Wang, C. -C. Wan, Thin solid films, **516**, 5046-5051 (2008)

81. X. Wang, Z. Yang, N. Li, Z. Liu, Z. Yang, Z. Wang, J. Electrochem. Soc., **157**, D546-D549 (2010)

82. Z. Wang, R. Obata, H. Sakaue, T. Takahagi, S. Shingubara, Electrochmica Acta, **51**, 2442-2446 (2006)

83. M. Hasegawa, N. Yamachika, Y. S. -Diamand, Y. Okinaka, T. Osaka, Appl. Phys. Lett., **90**, 101916 (2007)

84. Zhifeng Yang, Na Li, Xu Wang, Zhixiang Wang, Zenglin Wang, Electrochem. and Solid-State Lett., **13**, D47-D49 (2010)

85. Li Zan, Z. Liu, Z. Yaong, and Z. Wang, Electochem. and Solid-State Lett., **14**, D107-D109 (2011)

86. M. Hasegawa, N. Yamachika, Y. Okinaka, Y. S. -Diamand, and T. Osaka, Electrochemistry (tokyo, Jpn.), **75**, 349 (2007)

87. X. Wang, Q. Shen, Z. Shu, Int. J. Electrochem. Sci., **8**, 4670-4678 (2013)

88. F. Hanna, Z. Abdel Hamid, and A. Abdel Aal, Mater. Lett., **58**, 104 (2003)

89. F. Inoue, H. Philipsen, A. Radisic, S. Armini, Y. Civale, S. Shingubara, and P. Leunissen, J.

Electrochem. Soc., **159**, D437-D441 (2012)

90. J. Li and P. Kohl, J. Electrochem. Soc., **149**, C631 (2002)

91. D. Plana, A. Campbell, S. patole, G. Shul, and R. Dryfe, Langmuir, **26**, 10334 (2010)

92. I. Ohno, Mater. Sci. Eng., A146, **33** (1991)

93. Y. -M. Lin and S. -C. Yen, Appl, Surf, Sci, **178**, 116 (2001)

94. S. Aksu and F. Doyle, J. Electrochem. Soc., **149**, B340 (2002)

95. Z. Jusys, R. Pauliukaite and A. Vaskelis, Phys. Chem. Chem. Phys., **1**, 313 (1999)

96. R. Pauliukaite, G. Stalinionis, Z. Jusys, and A. Vaskelis, J. Appl. Electochem., **36**, 1261 (2006)

97. C. H. Lee, S. Hwang, S. –C. Kim, and J. J. Kim, Electrochem. Solid-State Lett, **9**, C157 (2006).

98. Bohren, C. F.; Huffman, D. R., Absorption and scattering of light by small particles, p 541, Wiley-Interscience, New York (1983).

99. R Manu, Sobha Jayakrishnan, bull. Mater. Sci., **34**, 347-356 (2011)

100. S. -L. Ko, J. -Y. Lin, Y.-Y. Wang, C. -C. Wan, Thin solid films, **516**, 5046 (2008)

101. P. P. Lau, C. C. Wong, and L. Chan, Appl. Surf. Sci., **253**, 2357 (2006)

102. T. Tsunoda, T. Okabe, and H. Honma, J. Electrochem. Soc., **151**, C610 (2004)

국문 초록

구리 무전해 도금은 극대규모 집적 회로의 구리 배선을 비롯하여 다양한 분야에 응용될 수 있다. 이를 위해서 용액의 특성에 관한 이해와 측정이 필수적이며, 다양한 인시츄 또는 익스시츄 분석 방법이 보고되었다.

본 연구에서는 틴-팔라듐 콜로이드를 이용하여 용액의 안정성과 반응성을 측정하는 인시츄 투과율 측정방법을 제안하고 가용성에 대하여 고찰하였다. 이 방법은 간단하면서도 시간에 따른 특성 분석이 가능하다는 장점을 가지고 있다. 구리 입자와 박막의 물성 관계를 관찰하거나 관통 실리콘 비아에서 씨앗층 형성하는데 적용할 수 있는 용액을 개발하는 데에 본 측정방법을 응용하였다.

먼저, 구리 무전해 도금 용액의 기본적인 거동을 확인하기 위하여 틴-팔라듐 콜로이드 용액을 주입하여 투과율 변화 및 구리 입자의 크기 변화를 관찰하였다. 투과율과 구리 입자 성장의 관계를 기반으로 안정성과 반응성 등의 용액 성능을 결정하는 중요한 요소인 착화제, 산화제, 첨가제의 영향을 확인하였다.

착화제의 특성 평가에서는 인시츄 투과율 측정이 각 용액의 안정성과 반응성을 잘 나타내 준다는 것을 확인하였다. 또한, 틴-팔라듐 촉매를 사용했기 때문에 실제 반응 환경을 반영할 수 있음을 보여주었다. 이러한 결과는 탄탈륨 기판에서 전착한 박막에서의 결과와 비교함으로써 본 측정 방법의 실용성을 증명하였다.

같은 방법으로 산화제를 평가하였다. 알데하이드를 기반으로 하는 산화제의

경우 비슷한 투과율 곡선과 구리 입자의 특성을 보였고, 이를 통해 반응성을 예측할 수 있었다. 반면에, 나머지 산화제는 특성 평가에 제한적이었는데, 이는 장비 개선을 통해 해결 될 수 있을 것으로 예상한다. 이러한 결과들은 더 다양한 용액에 적용이 가능하다는 것을 시사하였다.

구리 수퍼필링에 일반적으로 사용되는 유기 첨가제들이 반응성에 주는 영향을 확인하였다. 투과율 곡선의 변화는 가속 및 감속 효과를 모두 보여주었고, 작용하는 농도 범위 또한 실제 구리 박막 전착에서와 일치하였다. 또한, 구리 입자의 관찰을 통해서도 용액의 반응성 및 구리 박막의 표면 거칠기를 어느 정도 예상할 수 있었다. 본 측정법의 한 응용으로써, 인시츄 측정으로부터 얻은 구리 입자들과 구리 박막의 물성을 측정하고 비교하였다. 완벽하게 정량적인 비교는 어려웠지만 그레인 크기와 표면 거칠기 측면에서 상당한 관계를 가지고 있음을 확인하였다.

다른 응용을 위해, 본 투과율 측정법을 통해 우수한 안정성과 반응성을 확인 한 용액 들 중에 EDTA-HCHO를 기반으로 한 용액을 선택하였다. 이 용액을 이용하여 높은 종횡비를 갖는 비아에서 구리 씨앗층을 형성하고자 하였다. 안정성을 좀 더 향상 시키기 위하여 RE-610과 2,2’-다이피리딜을 첨가해서 박막을 전착하였다. 구조적인 단점을 가지고 있는 비-보쉬 비아는 최적화된 공정을 요구하였다. 그의 일환으로 강제 대류 시스템을 도입하고 전처리 시간을 최적화 하였다. 이를 통해, 등각전착된 구리 씨앗층을 얻었고, 전해도금을 통해 결함 없는 채움을 얻을 수 있었다.

결론적으로, 본 연구에서 제안된 인시츄 투과율 측정법은 다양한 용액의 성능 측정뿐 만 아니라 물성 예측에도 적용 가능한 것을 확인하였다. 또한, 구리 배선에서 다양한 분야에 적용될 수 있음을 시사하였다.

주요어: 무전해 도금, 구리, 안정성, 반응성, 인시츄 분석, 착화제, 산화제, 유기 첨가제, 박막 특성, 씨앗층

학 번: 2008-21073

Appendix I - White Pigment in Electronic Paper

Preparation of PS/TiO_2 as a white pigment for electrophoretic displays

I. Introduction

Electronic paper (e-paper), proposed by B. Comiskey in the 1970s,[A1] has arisen as a promising candidate for paper-like displays. It has remarkable advantages compared to conventional displays, such as portability, high brightness, high contrast ratio, long-term stability and low power consumption.[A1-A3] E-paper is composed of two parts: a thin film transistor (TFT), which controls the E-paper by generating an electric field, and microcapsules or micro-compartments that encapsulate nanosized charged pigments dispersed in a dielectric media with low dielectric constant. When an electric field is applied between two electrodes by the TFT, the charged particles migrate from one electrode to the other, based on their relative charge. Technology for the production of TFT electrodes from the liquid crystal display (LCD) and semiconductor device industry can be easily adapted.[A2-A3] However, the technology for the production of a charged pigment has not yet been fully established. Thus, the development of a charged particle with improved long-term stability, optical characteristics, and dynamic characteristics, is still a key issue for enhancing the performance of E-paper.

Long-term stability can be obtained by adjusting the density of a pigment to that of the dielectric liquid, or by introducing a stabilizing agent that causes steric hindrance among the particles.[A4-A5] The enhanced stability of suspension allows images to be maintained, even in the off-state. In order to obtain good optical characteristics of the pigment, which is represented by a high contrast ratio, it is important to select a proper material for the pigment, and to retain its property during operation.[A5] The dynamic characteristics, represented by the response time, are intimately related to the surface charge of the pigment,[A6-A8] with higher absolute value in surface charge corresponding to faster transfer to the electrode. Conventionally, the surface charge expressed by zetapotential can be modified by the addition of a charge control agent (CCA), such as anionic, cationic, or polymeric surfactants. The zetapotential of pigments is defined by the molecular structure of the surfactant, the direction of adsorption, and the amount of adsorbate.[7-8A7-A8] The surface charge of pigment with CCA is shifted negatively or positively, depending on the CCA. Thus the CCA enables the pigment to have the desirable zetapotential under various conditions.

Among various pigments, titanium oxide (TiO_2) has been adopted as the raw material for white pigment, because it has a high refractive index, which determines the whiteness of the color. To be used as a pigment, TiO_2 (4.2 g/cm^3) should be modified to have a lower density than in its natural state. Polymer coating has been introduced for lowering the density, so that density similar to that of dielectric media can be obtained.[A2-A6,A9-A14] However, polymer coating causes

deterioration of the reflectance of TiO_2, which has led to inverse structures like polymer/TiO_2 [A12,A14] being suggested to preserve the optical characteristics of TiO_2. This concept can be used to control the density of TiO_2 particles without deteriorating its reflectance. However, the zetapotential control, which is strongly dependent on the surface characteristics, became vibrant with the new structure. Studies on the zetapotential control of polymer/TiO_2 and the mechanism of the adsorption of CCA on TiO_2 have been lacking.

In this study, we propose two types of surface treatment processes of polymer/TiO_2 for high zetapotential; the addition of ionic and non-ionic surfactants and the surface modification by silane-based surfactants. We reported on how the zetapotential is affected by silane-based surfactants with an amino group and organic acid and the adsorption of various surfactants under various concentrations. The mechanism of how the surfactant and organic acid affect the zetapotential is discussed. In addition, the effects of dielectric fluid were considered with the addition of surfactants.

II. Experimental

2.1. Materials

Polystyrene (PS) with a mean diameter of 200 nm was purchased as a latex microsphere suspension from Thermo Scientific. It was dispersed in deionized (D. I.) water (10 wt.%), with divinylbenzene (DVB) for better dispersion. Titanium (IV) butoxide (TBO, 97%), (3-aminopropyl)triethoxy silane (APTES), ethyltriethoxy silane (ETES), (3-Aminopropyl)trimethoxysilane (APTMS), N-[3-(Trimethoxysilyl)propyl]ethylenediamine (AEAPTMS), tetraoctylammonium bromide (TOAB), Span 80 and tetrachloroethylene (TCE, >99%) were adapted from Sigma Aldrich. Acetic acid (99.7%) was obtained from JUNSEI, and ethanol (EtOH, 97%) was supplied by DAEJUNG. Isopar G manufactured by Exxon mobile and Halo C oil 0.8 made by Halocarbon®, and OLOA 1200 by the Chevron Chemical Co. were used.

2.2. Preparation of PS/TiO_2 particles

TiO_2 coated PS nanoparticles were prepared by the hydrolysis reaction of TBO in a solvent mixture of EtOH and distilled water. The surface coverage of TiO_2 on PS was controlled by varying the solvent mixture composition, or the concentration of TBO. The composition of solvent mixture (EtOH:distilled water) was altered from 0:1 to 1:0, and the concentration of

TBO was varied in the range of 0.01 M to 1.0 M. TBO was added to the solvent mixture with vigorous stirring. After 0.5 g of PS latex particles was dispersed in the solution, ultrasound was applied for 30 min, leading to the hydrolysis reaction of TBO. The TiO_2 coated PS was separated by centrifugation (4000 rpm), and dried at room temperature for 12 hrs, followed by post-heat treatment performed at 80℃ for 2 hrs.

2.3. Treatment of PS/TiO_2 particles with additives

There were three kinds of surfactants, tetraoctylammonium bromide (TOAB), Span 80, and OLOA1200, which were added to prepared solution. For the surface modification, 0.11 g of PS/TiO_2 particles was dispersed in 4 ml of TCE through the ball-milling process (370 rpm) for 10 min. An additional 12 ml of TCE and various concentrations of ETES, APTES, APTMS, and AEAPTMS were added. The mixture was heated to 50℃ with stirring, which was maintained for 6 hrs. To separate the PS/TiO_2, centrifugation (10 min) was carried out twice at 8000 rpm. After dried in a vacuum oven at 40℃ for 5 hrs, the particles were re-dispersed in TCE with acetic acid, to measure the zetapotential.

2.4. Characterization

For the qualitative characterization of PS/TiO_2, transmission electron microscope (TEM, JEM-3000F) and X-ray photoelectron spectroscope (XPS, AXIS-His) analyses were conducted. Fourier transform infrared (FT-IR, Nicolet 6700) spectra were collected, to characterize the surface functional groups attached to the TiO_2 surface. The surface charge of a treated PS/TiO_2 was measured in TCE media by a zetapotential analyzer (ELS-Z, Ostuka).

III. Results and discussion

TiO_2 coating on PS is an essential process for adjusting the density of PS (1.1 g/cm^3) to that of dielectric fluid (TCE, 1.6 g/cm^3). TiO_2 can be synthesized by the hydrolysis reaction and the condensation reaction of TBO ($Ti(O^tBu)_4$), as described below.[A15-A16]

Hydrolysis reaction: $Ti(O^tBu)_4 + 4H_2O \leftrightarrow Ti(OH)_4 + 4(Bu)OH$ ---------- (1)

Condensation reaction: $Ti(OH)_4 \leftrightarrow TiO_2(s) + 2H_2O$ ---------- (2)

Fig. A1 represents the TEM images of as-prepared PS and PS/TiO_2 particles, synthesized by varying the ratio of EtOH and H_2O from 1:0 to 0:1 before carrying out the surface modification with APTES. TiO_2 coating on PS can be achieved by several factors such as zetapotential difference, ultrasonic effect and heat treatment.[A12,A14] As-prepared PS particles have spherical shape with a size of 200 nm, as shown in Fig. A1(a). Despite changes in the shape and size, compared to the as-prepared PS, it was confirmed for PS/TiO_2 that Ti was uniformly distributed over the PS surface from the line scanning images, as shown in the insets of Figs. A1 (b)-(d). In addition, the XPS spectrum of Ti shown in Fig. A2 also demonstrated the formation of TiO_2, exhibiting peaks of Ti $2p_{1/2}$ located at 465 eV, and $2p_{3/2}$ at 459.2 eV.[A17-A18]

The density of PS/TiO_2 was controlled for matching its density to that of TCE (1.6 g/cm^3), by changing the ratio of EtOH to H_2O, and the concentration of TBO. First, the effect of the ratio of EtOH to H_2O on the density of PS/TiO_2 was studied. As shown in Fig. A3 (a), the

density of PS/TiO_2 increased after the TiO_2 coating, because the density of TiO_2 is higher than that of PS. Although it was expected for the density to increase according to the H_2O content because of the enhanced hydrolysis reaction, the density showed the opposite trend. The particle density decreased from 1.71 g/cm^3 to 1.56 g/cm^3 with the increase in H_2O content. It is well known that the hydrolysis reaction of titanium tetrabutoxide ($Ti(O^tBu)_4$) to $Ti(OH)_4$ in water is favorable, while the condensation of $Ti(OH)_4$ to TiO_2 is restricted in high concentrations of H_2O.[A19] From the experimental results of this study, and a conclusion from the reference,[A15] we could infer that the condensation reaction is more strongly affected by the H_2O content. Therefore, in this study, the density of PS/TiO_2 decreased in high concentrations of H_2O, for the same reaction time of 30 min.

To consider the dispersity of PS/TiO_2, which is highly related to the stability of the pigment, the size distribution was compared in TCE. Fig A3 (b) indicates that the PS/TiO_2 prepared in EtOH-rich solution resulted in a narrow size distribution in TCE, because EtOH brought about enhanced dispersion of TBO, preventing the formation of aggregated TiO_2 on the PS surface.[A20]

We also tried to control the density of PS/TiO_2 by varying the TBO concentration. Experiments were performed with a 1:1 ratio of EtOH and H_2O. As shown in Fig. A4, the density of PS/TiO_2 was proportional to the TBO concentration, as expected. Based on the relationship, a density of 1.59 g/cm^3, which matches that of TCE, could be obtained with 0.24

M of TBO. By controlling the density of PS/TiO_2 while varying the $EtOH/H_2O$ ratio and TBO concentration, the density and the size distribution could be adjusted successfully.

As a second step for the preparation of a positively charged white pigment, surface modification of the density-controlled PS/TiO_2 was carried out with 0.1 M APTES, which contains silane and amine functional groups. It was expected that APTES functions as a cationic surfactant in the presence of protons dissociated from acetic acid, as suggested by Park *et al.*[A21] APTES is adsorbed by reciprocal action with TiO_2, and change in the zetapotential takes place by the interaction between the amine functional group attached at the end of the APTES and the proton from the acetic acid, as shown in Fig. A5. FT-IR analysis of PS/TiO_2 and PS/TiO_2 treated with APTES supported the interaction between APTES and TiO_2, as shown in Fig. A6. In the PS/TiO_2 spectra, O-H stretching at 3350-3500 cm^{-1}, C-H stretching at 2800-3000 cm^{-1}, $–CH_2$ stretching at 2935 cm^{-1}, and C=C stretching at 1600 cm^{-1} were observed.[A4] After the surface modification with APTES, strong Si-O-Si stretching around 1090 cm^{-1} and N-H stretching at 3400 cm^{-1} newly appeared, while –OH stretching decreased. In particular, Si-O-Si stretching corresponds to siloxane groups originating from polymerized APTES on the Ti surface, as described in Fig A6.[A22] Thus, it can be concluded that the APTES was grafted onto the Ti surface initiated from the –OH on Ti, with the remaining $–NH_2$ at the end group.

The solid triangles in Fig. A7 describe the zetapotential of PS/TiO_2 treated with 0.1 M APTES, which increased from -41 mV to 75 mV, according to the concentration of acetic acid.

To elucidate the function of the amine group and proton, zetapotential measurements were carried out under two different conditions. First, the zetapotential measurement of as-prepared PS/TiO_2 without surfactant was performed, with the addition of the acetic acid that provides proton, as shown in Fig. A7. No change in zetapotential was observed for different concentrations of acetic acid, which means the proton itself has no influence on the surface charge of PS/TiO_2 without APTES. Secondly, PS/TiO_2 treated with 0.1 M ETES was tested, to examine the zetapotential with the addition of acetic acid, as indicated by circles in Fig. A7. Unlike with APTES, the zetapotential was independent of the acetic acid concentration with ETES. ETES has the same structure as APTES, except for an amine functional group, as summarized in Table 1. Thus, this result provides a clue about the role of the amine functional group. Considering that ETES did not show a positive shift in zetapotential, even with a high concentration of acetic acid, it becomes apparent that the combination of an amine group and a proton are keys making a positive shift of the zetapotential of PS/TiO_2.

After we confirmed the role of APTES and acetic acid in the zetapotential, the effect of the concentration of APTES was considered. Fig. A8 illustrates the variation of the zetapotential with changes in concentration of APTES from 0.05 M to 0.4 M. In all cases, an increase in zetapotential to a positive value was observed. At 0.05 M APTES concentration, the zetapotential was raised up to 30 mV. In contrast, a relatively great increase of about 120 mV was shown with 0.1 M APTES concentration. However, at a higher concentration of APTES

over 0.1 M, the zetapotential was saturated at 30~44 mV again. It has been reported that a high concentration of APTES leads to the formation of thick silicone organic copolymer.[A23] This might lead to the decrease in adsorption sites for protons, which could result in the relatively smaller increment of the zetapotential at high concentration of APTES. From these results, it could be speculated that 0.1 M APTES is a suitable concentration to cover the PS/TiO_2, supplying the maximum sites to combine the protons.

In addition, the comparison of optimized condition with APTES was performed with 0.1 M APTMS and AEAPTMS to contemplate the effect of structural characteristics of surfactants on zetapotential. APTMS has similar structure, however it has methoxy group, and AEAPTMS is one of the methoxy silane based surfactant with two amine groups. Fig. A9 presented the zetapotential changes with 0.1 M APTES and APTMS. The zetapotential was almost linearly increased with APTES. However, with APTMS, the initial zetapotential before the addition of acetic acid was very negative about -72 mV, which is thought to be due to the different surface state. When 0.29 M acetic acid was added, the zetapotential was shifted to positive direction to -27 mV, whereas it was saturated even at high concentration of acetic acid. It was because the relatively bulky surfactants served decreased and limited adsorption probability.[A24] Besides, the effects of number of amine functional group on the zetapotential was also considered by comparison of 0.1 M APTMS and AEAPTMS that has two amine groups as summarized in Table A1. As compared in Fig. A10, clear difference could be observed in the zetapotential as a

function of acetic acid. Initial zetapotential of them were similar. However, gradual shift to positive direction was observed with AEAPTMS treated PS/TiO_2 to 20 mV according to the concentration of acetic acid. Since the zetapotential changes happened with the combination of proton and amine group of surfactants, higher number of amines supported the adsorption site for proton combination so that the zetapotential continuously increased.[A25] Consequently, it was found that the zetapotential was affected by the structure characteristics and the functional groups of surfactants. Finally, PS/TiO_2 prepared in a mixture of EtOH and H_2O with 0.24 M TBO thus had 1.6 g/cm^3 in density, and showed 75 mV in zetapotential at 0.1 M APTES and 5 M acetic acid in TCE.

As a second method for the control of zetapotential, ionic and non-ionic surfactants such as OLOA 1200, TOAB and Span 80 were added to PS/TiO_2 dispersed in TCE as marked by square in Fig.A11. The molecular structures of surfactants were described in Table A2. When OLOA 1200 was added to 5 wt. %, the zetapotential was decreased from -2 mV to -60 mV and saturated, whereas the lowest value and saturation tendency were observed in the presence of TOAB and Span 80 despite the difference in the concentration range. The saturated value was 10mV with TOAB and 0 mV with Span 80. The surface area that can be covered by surfactants is limited so that the change of zetapotential became decreased at high concentration of surfactants. It was found that the achievement of positively charged PS/TiO_2 with high absolute value over 50 mV was hard with PS/TiO_2 in TCE. Therefore, in addition to the roles of

surfactants, the effects of characteristics of solvents, dielectric fluids, were considered with cyclohexane, Halo C oil 0.8, and Isopar G that has different properties as shown in Table 3. Especially, the mixture of dielectric fluids such as cyclohexane+TCE (v:v=8:2) or Halo C oil 0.8+Isopar G (v:v=1:1).[A2,A3,A5] The densities of mixed dielectric fluids were 1.28 g/cm^3 and 1.23 g/cm^3, respectively. Using these dielectric fluids, the change of zetapotential of as-prepared PS/TiO_2 (1.6 g/cm^3) was observed with surfactants as presented in Fig. A11. It was noted that TOAB was not soluble to Halo C oil 0.8 + Isopar G. As compared to the behaviors of zetapotential changes with same surfactants used for TCE in different dielectric fluids, it was so difficult to explain those phenomena by consistent theory or hypothesis. In the case of OLOA 1200, PS/TiO_2 had 70 mV of zetapotential in cyclohexane+TCE whereas negative changes were observed with other dielectric fluids. However, the addition of TOAB in cyclohexane+TCE showed opposite trends to decreased and saturated to 0 mV. Considering the Span 80 case, there was no significant changes in zetapotential with mixed dielectric fluids. Therefore, further study to verify the roles of dielectric fluids on the determination of surface charge or the adsorption behaviors is required. One more thing that should be contemplated is the density difference between PS/TiO_2 and dielectric fluids. The density of PS/TiO_2 used above conditions was controlled to 1.6 g/cm^3, which is the density of TCE. Fig. A12 and A13 indicated the effect of density difference on the zetapotential. Square marks meant the zetapotential with 1.6 g/cm^3 of PS/TiO_2, and circle represented the zetapotential measured with 1.28 g/cm^3 of PS/TiO_2 ,which

were controlled to the similar density of dielectric fluids. In Halo C oil 0.8 + Isopar G as shown in Fig. A12, the change tendency was not significantly altered despite of the density difference with the addition of both OLOA 1200 and Span 80. However, positive shift about 10 mV was observed with Span 80. In contrast, when cyclohexane+TCE was used as a dielectric fluid, completely different with the addition of both OLOA 1200 and Span 80 as Fig. A13 depicted. Although 2.4 wt.% of OLOA addition led to 70 mV of zetapotential, it was changed to -60mV after control the density of PS/TiO_2 to that of dielectric fluid. In the same way, the addition of 0.25 wt. % of Span 80 showed 0 mV, however, it shifted to 25 mV after density control.

Given that the stability in dielectric fluid that is represented by density matching and the surface charge of PS/TiO_2, the surface modification with silane-based surfactants resulted in the outstanding improvements both on the dispersity and the zetapotential than the addition of ionic and non-ionic surfactants.

Table A1. Characteristics of Silane-based Surfactants

Name	Oxyl structure	Number of amine	Molecular structure
Ethyltriethoxysilane (ETES)	Ethoxy	0	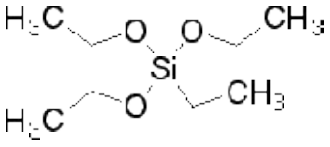
3-aminopropyltriethoxysilane (APTES)	Ethoxy	1	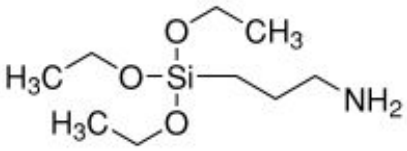
3-aminopropyltrimethoxysilane (APTMS)	Methoxy	1	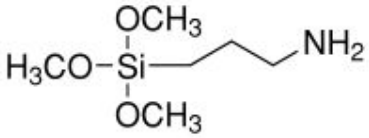
N-[3-(Trimethoxysilyl)propyl] ethylenediamine [AEAPTMS]	Methoxy	2	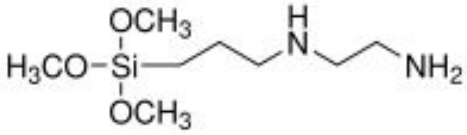

Table A2. Characteristics of Ionic and Non-ionic Surfactants

Name	Molecular structure
OLOA 1200	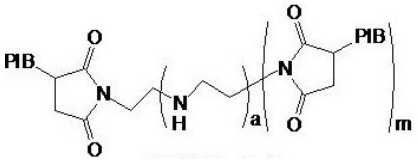
Tetraoctylammonium bromide (TOAB)	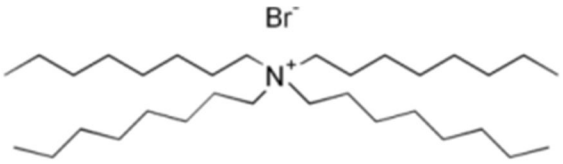
Span 80	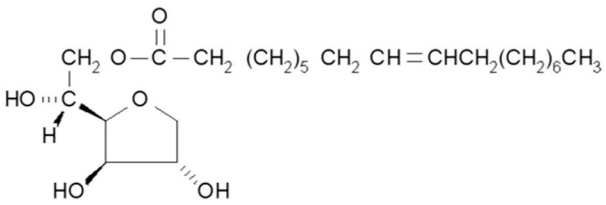

Table 3. Properties of Dielectric Fluids

Name	Molecular structure	Density (g/cm^3)	Dielectric constant
Tetrachloroethylene	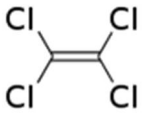	1.6	2.5
Halo C oil 0.8 (polychlorotrifluoroethylene)	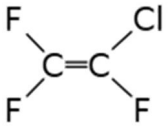	1.71	2.25
Isopar G (Isoparaffinic hydrocarbon solvent)		0.748	1.995-2.006
Cyclohexane		0.779	2.023

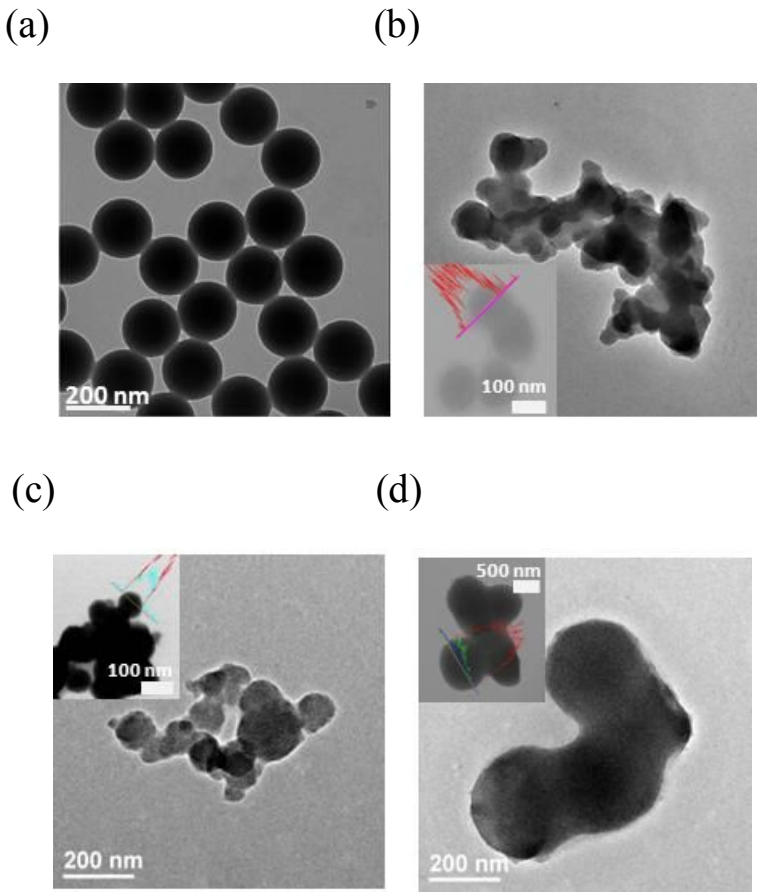

Fig. A1. TEM images of PS/TiO_2 and the distribution of Ti on the PS according to the ratio of EtOH and H_2O (EtOH:H_2O). (a) as-prepared PS, (b) 1:0, (c) 1:1, and (d) 0:1. The image inserts show the line scans of Ti observed by EDX.

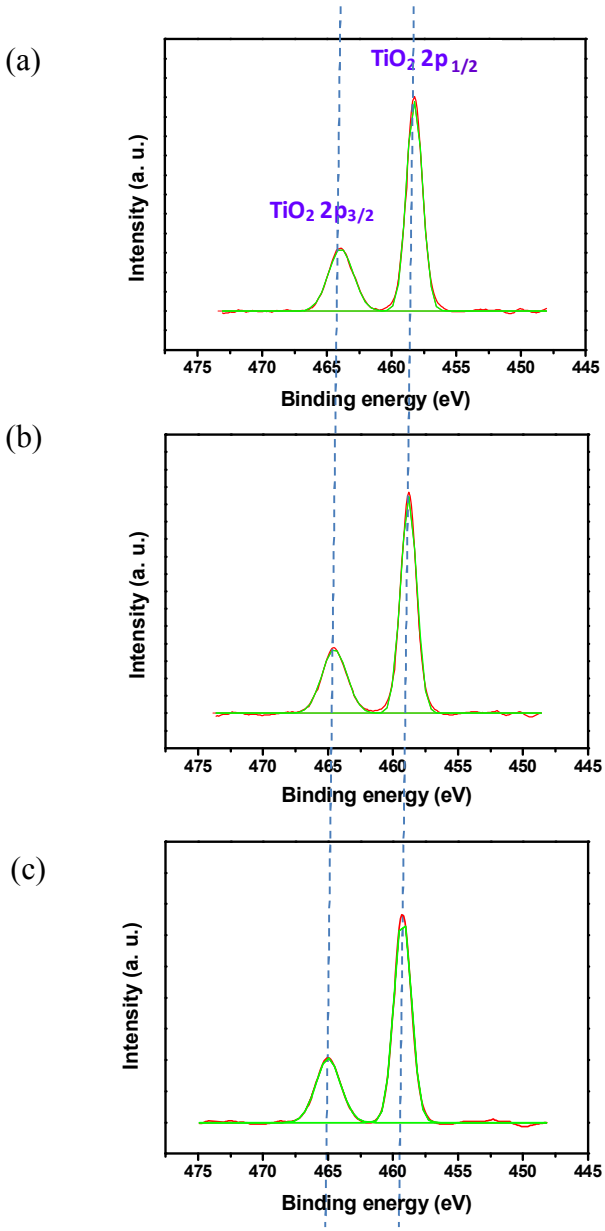

Fig. A2. XPS spectra taken from the samples prepared at various ratio of EtOH and H_2O to confirm the TiO_2 coating on PS (a) 1:0, (b) 1:1, and (c) 0:1.

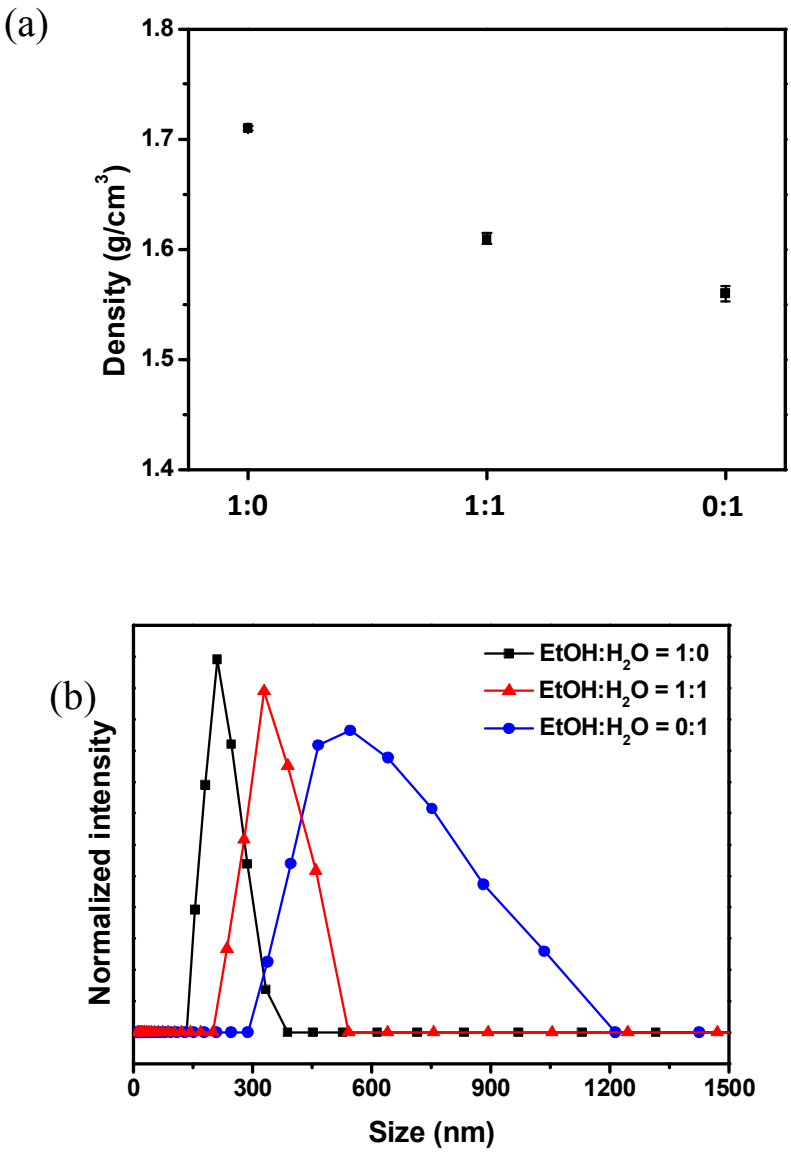

Fig. A3. (a) Density changes of PS/TiO_2, and (b) the size distribution, according to the ratio of EtOH and H_2O.

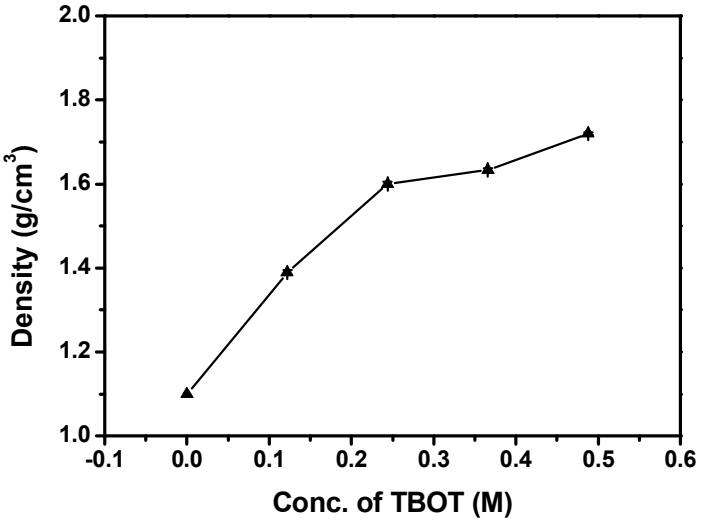

Fig. A4. The changes of PS/TiO_2 density as a function of concentration of TBO.

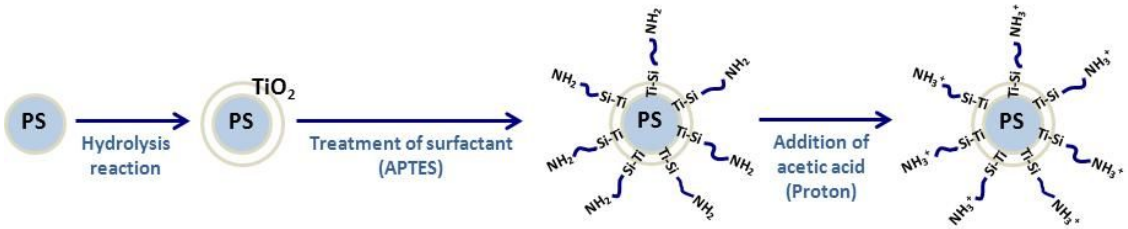

Fig. A5. The proposed mechanism for preparing white pigments with positive charge.

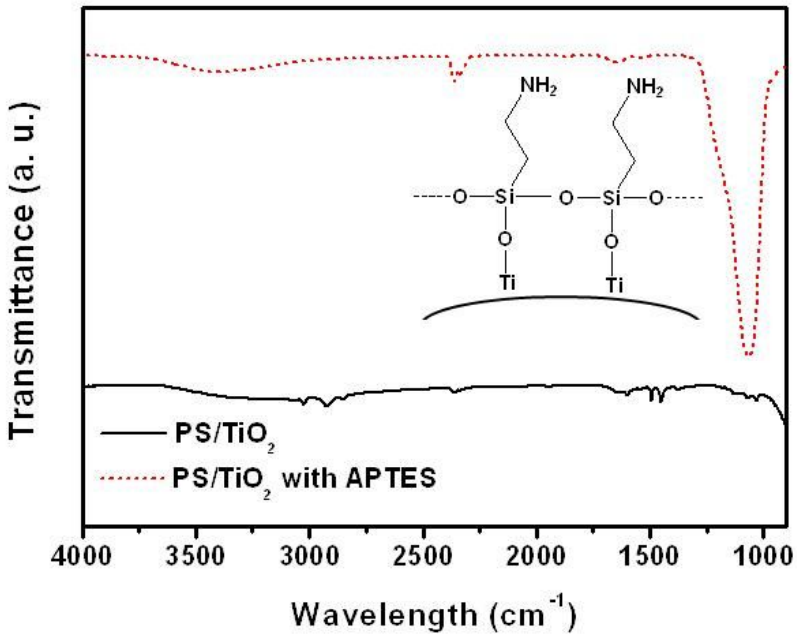

Fig. A6. FT-IR spectra of PS/TiO_2 and PS/TiO_2 treated with APTES.

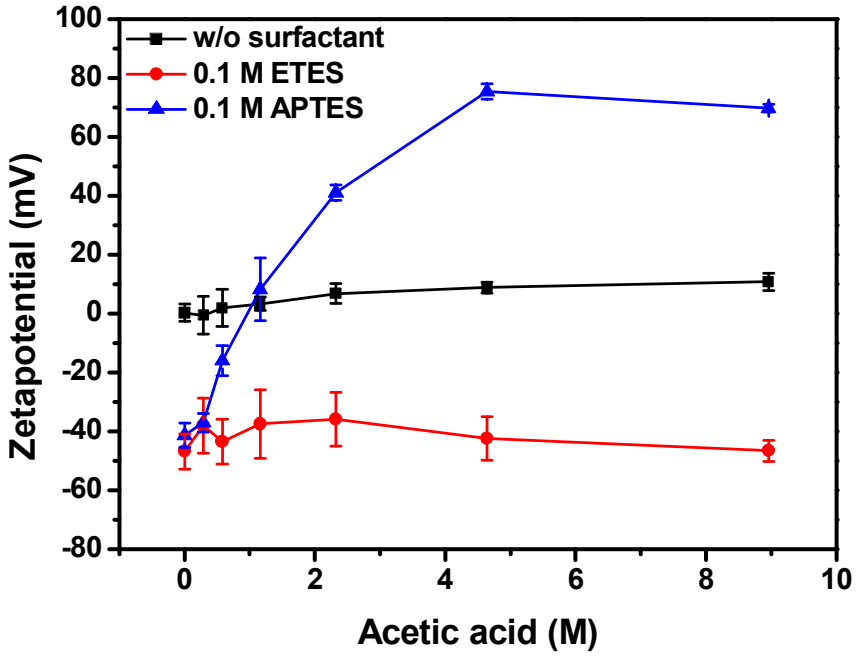

Fig. A7. The effects of the surfactant and the amine functional group on the zetapotential of PS/TiO_2.

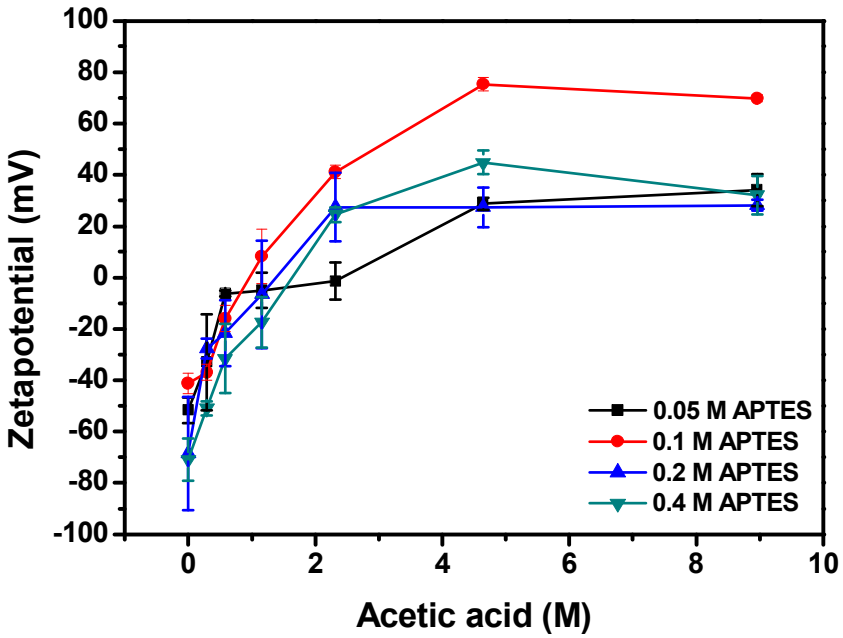

Fig. A8. Zetapotential changes according to the acetic acid concentration at various APTES concentrations.

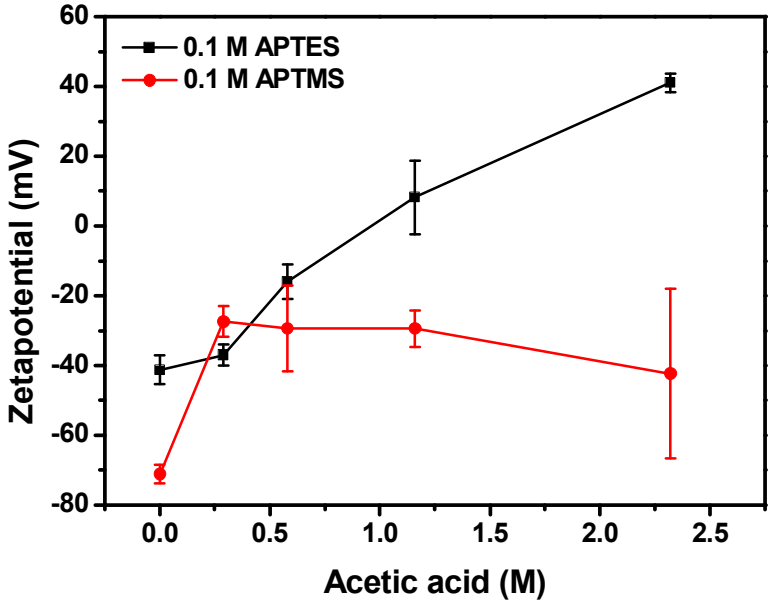

Fig. A9. Zetapotential changes according to the acetic acid concentration with 0.1 M APTES and 0.1 M APTMS.

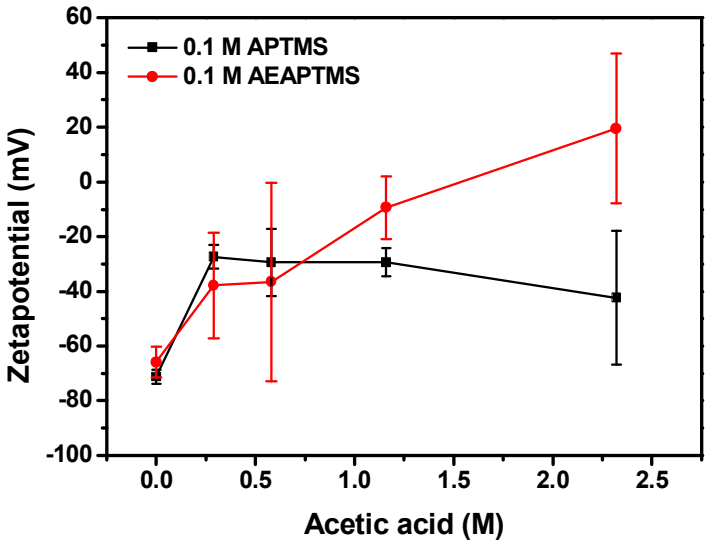

Fig. A10. Zetapotential changes according to the acetic acid concentration with 0.1 M APTMS and 0.1 M AEAPTMS.

(a)

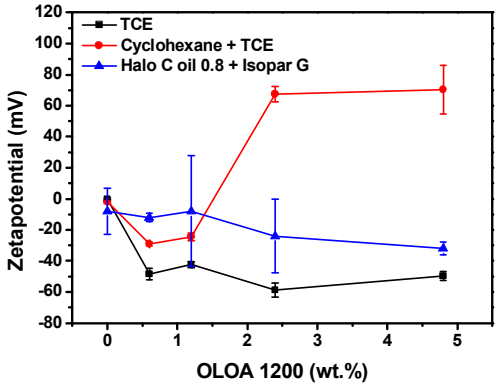

(b)

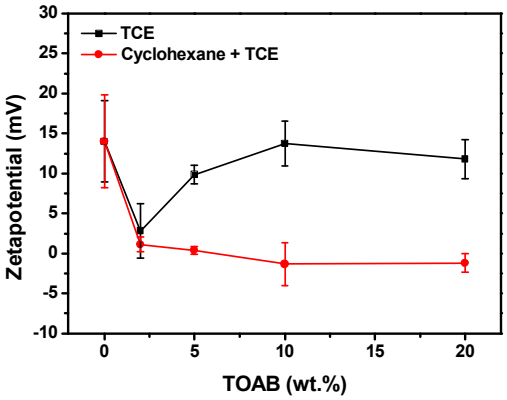

(c)

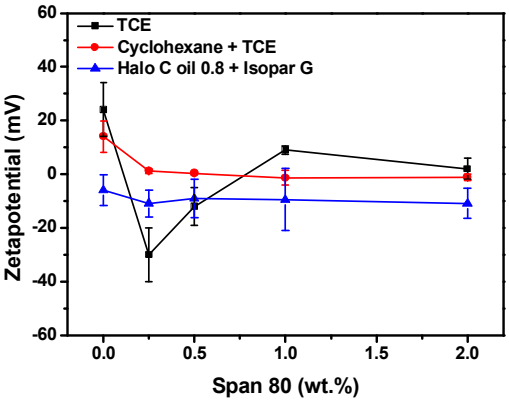

Fig. A11. Zetapotential changes of PS/TiO_2 with the addition of OLOA1200, TOAB, and Span 80 dispersed in different dielectric fluids; TCE, Cyclohexane + TCE (v:v=8:2), and Halo C oil 0.8 + Isopar G (v:v=1:1).

(a)

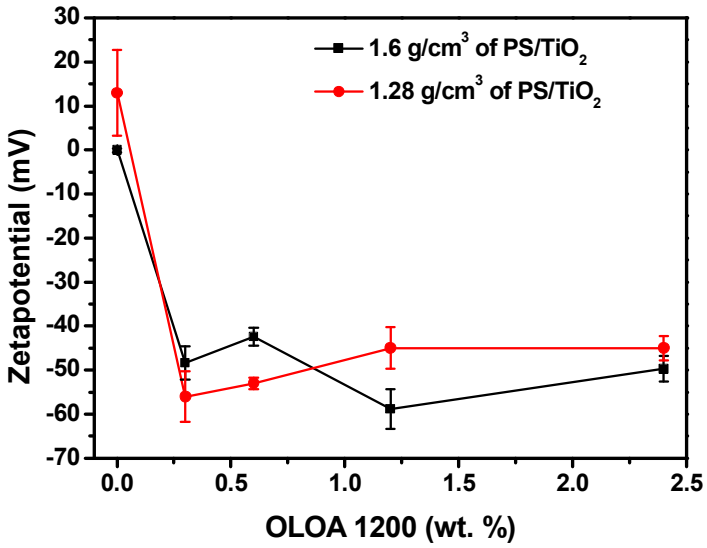

(b)

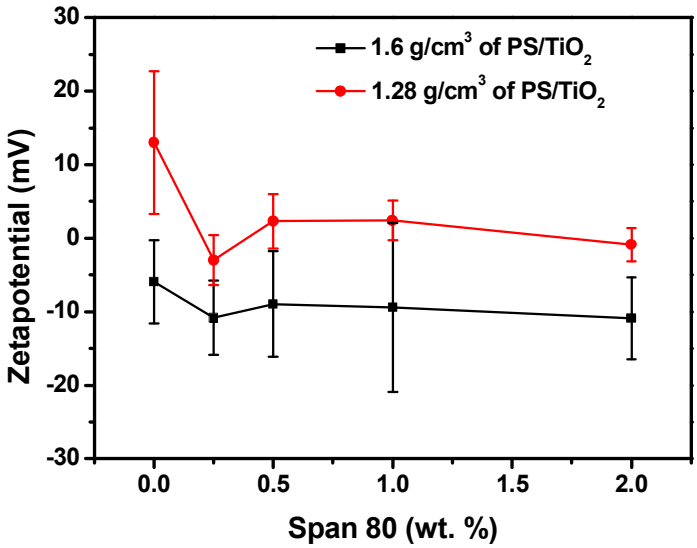

Fig. A12. Effects of PS/TiO_2 density on zetapotential dispersed in Halo C oil 0.8 + Isopar G with the addition of (a) OLOA 1200 and (b) Span 80.

(a)

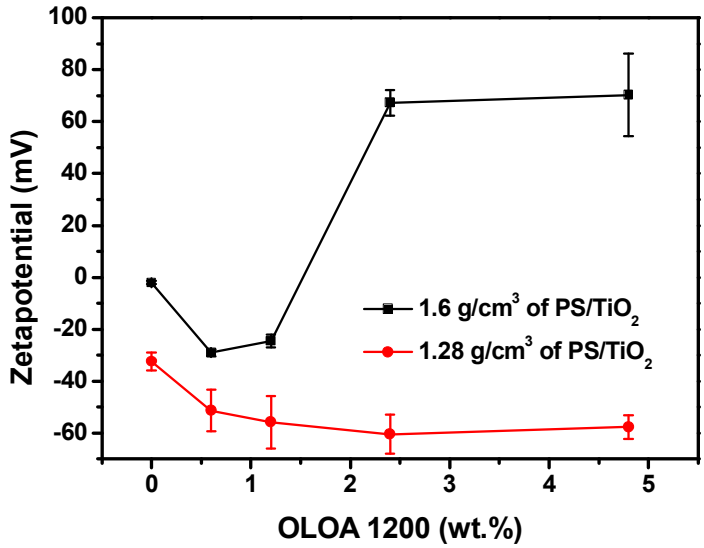

(b)

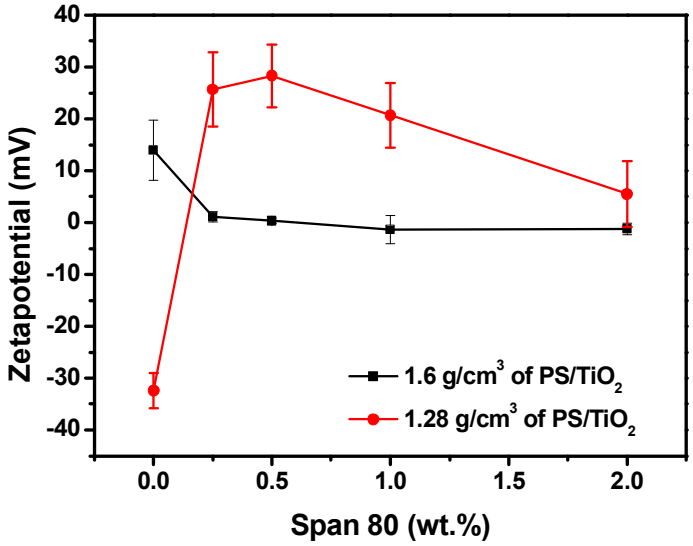

Fig. A13. Effects of PS/TiO_2 density on zetapotential dispersed in Cyclohexane + TCE with the addition of (a) OLOA 1200 and (b) Span 80.

IV. Conclusion

PS/TiO_2 particles were prepared for use as a white pigment in electronic displays. PS/TiO_2 could be obtained by the hydrolysis reaction of TBO, in a mixture of EtOH and H_2O. Changing the ratio of EtOH and H_2O, and the concentration of TBO, can be used to obtain a density of PS/TiO_2 that matches the density of TCE (1.6 g/cm^3). To achieve the positive surface charge of PS/TiO_2, its surface was modified with silane-based surfactants, which has an amino group. The positive shift of zetapotential is ascribed to the interaction between the amine group at the end of the grafted surfactants, and the proton that came from acetic acid. Finally, we achieved PS/TiO_2 with a density of 1.6 g/cm^2 and a zetapotential of 75 mV with the treatment of APTES. In other trials to make positively charged PS/TiO_2 by the addition of ionic and non-ionic surfactants, it was hard to obtain required zetapotential with the stability in dielectric fluids. Therefore, it was found that the surface modification with APTES and the addition of acetic acid satisfied the required properties for PS/TiO_2 for use as a white pigment in TCE.

V. References

A1. B. Comiskey, J. D. Albert, H. Yoshizawa, J. Jacobson, Nature **394** (1998) 253.

A2. C. A. Kim, M. K. Kim, M. J. Joung, S. D. Ahn, S.-Y. Kang, Y. E. Lee, K. S. Suh, J. Ind. Eng. Chem. **9** (2003) 674.

A3. D.-G. Yu, S.-H, Kim, J.-H An, J. Ind. Eng. Chem. **13** (2007) 438.

A4. B. Peng, F. Tang, D. Chen, X. Ren, X. Meng, J. Ren, J. Colloid Interface Sci. **329** (2009) 62.

A5. G. Yin, Z. Zheng, H. Wang, Q. Du, J. Colloid Interface Sci. **361** (2011) 456.

A6. C. A. Kim, S.-Y. Kang, G. H. Kim, S. D. Ahn, J. Oh, K. S. Suh, Mol. Cryst. Liq. Cryst. **499** (2009) 282.

A7. M. N. Patel, P. Griffin, J. Kim, T. E. Milner, K. P. Johnston, J. Colloid Interface Sci. **345** (2010), 194.

A8. S. K. Sainis, V. Germain, C. O. Mejean, E. R. Dufresne, Langmuir **24** (2008) 1160.

A9. M. K. Kim, C. A. Kim, S. D. Ahn, S.-R. Kang, K. S. Suh, Synth. Met. **146** (2004) 197.

A10. M. Badila, C. Brochon, A. Hebraud, G. Hadziioannou, Polymer 49 (2008) 4529.

A11. Y. T. Wang, X. P. Zhao, D. W. Wang, J. Microencapsulation **23** (2006) 762.

A12. I. B. Jang, J. H. Sung, H. J. Choi, I. Chin, Synth. Met. **152** (2005) 9.

A13. M. P. L. Werts, M. Badila, C. Brochon, A. Hebraud, G. Hadziioannou, Chem. Mater. **20**

(2008) 1292.

A14. X. Fang, H. Yang, G. Wu, W. Li, H. Chen, M. Wang, Curr. Appl. Phys. **9** (2009) 755.

A15. E. A. Barringer, H. K. Bowen, Langmuir **1** (1985) 414.

A16. H. T. Kim, H. Park, S. Y. Bae, K. O. Yoo, Korean J. Chem. Eng. **12** (1995) 516.

A17. M. Murata, K. Wakino, S. Ikeda, J. Elec. Spectrosc. Relat. Phenom. **6** (1975) 459.

A18. U. Diebold, T. E. Madey, Surf. Sci. Spectra **4** (1998) 227.

A19. X. Chen, S. S. Mao, Chem. Rev. **107** (2007) 2891.

A20. J. Chen, L. Gao, J. Huang, D. Yan, J. Mater. Sci. **31** (1996) 3497.

A21. L. S. Park, J. W. Park, H. Y. Choi, Y. S. Han, Y. Kwon, H. S. Choi, Curr. Appl. Phys. **6** (2006) 644.

A22. G. Tan, L. Zhang, C. Ning, X. Liu, J. Liao, Thin solid films **519** (2011) 4997.

23. E. Ukaji, A. Furusawa, M. Sato, N. Suzuki, Appl. Surf. Sci. **254** (2007) 563.

A24. H. Salmio, J. Phys. Chem. C 111 (2007) 923.

A25. M. Lijima, J. Collod and Interface Sci. **337** (2009) 61.

Appendix II - CURRICULUM VITAE

CURRICULUM VITAE

Kyung Ju Park

Electronics Processing Research Laboratory
Department of Chemical and Biological Engineering
Seoul National University, Seoul 151-744, KOREA

Personal Information

Name: Kyung Ju Park
Date of Birth: April 17, 1985
Place of Birth: Seoul, Korea
Nationality: Republic of Korea
Sex: Female

Office Address

Build.302, 907
Seoul National University
San 56-1, Shillim-dong, Kwanak-gu
Seoul 151-744, Korea
Tel: +82-2-880-8940
E-mail: melongta@snu.ac.kr

EDUCATION

Doctor of Philosophy (March 2008 ~ present)

Department of Chemical and Biological Engineering, Seoul National University
Advisor: Prof. Jae Jeong Kim
Thesis: "*in-situ* transmittance evaluation of solutions for Cu electroless deposition and its applications"

Bachelor of Engineering (March 2004 ~ February 2008)

Chemical Engineering, Yonsei University

PROFESSIONAL ACTIVITIES

September 2013~present	Student Member, International Society of Electrochemistry
March 2008~ present	Student Member, The Korean Electrochemical Society
September 2009 ~ present	Student Member, The Electrochemical Society, USA
April 2008 ~ present	Member, Korea Institute of Chemical Engineering
January 2008	Elementary Education Program of Semiconductor Processing in Inter-University Semiconductor Research Center (ISRC) (Seoul National University)

SCHOLARSHIPS

Yonsei University

2nd semester, 2007	National science and technology scholarship
1st semester, 2007	University designated scholarship (truth)
2nd semester, 2006	University designated scholarship (freedom)
1st semester, 2005	University designated scholarship (freedom)
1st semester, 2004	Yonsei special awards

Seoul National University

2nd semester, 2012 ~present	Scholarships granted by Cheil Industries Inc.
2011	Scholarship student for school affairs support

2009~2010	Lecture & Research Scholarship
2008~2012	Brain Korea (BK21) scholarships of scientific technology

LIST OF PUBLICATIONS (Kyung Ju Park)

-International Journal-

[1] Kyung Ju Park, Myung Jum Kim, Taeho Lim, Hyo-Chol Koo, Jae Jeong Kim, "Conformal Cu Seed Layer Formation by Electroless Deposition in non-Bosch Through Silicon Vias", Electrochem. Solid-State Lett., 15(5), D26-28 (2012)

[2] Kyung Ju Park, Hyo-Chol Koo, Taeho Lim, Myung Jun Kim, Oh Joong Kwon, Jae Jeong Kim, "Evaluation of Stability and Reactivity of Cu Electroless Deposition Solution by *In-Situ* Transmittance Measurement", J. Electrochem. Soc., 158(9), D541-545 (2012)

[3] Kyung Ju Park, Kang Uk Lee, Myeong Ho Kim, Oh Joong Kwon, Jae Jeong Kim, "Preparation of PS/TiO_2 as a white pigment in electrophoretic display", Curr. Appl. Phys. in printing

[4] Taeho Lim, Kyung Ju Park, Myung Jun Kim, Hyo-Chol Koo, Kwang Hwan Kim, Seunghoe Choe, Young-Soo Lee, and Jae Jeong Kim, "Real-time observation of Cu electroless deposition: Adsorption behavior of PEG during Cu electroless deposition", J. Electrochem. Soc., 160 (12) D3015-D3020 (2013)

[5] Seunghoe Choe, Myung Jun Kim, Hoe Chul Kim, Taeho Lim, Kyung Ju Park, Sung-Ki Cho, Soo-Kil Kim, and Jae Jeong Kim, "Seed Repair by Electrodeposition in Pyrophosphate Solution for Acid Cu Superfilling", J. Electrochem. Soc., 160 (4) D202-D205, (2013)

[6] Kang Uk Lee, Kyung Ju Park, Oh Joong Kwon, Jae Jeong Kim, "Carbon sphere as a black pigment for an electronic paper", Curr. Appl. Phys., 13, 419-424 (2012)

[7] Taeho Lim, Kyung Ju Park, Myung Jun Kim, Hyo-Chol Koo, and Jae Jeong Kim, "Real-time Observation of Cu Electroless Deposition Using OCP Measurement Assisted by QCM", J.

Electrochem. Soc., 159, D724-D729 (2012).

[8] Myung Jun Kim, Sang Heon Yong, Hyun Seok Ko, Taeho Lim, Kyung Ju Park, Oh Joong Kwon, Jae Jeong Kim, “Superfilling of Cu-Ag using electrodeposition in cyanide-based electrolyte”, J. Electrochem. Soc., 159(11). D656-658 (2012)

[9] Myung Jun Kim, Sang Heon Yong, Hyun Seok Ko, Taeho Lim, Kyung Ju Park, Oh Joong Kwon, Jae Jeong Kim, “Superfilling of Cu-Ag using electrodeposition in cyanide-based electrolyte”, J. Electrochem. Soc., 159(11). D656-658 (2012)

[10] Myung Jun Kim, Taeho Lim, Kyung Ju Park, Oh Joong Kwon, Soo-Kil Kim, Jae Jeong Kim, “Characteristics of Pulse-Reverse Electrodeposited Cu thin films: II. Effects of Organic Additive”, J. Electrochem. Soc., 159(9), D544-548 (2012)

[11] Myung Jun Kim, Taeho Lim, Kyung Ju Park, Sung Ki Cho, Soo-Kil Kim, Jae Jeong Kim, “Characteristics of Pulse-Reverse Electrodeposited Cu thin films: I. Effects of the Anodic Step in the Absence of an Organic Additive”, J. Electrochem. Soc., 159(9), D538-543 (2012)

[12] Taeho Lim, Hyo-Chol Koo, Kyung Ju Park, Myung Jun Kim, Soo-Kil Kim, Jae Jeong Kim, “Optimization of Catalyzing Process on Ta Substrate for Copper Electroless Deposition Using Electrochemical Method”, J. Electrochem. Soc., 159(3), D142-D147 (2012)

[13] Taeho Lim, Hyo-Chol Koo, Kwang Hwan Kim, Kyung Ju Park, Myung Jun Kim, Oh Joong Kwon, Jae Jeong Kim, “Room-Temperature Electroless Deposition of CoB Film and its Application as In Situ Capping during Buffing Process”, Electrochem. Solid-State Lett., 14(9), D95-D98 (2011)

[14] Myung Jun Kim, Sung Ki Cho, Hyo-Chol Koo, Taeho Lim, Kyung Ju Park, Jae Jeong Kim, “Pulse Electrodeposition for Improving Electrical Properties of Cu Thin Film” J. Electrochem. Soc., 157(11), D564-D569 (2010)

[15] Myung Jun Kim, Kyung Ju Park, Taeho Lim, Oh Joong Kwon, and Jae Jeong Kim, “Fabrication of highly conductive and oxidation-resistive Cu-Ag interconnection using electrodeposition: the mechanism of superfilling and the properties of Cu-Ag film”, in preparation

[16] Myung Jun Kim, Taeho Lim, Kyung Ju Park, Soo-Kil Kim, and Jae Jeong Kim, “Pulse-

reverse electrodeposition of Cu for metal interconnection: I. Effects of anodic steps on the competitive adsorption of the additives used for superfilling", in preparation.

[17] Myung Jun Kim, Taeho Lim, Kyung Ju Park, Soo-Kil Kim, and Jae Jeong Kim, "Pulse-reverse electrodeposition of Cu for metal interconnection: II. Enhancement of Cu superfilling and leveling", in preparation.

-Conference Proceedings-

(International)

[1] Kyung Ju Park, Taeho Lim, Myung Jun Kim, Kang Uk Lee, and Jae Jeong Kim, "in-situ Transmittance Measurement for Characterization of Organic Additives in Cu Electroless Deposition", 64th annual Meeting of ISE, 2013, Santiago de Queretaro, to be presented

[2] Kwang Hwan Kim, Taeho Lim, Kyung Ju Park, Hyo-Chol Koo, Myung Jun Kim, and Jae Jeong Kim, "Cu Electroless Deposition on Ru Barrier-Investigation of Growth Phenomena and Film Properties", 222nd Meeting of ECS, 2012, Hawaii

[3] Kyung Ju Park, Taeho Lim, Myung Jun Kim, Jae Jeong Kim, "Investigation of Reations and Additive Effects in Electroless Deposition by In situ Transmittance Measurement", 222nd Meeting of ECS, 2012, Hawaii

[4] Taeho Lim, Kyung Ju Park, Myung Jun Kim, Oh Joong Kwon, Jae Jeong Kim, "Investigation of Cu Electroless Deposion Mechanism by Open Circuit Potential Measurement", 220th Meeting of ECS, 2011, Boston

[5] Myung Jun Kim, Tae Ho Lim, Kyung Ju Park, Oh Joong Kwon, Jae Jeong Kim, "Synthesis of pd-Au Nanoalloys Using Electrodeposition", 218th Meeting of ECS, 2010, Las vagas

[6] Kang Uk Lee, Oh Joong Kwon, Kyung Ju Park, Bum Koo Cho, Sang Hyun Yong, M.G. Yeo, Jae Jeong Kim, "The Characteristics of Black Pigment Prepared by Grafting Polymerization", 218th Meeting of ECS, 2010, Las vagas

[7] Hyo Jun Lee, Myung Jun Kim, Tae Ho Lim, Kyung Ju Park, Jae Jeong Kim, Oh Joong

Kwon, “Electrodeposition of Cu-Ag Film in Cyanide Based Electrolyte”, 218th Meeting of ECS, 2010, Las vagas

[8] Kyung Ju Park, Hyo-Chol Koo, Taeho Lim, and Jae Jeong Kim, “Evaluation of Stability and Reactivity of Solutions by In Situ Transmittance in Electroless Deposition”, 216th Meeting of ECS, 2009, Vienna

[9] Jae Jeong Kim, Sung Ki Cho, Kyung Ju Park, Myung Jun Kim, and Hyo-chol Koo, "Cu filling in through silicon via (TSV) using electroless and electroplating for 3D interconnection", 215th Meeting of ECS, 2009, San Francisco

(domestic)

[1] Myeong Ho Kim, Kyung Ju Park, Kang Uk Le, Jae Jeong Kim, Oh Joong Kwon, "Synthesis of black pigment with Couette-Taylor vortex for electrophoretic display application", Fall Meeting for Korean Institute of Chemical Engineers, 2012, Busan

[2] Kwang Hwan Kim, Taeho Lim, Kyung Ju Park, Myung Jun Kim, Jae Jeong Kim, "Cu electroless deposition in NH_2NH_2 based solution Investigation of electrochemical behavior and Cu film growth phenomena", Fall Meeting for Korean Institute of Chemical Engineers, 2012, Busan

[3] Hoe Chul Kim, Myung Jun Kim, Taeho Lim, Kyung Ju Park, Kwang Hwan Kim, Seunghoe Choe, Hyuk Jin Seo, Jae Jeong Kim, Soo-Kil Kim, “Charateristics of electrodeposited Cu films with various additives”, Spring Meeting for Korean Institute of Chemical Engineers, 2012, Jeju

[4] Myeong Ho Kim, Kyung Ju Park, Kang Uk Lee, Jae Jeong Kim, Oh Joong Kwon, “Preparation of black pigment using radical polymerization with Couette Taylor vortex in electrophoretic display”, Spring Meeting for Korean Institute of Chemical Engineers, 2012, Jeju

[5] Kyung Ju Park, Myung Jun Kim, Taeho Lim, Hyo-Chol Koo, Jae Jeong Kim, “Conformal Cu seed layer formation by electroless deposition in high aspect ratio of non-bosch through silicon vias”, The 19th Korean Conference on Semiconductors, February, 2012, Seoul

[6] Taeho Lim, Hyo-Chol Koo, Kyung Ju Park, Myung Jun Kim, Soo-Kil Kim, Jae Jeong Kim,

"Optimization of catalyzing process on Ta substrate for Copper electroless deposition using electrochemical method", The 19th Korean Conference on Semiconductors, February, 2012, Seoul

[7] Kyung Ju Park, Kang Uk Lee, Jae Jeong Kim, Oh Joong Kwon, "Preparation and cheracterization of PS/TiO_2 with treatment of 3-aminopropyltriethoxysliane and acetic acid in electrophoretic display",Fall Meeting for Korean Institute of Chemical Engineers, 2011, Incheon

[8] Myung Jun Kim,Taeho Lim, Kyung Ju Park, Jae Jeong Kim, "The influences of the dissolution in pulse-reverse electrodeposition on the propertise of Cu thin films", Fall Meeting for Korean Institute of Chemical Engineers, 2011, Incheon

[9] Taeho Lim, Kyung Ju Park, Myung Jun Kim, Jae Jeong Kim, "Investigation of Cu Electroless Deposition Mechanism : Effect of Cu Electroless Deposition", Fall Meeting for Korean Institute of Chemical Engineers, 2011, Incheon

[10] Kang Uk Lee, Kyung Ju Park, Jae Jeong Kim, Oh Joong Kwon, "Application of carbon sphere for electronic paper", Fall Meeting for Korean Institute of Chemical Engineers, 2011, Incheon

[11] Kwang Hwan Kim, Taeho Lim, Kyung Ju Park, Jae Jeong Kim, "Electroless Cu deposition on Ru - The investigation of the growth mechanism and thin film properties", Spring Meeting for Korean Institute of Chemical Engineers, 2011, Changwon

[12] Taeho Lim, Hyo-Chol Koo, Kyung Ju Park, Myung Jum Kim, Jae Jeong Ki, "Investigation of Copper Electroless Deposition Mechanism by Open Circuit Potential Measurement", The 18th Korean Conference on Semiconductors, 2011, Jeju

[13] Kyung Ju Park, Hyo-Chol Koo, Taeho Lim, Myung Jum Kim, Jae Jeong Kim, "in situ Transmittance Measurement for Monitoring of Solution Performance in Copper Electroless Deposition", The 18th Korean Conference on Semiconductors, 2011, Jeju

[14] Kyung Ju Park, Taeho Lim, Myung Jum Kim, Jae Jeong Ki, "Evaluation of Cu ELD solution using in situ transmittance measurement", Fall Meeting for Korean Institute of Chemical Engineers, 2010, Daejeon

[15] Kang Uk Lee, Oh Joong Kwon, Kyung Ju Park, and Jae Jeong Kim, “Grafting polymerization on the carbon black for electrophoretic display pigment”, Spring Meeting for Korean Institute of Chemical Engineers, 2010, Daegu

[16] Kyung Ju Park, Hyo-Chol Koo, and Jae Jeong Kim, “Optimization of process for Cu seed layer formation in through silicon via (TSV)”, Spring Meeting for Korean Institute of Chemical Engineers, 2009, Gwangju

-Patent-

(domestic)

*Patent registration

[1] Jae Jeong Kim, Oh Joong Kwon, Kyung Ju Park, “Method of fabricating coated particles”, registration number 1148004, 2012

* Patent application

[1] Jae Jeong Kim, Oh Joong Kwon, Kyung Ju Park, Kang Uk Lee, “Carbon sphere of particle-uniformity and small size-distribution and the use thereof”, application number 10-2012-0001386

[2] Jae Jeong Kim, Oh Joong Kwon, Kyung Ju Park, Myeong Ho Kim, “Method of manufacturing electrophoretic micro-capsules”, application number 10-2012-0001385